Characterization of a novel OTX2-driven stem cell program in Group 3 and Group 4 medulloblastoma

by

Margaret Stromecki

A Thesis submitted to the Faculty of Graduate Studies of

The University of Manitoba

in partial fulfillment of the requirements of the degree of

MASTER OF SCIENCE

Department of Biochemistry and Medical Genetics,

University of Manitoba,

Winnipeg, MB

Copyright © 2017 by Margaret Stromecki

TABLE OF CONTENTS

Abstract……..…….vi

Acknowledgements……vii

List of Tables...……...……...……viii

List of Figures……...…. ix

List of Abbreviations…….….xi

CHAPTER 1: INTRODUCTION…..……..……1

1.1.0 OVERVIEW…..……...…….1

1.1.2 Medulloblastoma…….……...2

1.1.2 a) Symptoms and clinical presentation…….……..2

1.1.2 b) Histology…….……...….4

1.1.2 c) Current standard treatment…….……5

1.1.3 Wnt…….…….……...6

1.1.1 a) Incidence and demographics…….…….6

1.1.3 b) Genetic and molecular alterations…….……7

1.1.3 c) Cell of origin…….……..9

1.1.3 d) Treatment options…….……10

1.1.4 SHH…….……10

1.1.4 a) Incidence and demographics…….……...10

1.1.4 b) Genetic and molecular alterations…….……...11

1.1.4 c) Cell of origin…….……12

1.1.4 d) Treatment options…….……14

1.1.5 Group 3…..……...15

1.1.5 a) Incidence and demographics……...……15

1.1.5 b) Genetic and molecular alterations…..…….…..15

1.1.5 c) Cell of origin…….……17

1.1.6 Group 4…….…….……...18

1.1.6 a) Incidence and demographics…….…...18

1.1.6 b) Genetic and molecular alterations…….…...……18

1.1.6 c) Cell of origin…….……...…….19

1.1.6 d) Treatment options for Group 3 and 4 MB…….…….19

1.2.0 CEREBELLAR DEVELOPMENT AND MOLECULAR REGULATION OF STEM/ PROGENITOR CELLS.……..…….20

1.2.1 Cerebellum structure and function…….....…….20

1.2.2 Human cerebellum development……...……..……21

1.3.0 OTX2…….…….……...…...27

1.3.1 OTX2 and its role in the developing nervous system…….…..……27

1.3.2 OTX2 and dopaminergic neurons…….…….…..30

1.3.3 OTX2 and glutamatergic progenitors of the thalamus…….…..…..31

1.3.4 OTX2 in the choroid plexus……..……..……..….31

1.3.5 OTX2 and its role in the pineal gland and eye development……...…..…...32

1.3.6 OTX2 and its role in medulloblastoma…….…….…...33

1.4.0 CANCER STEM CELLS……..…….…….35

1.4.1 The cancer stem cell theory…….……35

1.4.2 The first cancer stem cells: assays……...……..……..36

CHAPTER 2: RATIONALE AND HYPOTHESIS……..……41

2.1 RATIONALE……..……41

2.2 HYPOTHESIS AND RESEARCH AIMS……..……41

CHAPTER 3: MATERIALS AND METHODS…….……..….43

3.1 Cell culture……..……43

3.2 Tumorsphere assays……45

3.3 Small interfering RNA..……..45

3.4 Gene expression profiling and analyses…….……47

3.5 Chromatin immunoprecipitation sequencing……..47

3.6 Immunofluorescent staining……48

3.7 Western Blot……49

3.8 Real Time-qPCR ……50

3.9 Lentiviral transduction…….50

3.10 RHO pulldown..…..……50

3.11 Group 3 and Group 4 MB patient sample analysis……52

3.12 Intracerebellar transplantation……...52

3.13 Statistical tests...……53

CHAPTER 4: RESULTS……55

4.1 AIM 1: To validate the effects of OTX2 on self-renewal/differentiation following OTX2 knockdown…….55

4.1.1 OTX2 knockdown decreases MB self-renewal in both well-established and recently

derived cell lines *in vitro* ….……55

4.1.2 OTX2 knockdown increases differentiation in both well-established and recently derived MB cell lines *in vitro*...…….58

4.1.3 OTX2 knockdown inhibits tumor growth and decreases tumor initiating capacity from D283 tumorspheres *in vivo*.…….…….60

4.2 AIM 2: To determine the relationship between OTX2 and select neural differentiation genes in regulating cell function *in vitro*. ……...…….…..62

4.2.1 Global gene expression analysis and ChIP-sequencing reveal a negative correlation between OTX2 and expression of a large cohort of axon guidance genes in MB cells……62

4.2.2 Axon guidance genes are negatively correlated with OTX2 expression in tumorspheres from established and recently derived MB cell lines as well as Group 3 and Group 4 patient samples…..…….…….68

4.2.3 Increased semaphorin levels are inversely correlated with tumorsphere formation, self-renewal and growth in MB tumorspheres…….…….76

4.3 AIM 3: To investigate the downstream pathways known to modulate the effects of select neural differentiation genes following OTX2 knockdown in Group 3 and Group 4 MB stem cells. …….…….…….…….…….……89

4.3.1 OTX2 limits RHO pathway activation.…….…….……..89

4.3.2 Decreased RHO activity partially rescues tumorsphere formation in OTX2 knockdown MB stem cells…….…….…….93

CHAPTER 5: DISCUSSION…….…….……...96

5.1 *In vitro* MB studies in stem cell-enriched conditions are the most biologically relevant……96

5.2 OTX2 inhibits neural differentiation and axon guidance gene expression in MB stem cells..96

5.3 Axon guidance cues can promote or inhibit tumor progression in a cell context dependent manner…….…….…….98

5.4 Semaphorin signaling genes and their tumor suppressive role in Group 3 and 4 MB stem cells…….…….……100

5.5 Transcriptional regulation of the semaphorin genes by OTX2…….…….……...103

5.6 Downstream semaphorin pathway signaling is negatively correlated with OTX2……..….104

5.7 Future Directions.…….……106

5.8 Summary…….……..107

CHAPTER 6: REFERENCES…….……..…109

APPENDIX A: SUPPLEMENARY TABLES…….……...121

ABSTRACT

Medulloblastoma (MB) is a primary pediatric brain cancer that is frequently accompanied by metastasis and poor long-term prognosis. Our goal is to identify new signaling pathways that regulate the treatment-resistant MB cellular phenotypes, namely the stem cells. The *OTX2* gene, which is amplified or overexpressed in the majority of Group 3 and 4 MBs, is a central regulator of stem cell function in these tumors. Here, we characterized the OTX2 regulatory network and identified a negative correlation between OTX2 and axon guidance genes in Group 3 and 4 MB stem/progenitor cells and tumors. Functional validation studies demonstrated that increased levels of semaphorin 4D (SEMA4D), L1 Cell Adhesion Molecule (L1CAM), and neuropilin-1 (NRP1) are associated with decreased self-renewal and that the downstream RHO signaling may be contributing to these effects. Our results offer critical insights into the molecular drivers of these aggressive tumors and provide a framework to pursue novel therapies.

ACKNOWLEDGEMENTS

First and foremost I would like to thank my supervisor Dr. Tamra Werbowetski-Ogilvie for her mentorship, guidance and support throughout my graduate training. I am very grateful for the opportunity she gave me to join her lab as a Master's student in 2015. This thesis could not have been assembled without her guidance and expertise. She is an inspiring woman in medical science research and I hope to be as good a mentor as she one day.

I would like to acknowledge and thank my committee members, Dr. Mark Nachtigal and Dr. Sari Hannila for their time and constructive criticism. I am grateful for their guidance during my graduate training and for their support of my career goals.

I am also very appreciative for the support I have received from each of the Ogilvie Lab members. Ms. Ludivine Morrison for her patience, technical support and for conducting the RHO-activity pulldowns used in this study. I convey my thanks to Nazanin Tatari for conducting the immunofluorescence staining and animal surgeries and, Lisa for her mentorship and support. A special thanks to Dr. Ravinder Kaur for orienting and teaching me numerous experimental protocols and tissue culture techniques while Dr. Ogilvie and Ludivine were still away on their maternity leaves and throughout my first year. In addition, I would also like to thank Pratima and Vasu for their friendship and support. I have made some great friends in the lab that I am so grateful for!

I must also extend a thank you to Gareth Palidwor from The Ottawa bioinformatics Core Facility for his gene expression and ChIP-sequencing analysis, and to Patryk Skowron from Arthur and Sonia Labatt Brain Tumour Research Centre and Program in Developmental and Stem Cell Biology for his Group 3 and Group 4 medulloblastoma patient sample analysis.

This project could not have been completed without support from the following agencies; Canada Research Chairs, Canadian Institute of Health Research and Dr. Paul T. Thorlakson Foundation.

Of course, I thank my family and friends for their unconditional love and encouragement throughout my academic endeavors. I could not have done this without them. Thank you to Riley for his love and comic relief, which keeps me sane.

LIST OF TABLES

Table 1.0: Properties of cell lines used…….....44

Table 1.1: List of primer sequences used for Real Time qPCR…….…….....51

Table 1.2: Axon guidance pathway genes that were significantly and differentially expressed following OTX2 knockdown and the number of OTX2 binding peaks/overlaps within -5kb-+2kb of their transcriptional start sites. ……..66

Table 1.3: Correlation between OTX2 and expression of axon guidance genes in Group 3 and 4 MB patient samples ……...73

Table 1.4: Gene Set Enrichment Analysis revealed that genes associated with SEMA4D signaling were enriched in gene sets that were downregulated in D283 scramble relative to OTX2 knockdown tumorspheres……...…….....90

Table 1.5: Gene Set Enrichment Analysis results for Reactome and KEGG databases identified pathways significantly enriched in gene sets that were downregulated in D283 scramble relative to OTX2 knockdown tumorspheres……...91

Table S1: Neuronal differentiation genes that are significantly and differentially expressed following OTX2 knockdown in D283 tumorspheres……...121

Table S2: Axon guidance genes that are significantly and differentially expressed following OTX2 knockdown in D283 tumorspheres……...127

Table S3: Gene Set Enrichment Analysis revealed that genes associated with semaphorin interactions were enriched in gene sets that were downregulated in D283 scramble relative to OTX2 knockdown tumorspheres. ……..……130

LIST OF FIGURES

Figure 1.0: Molecular subgroups of medulloblastoma……3

Figure 1.1: Normal WNT signaling……..……8

Figure 1.2: Normal SHH signaling. …….…….13

Figure 1.3: Nervous system and cerebellum development……..…..23

Figure 1.4: Midbrain-Hindbrain boundary.…..…….…….24

Figure 1.5: The gray matter of the cerebellum during development.…..…….…..……....26

Figure 1.6: The OTX2 gene and protein….. …….28

Figure 1.7: Cancer stem cell survival with conventional chemotherapy……..38

Figure 1.8: Cancer stem cell isolation……40

Figure 3.1: Tumorsphere assay…….…46

Figure 4.1: Knockdown of OTX2 in Group 3 and Group 4 MB tumorspheres decreases self-renewal……..56

Figure 4.2: Knockdown of OTX2 in Group 3 and Group 4 MB tumorspheres increases neural differentiation……59

Figure 4.3: OTX2 knockdown decreases tumor growth and tumor initiating capacity *in viv*o…61

Figure 4.4: OTX2 knockdown increases expression of neuronal differentiation and axon guidance genes……...……63

Figure 4.5: Axon guidance genes are negatively correlated with OTX2 expression in D283 and D341 cell lines……..….69

Figure 4.6: Semaphorin genes are negatively correlated with OTX2 expression in D283 and D341 cell lines…….……..…71

Figure 4.7: Semaphorin genes are negatively correlated with OTX2 expression in established and recently derived MB cell lines as well as patient samples…….75

Figure 4.8: Recombinant L1CAM Fc treatment decreased self-renewal……..77

Figure 4.9: Recombinant SEMA4D Fc treatment decreased self-renewal……78

Figure 4.10: Recombinant NRP1 Fc treatment decreased self-renewal……79

Figure 4.11: Recombinant semaphorin protein treatment does not significantly affect cell number or viability of D283 tumorspheres……..80

Figure 4.12: Decreased levels of L1CAM in OTX2 knockdown cells results in no rescue of tumorsphere formation and growth……...…….82

Figure 4.13: Decreased levels of SEMA4D in OTX2 knockdown cells results in a partial rescue of tumorsphere formation and growth……...……83

Figure 4.14: Decreased levels of NRP1 in OTX2 knockdown cells results in a partial rescue of tumorsphere formation and growth……84

Figure 4.15: Decreased levels of semaphorin pathway genes in MB3W1 OTX2 knockdown tumorspheres results in a partial rescue of tumorsphere formation and growth……85

Figure 4.16: Decreased levels of semaphorin pathway genes in D283 and MB3W1 OTX2 knockdown tumorspheres does not significantly affect viability……..88

Figure 4.17: OTX2 levels are negatively correlated with activation of RHO signaling genes….92

Figure 4.18: OTX2 levels are negatively correlated with activation of RHO signaling……...94

Figure 5.0: Working model depicting the oncogenic role OTX2 plays in high OTX2 expressing Group 3 and 4 MBs……..…….…….…….……...…99

Figure 5.1: Vertebrate membrane bound and secreted semaphorin signaling molecules and receptors…….……...…101

Figure 5.2: Downstream semaphorin pathway signaling…….……..……...…105

LIST OF ABBREVIATIONS

~	Approximately
3D	Three dimensional
µg	Microgram (weight)
µl	Microliter (volume)
µM	Micromolar (concentration)
°C	Degrees Celsius
ADP	Adenosine diphosphate
ANOVA	Analysis of variance
APC	Adenomatous polyposis coli
ATP	Adenosine triphosphate
ATOH1	Atonal homologue 1
AVE	Anterior visceral endoderm
BBB	Blood brain barrier
BET	Bromodomain and extraterminal domain family
BrdU	Bromodeoxyuridine
BSA	Bovine serum albumin
CDK	Cyclin dependent kinase
cDNA	Complementary DNA
CGNPs	Cerebral granular neural precursors
ChIP	Chromatin immunoprecipitation
CK1	Casein kinase 1
CSF	Cerebral spinal fluid
CTNNB1	β-catenin gene
DMSO	Dimethyl sulfoxide
DMEM	Dulbecco's modified eagle medium
EGL	External granule layer
EMEM	Eagle's minimum essential medium
FZD	Frizzled
GABA	Gamma-Aminobutyric acid
GAPDH	Glyceraldehyde 3-phosphate dehydrogenase
GBX2	Gastrulation brain homoebox 2
GFP	Green fluorescent protein
GLI1/2/3	Glioma-associated oncogene family transcription factors
GSK3	Glycogen synthase kinase 3
HEPES	4-(2-hydroxyethyl)-1-piperazineethanesulfonic acid
HES	Hairy and enhancer of split
IF	Immunofluorescence
IGL	Internal granular layer
IPA	Ingenuity pathway analysis
KD	Knockdown
kDa	Kilodalton
L1CAM	L1 cell adhesion molecule
LCA	Large cell/anaplastic
MATH1	A basic helix-loop-helix transcription factor

MB	Medulloblastoma
MBEN	Medulloblastoma with extensive nodularity
min	Minutes
mL	Microliter (volume)
mg	Microgram
mTOR	Mammalian target of rapamycin
MYC	Myelocytomatosis
NaCl	Sodium chloride
NEUROD	Neuronal differentiation gene
nM	Nanomolar
NOD-SCID	Nonobese diabetic/severe combined immunodeficiency
NRP1	Neuropilin 1
OTX2	Orthodenticle homeobox2
PI3K/Akt	Phosphatidylinositol 3-kinase and protein kinase B
PBS	Phosphate buffered saline
PTCH	Patched
PTEN	Phosphatase and tensin homolog
qPCR	Quantitative real time polymerase chain reaction
RNA	Ribo-nucleic acid
RPE	Retinal pigmented epithelium
RT	Room temperature
SDS	Sodium dodecyl sulphate
SEMA	Semaphorin
SEMA4D	Semaphorin 4 D
SHH	Sonic hedgehog
shRNA	Short hairpin RNA
siRNA	Small interference RNA
SMO	Smoothened
SSEA3	Stage specific embryonic antigen 3
SUFU	Suppressor of fused
TBS	Tris EDTA buffer
TCF/LEF	T cell factor/lymphoid enhancer factors
TP53	Tumor protein 53
Trp53	Transformation-related protein 53
TSS	Transcriptional start site
WNT	Wingless/Integrated

CHAPTER 1: INTRODUCTION

1.1.0 OVERVIEW

Brain tumors are the deadliest forms of childhood cancer, accounting for 35% of cancer related deaths in Canadian children 0-14 (Canadian Cancer Society Statistics, 2016). Medulloblastoma (MB) is the most common malignant primary pediatric brain tumor. It is divided into five subtypes based on genetic, molecular, and clinical treatment outcomes: Wingless (WNT), Sonic Hedgehog (SHH) *TP53*+, SHH *TP53-,* Group 3 and Group 4 [1-3]. As the names imply, the signaling pathways associated with tumor progression remain largely undefined for both Group 3 and 4 MB, yet they exhibit the worst prognosis [1,3]. These subgroups originate from neural stem/progenitor cells that often disseminate through the cerebrospinal fluid, evade treatment, and induce metastasis and recurrence [4-7]. Furthermore, young patients who survive long-term commonly suffer from cognitive deficits and physical dysfunction due to toxicities associated with chemotherapy and radiation [2]. Thus, there is a critical need to define the molecular mechanisms contributing to Group 3 and 4 MB pathogenesis in order to develop better prognostic tools and therapies with less toxic effects. My thesis aims to define the molecular signatures that contribute to Group 3 and 4 MB pathogenesis with a focus on genes that are molecular regulators of self-renewal or stem cell function.

A hallmark of Group 3 and 4 MB is the amplification or overexpression of orthodenticle homeobox 2 (*OTX2*). OTX2 is a transcription factor that is essential during forebrain, midbrain and hindbrain patterning [8, 9,10]. Our lab has demonstrated that OTX2 knockdown (KD) decreases the self-renewal capacity of Group 3 and 4 MB cells grown in stem cell conditions *in vitro* [11]. However, the exact mechanisms by which OTX2 enhances self-renewal and inhibits differentiation in Group 3 and 4 MB are still unknown. Thus, the aims of my thesis are: 1) To

validate the effects of OTX2 on self-renewal/differentiation following OTX2 KD, 2) To determine the relationship between OTX2 and select neural differentiation genes in regulating Group 3 and 4 MB cell function *in vitro,* and 3) To investigate the downstream pathways known to modulate the effects of select neural differentiation genes following OTX2 KD in Group 3 and Group 4 MB stem/progenitor cells.

1.1.1 Medulloblastoma

MB is the most common malignant primary pediatric brain tumor that develops in the cerebellum or fourth ventricle of the brain (World Health Organization, 2016) [12]. It is an embryonal tumor that originates from stem and progenitor cells during neurogenesis [1, 13]. Recent advances in genomic sequencing and microarray technologies have improved our understanding of MBs molecular and cellular heterogeneity. Currently, MB is divided into 5 distinct subtypes based on genomic alterations, transcriptional profiles, and response to treatment: WNT, SHH tumor protein p53 (*TP53)*+, SHH *TP53-,* Group 3 and Group 4 (Figure 1.0) [1-4, 14]. This new molecular profiling has improved risk stratifications and treatment regimes for patients. Despite this, children still suffer from long-term cognitive and physical dysfunction due to the toxicities associated with aggressive treatment. Therefore, there is a critical need for the development of more targeted and less toxic therapies. By understanding the regulatory pathways of the developing nervous system, we can gain insight into the molecular mechanisms contributing to MB initiation, progression and metastasis.

1.1.1 a) Symptoms and clinical presentation

Due to MBs close proximity to the fourth ventricle, patients often experience increased intracranial pressure and hydrocephalus as a result of cerebrospinal fluid (CSF) blockage and accumulation in the brain [15]. Hydrocephalus is responsible for many of the initial symptoms of

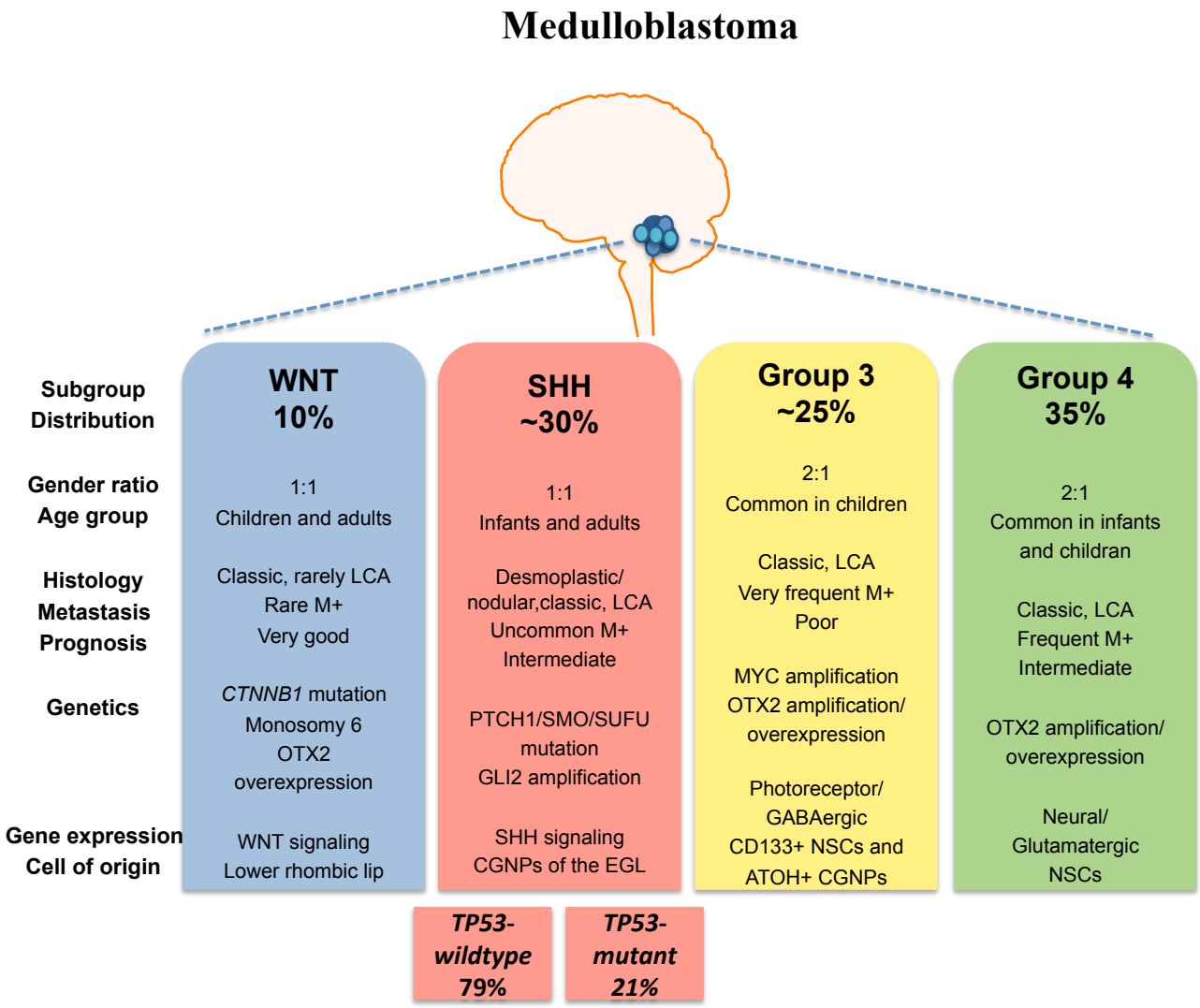

Figure 1.0: Molecular subgroups of medulloblastoma.
Medulloblastoma is divided into 5 subtypes based on genetic, molecular, and clinical treatment outcomes into: WNT, SHH *TP53-wildtype*, SHH *TP53-mutant*, Group 3 and Group 4. Adapted from Kool *et al*., 2012.

disease including morning headaches, vomiting, reduced balance or ataxia, elevated eyes and papilledema [16, 17]. Some patients that develop MB tumors in the lateral cerebellar hemispheres commonly present with unsteadiness and muscle weakness with no signs of hydrocephalus [15, 17]. Other patients can exhibit a head tilt or stiff neck, resulting from herniation of the vertebral bodies [17]. On average, children are diagnosed within 2-3 months from their onset of symptoms via imaging. On computed tomography (CT) scans, MB tumors appear as dense or very dense well-defined midline or lateral cerebellar lesions [17], while via magnetic resonance imaging (MRI), tumors appear as midline inferior vermian lesions infiltrating the fourth ventricle [17].

1.1.1 b) Histology

Previous MB risk stratification was primarily based on the histology of the tumor, presence of metastasis, and the age of the patient. Despite advances in molecular technologies, most hospitals still rely on histology for risk stratification and subtyping. With hematoxylin and eosin staining (H&E), MB tumors appear as undifferentiated cells with large blue stained nuclei [1]. Accordingly, MBs are described as small blue cell cerebellar malignancies [1] and are divided into 4 histological variants; classic, large cell/anaplastic (LCA), desmoplastic/nodular, and MB with extensive nodularity (MBEN) [1, 2, 18, 19]. Classic MBs are observed in 70% of MB cases and contain small, round undifferentiated cells with high nuclear-to-cytoplasmic ratios and hyperchromatid nuclei [18]. About 40% of classic MBs exhibit Homer Wright rosettes (named after the pathologist who categorized MB separately from other CNS tumors in 1910) [18]. In addition, β-catenin nuclear accumulation is associated with excellent clinical outcome in the classic histological MB variant [20]. Conversely, LCA MBs are characterized by marked nuclear pleomorphisms, large nuclei, prominent nucleoli and ample cytoplasm [19]. LCA histology is associated with malignant MBs and the majority exhibits intermingled areas of anaplastic and/or

classic tumor cells [19]. Anaplastic MBs contain distinctive nuclear molding and high mitotic counts [19]. Desmoplastic/nodular MBs contain nodules of differentiated neuron-like cells surrounded by internodular zones, that are composed of highly proliferative cells [18]. While MBEN MBs are characterized by expanded nodular regions with elongated reticulin-free, neuropil-rich (unmyelinated axons) zones containing uniform neuron-like tumour cells [18]. Moreover, MBENs typically have a good prognosis and commonly arise in infants [18, 19]. Interestingly, desmoplastic/nodular and MBEN MBs are only found within the molecular SHH subgroup while the other histological variants appear across all the molecular classifications.

1.1.1 c) Current standard treatment

Standard therapy for MB patients consists of maximal safe surgical resection, chemotherapy, and radiation therapy. As mentioned above, the histology, age of the patient, metastatic status and extent of resection are still critical factors that determine patient risk stratification and prognosis. Patients over the age of 3 are categorized as high-risk if they display $\geq 1.5 cm^2$ residual disease, evidence of metastases and/or CSF dissemination [21,15]. Average-risk patients include those with near-total resection with ≤ 1.5 cm^2 residual disease and no evidence of CSF dissemination [15]. A randomized controlled trial by Albright *et al.* on 233 children with differing chemotherapy regimes demonstrated that residual tumor ≤ 1.5 cm^2 was associated with improved 5-year progression-free survival in 20% of patients with no evidence of metastasis, and in 11% of patients with metastasis or aggressive disease [14]. In contrast, patients younger than 3 years of age make up a separate treatment group. These young patients are recommended a treatment regime that only consists of surgical resection and high dose adjuvant chemotherapy in order to protect their developing nervous systems from radiation therapy [21,15].

After surgical resection, high-risk patients undergo radiation therapy (54-55.8 Gy) with

high-dose craniospinal irradiation (CSI) (36.0 Gy) and adjuvant chemotherapy [16]. Average-risk patients undergo radiation therapy (54-55.8 Gy) with a reduced-dose of CSI (23.4 Gy) and adjuvant chemotherapy [16]. Adjuvant chemotherapy consists of the cytotoxic and alkylating agents, vincristine, cisplatin, cyclophosphamide, lomustine and carboplatin [22-24], administered in the most favorable combinations built upon the patient's risk stratification.

Follow-up appointments include imaging of the brain and spinal cord every 3 months following diagnosis for 1 year, and then twice a year for an additional 2 years [25]. Although >80% of patients can achieve disease control with these standard treatments, it is well recognized that long-term survivors live with permanent neurocognitive damage [25]. This is especially true in younger children and thus management of the disease and new treatment approaches need to better protect the developing nervous systems of these young patients. Understanding the molecular heterogeneity and the signaling pathways contributing to disease progression within and between tumors will be imperative. Fortunately, new microarray and whole genome sequencing technologies with larger patient datasets have already improved our understanding of MBs heterogeneity. I will take the next few sections to outline in detail the main characteristics including incidence and demographics, genetic and molecular alternations, cell of origin, and treatment options of each MB molecular subtype discovered to date.

1.1.3 WNT

1.1.3 a) Incidence and demographics

The Wingless (WNT) subtype accounts for 10% of all MB cases and has the best long-term prognosis with a 5-year survival rate of over 90% [1, 4]. The 5-10% who do not survive often succumb to complications from therapy or secondary neoplasms caused by radiation therapy [26]. WNT-activated tumors commonly occur in children (3-16 years of age) and are rarely seen in

infants [26]. The overall incidence of MB is higher in males than females, however, for the WNT subtype, the distribution is 1:1 between sexes [1, 3, 26, 27]. Most WNT tumors have a classic histology but some appear as LCA as well [1, 4, 26].

1.1.3 b) Genetic and molecular alterations

As the name implies, aberrant activation of the WNT/β-catenin signaling pathway is responsible for the pathogenesis of this MB subtype. In the canonical-WNT signaling pathway, β-catenin is normally kept at low levels in the absence of WNT ligand [28]. Briefly, axin scaffold proteins phosphorylate β-catenin when WNT is not present, recruiting proteasomal degradation proteins such as, E3 ligase to degrade β-catenin [28]. The axin scaffold consists of axin, adenomatous polyposis coli (APC), casein kinase 1 (CK1), and glycogen synthase kinase 3 β (GSK3β). CK1 and GSK3β are responsible for the phosphorylation of β-catenin, preventing it from entering the nucleus [28]. However, when WNT is present, it binds to the seven-transmembrane receptor frizzled (FZD), recruiting low-density lipoprotein receptor related protein (LRP6) and Disheveled (DVL) to the membrane. At the membrane, phosphorylated LRP6 signals axin, CK1, and GSK3β to the membrane. As the axin scaffold proteins are recruited to the membrane, phosphorylation of β-catenin is reduced. β-catenin then accumulates in the cell, enters the nucleus, and turns on T cell factor/lymphoid enhancer factor (TCF/LEF) target gene expression. TCF/LEF target genes include myelocytomatosis *(c-MYC)* and cyclin D1 *(CCND1),* which ultimately increases cell proliferation (Figure 1.1) [27]. WNT signaling is a critical regulator of midbrain-hindbrain development and of self-renewal in neural precursors [27, 29].

The initial indicator that demonstrated WNT signaling mutations caused MB came from studies on Turcot syndrome patients. Turcot syndrome predisposes individuals to WNT MB (by

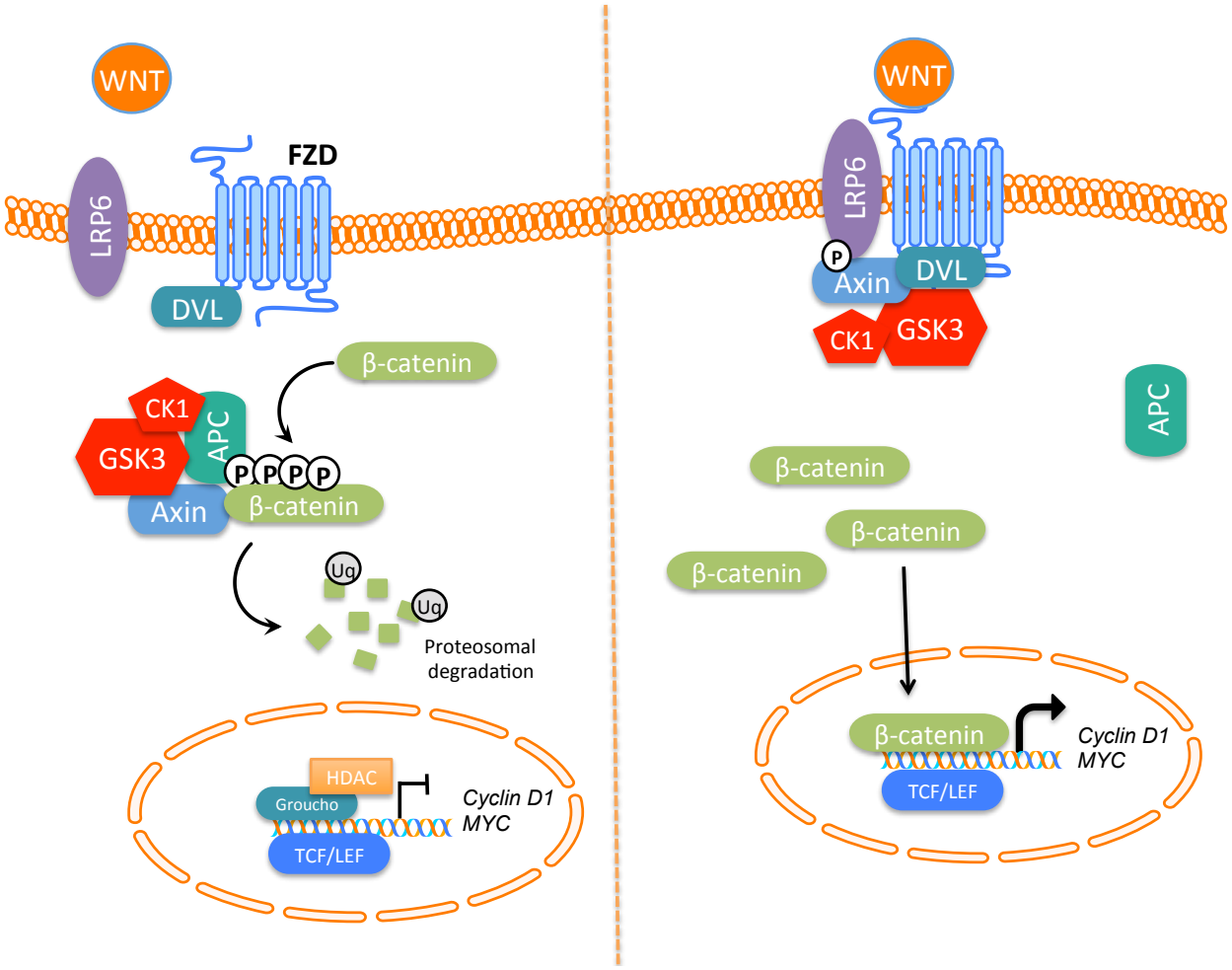

Figure 1.1: Normal WNT signaling.
In the absence of WNT, axin scaffold proteins bind together in a multi-protein destruction complex and phosphorylate β-catenin. Phosphorylation signals the degradation of β-catenin, allowing Groucho (co-repressor) proteins to inhibit TCF/LEF expression. When WNT is present, it binds to the G protein-coupled receptor, FZD, and recruits part of the axin scaffold protein complex to the membrane. This allows non-phosphorylated β-catenin to accumulate in the cell and translocate into the nuclease to turn on the expression of *Cyclin D1* and *MYC*. Adapted from MacDonald *et al*., 2009, and Lee *et al*., 2012.

92-fold) due to heterozygous germline mutations in *APC* (wildtype *APC* allele is lost) [1, 30, 31]. Conversely, sporadic WNT-activated MBs account for 70-90% of all cases, and develop due to somatic miscoding mutations in the β-catenin encoding gene, *CTNNB*1 and *APC* [1, 26, 27, 32].

Monosomy 6 is a characteristic chromosomal aberration observed in 90% of WNT-activated MBs [1, 4]. Interestingly, the WNT signaling genes are not encoded on chromosome 6. However, WNT MBs also exhibit mutations in downstream WNT signaling genes dickkopf-related protein 1 (*DKK1)*, *DKK2*, and Wnt-inhibitory factor 1 (*WIF1)* [1, 26]. thus, further investigation into aberrant WNT signaling function is necessary for the development of less toxic, more targeted therapies.

1.1.3 c) Cell of origin

WNT-activated tumors are believed to originate from the cells in the lower rhombic lip of the developing dorsal brainstem (to be discussed in more detail later) [1, 5]. *CTNNB1* is responsible for normal differentiation and migration of lower rhombic lip progenitors. Gibson *et al*., demonstrated that activating mutations in *CtnnbB1* generated cell accumulations in dorsal brainstem as a result of disrupted progenitor cell differentiation and migration [5]. This was complimented by positive staining of lower rhombic lip markers oligodendrocyte transcription factor 3 (OLIG3) and paired box gene 6 *(*PAX6), and negative staining for granule neural precursor markers in the cell deposits observed by *Gibson et al.* [5]. Notably, the same group showed that conditional *Ctnnb1* mutants accompanied by *Trp53* mutations in ventricular zone progenitors *(Blbp-Cre;Ctnnbl*$^{+/lox(Ex)}$*;Trp53*$^{flx/lxx}$*),* develop classic MB tumors in the dorsal brain stem with 10% penetrance which poses transcriptional profiles that recapitulated human WNT MBs [4,5]. While Robinson *et al.* modeled classic MB with 100% penetrance by adding a phosphatidylinositol 3-kinase (*Pik3ca)* mutant allele to the previous conditional model (*Blbp-*

Cre;Ctnnbl$^{+/lox(Ex)}$*;Trp53*$^{+/flx}$*; Pik3ca*^{E545k}*)* [33]. Collectively, these models will need to be further utilized for preclinical testing.

1.1.3 d) Treatment options

WNT-activated MB patients typically undergo tumor resection, chemotherapy and radiotherapy. However, due to their excellent prognosis, clinicians now recommended that WNT patients be treated less aggressively to reduce some of the long-term toxicities associated with standard treatment regimes. Reduced doses of CSI and extra tumor area radiation (tumor bed boosts) have demonstrated better preservation of intellectual functioning among patients [4]. Notably, the excellent outcomes in WNT-activated MB have been partially attributed to the tumoral blood vessels that feed into the cerebellar fenestrations of WNT MBs and establish a leaky blood brain barrier (BBB) [34]. This leaky BBB surrounding the tumor allows chemotherapy to more readily access the tumor cells.

Baryawno and collegues have demonstrated that inhibition of phosphoinositide 3-kinase (P13K) and protein kinase B (AKT) signaling with a small molecule inhibitor, OSU03012, suppresses MB proliferation and expansion via cross talk with WNT signaling [35]. P13K/AKT inhibition activates GSK3β which inhibits β-catenin function and in turn downregulates *CCND1* and *c-MYC* transcription factor expression [35]. Continued research aimed at investigating WNT signaling and its downstream signaling targets could lead to even better long-term treatment outcomes and improved quality of life for patients.

1.1.4 SHH

1.1.4 a) Incidence and demographics

Sonic hedgehog (SHH) activated MBs account for ~30% of MB cases and exhibit an intermediate to poor prognosis with a 5-year survival rate of 75% [4]. They frequently appear in infants <3 years old and adults dichotomously [4]. The gender ratio for SHH MB is similar to

WNT at 1:1 [4, 26]. Recent molecular studies suggest 21% of SHH-activated MBs contain an inactivating *TP53* mutation [36]. Thus, SHH tumors have been further subdivided into SHH-activated *TP53*-wildtype and SHH-activated *TP53*-mutant [36]. This mutation appears in patients between 5-18 years of age, the age group with the lowest frequency of SHH MBs [36]. Importantly, SHH *TP53*-mutant tumors also exhibit frequent metastatic dissemination and have a poor prognosis in comparison to the SHH *TP53*-wildtype [1, 2, 36]. As mentioned previously, SHH MB is the only subtype to exhibit desmoplastic/nodular histology and MBEN, but classic and LCA histology are found in this subtype as well [3, 26].

1.1.4 b) Genetic and molecular alterations

The SHH subtype exhibits driver mutations in the Sonic Hedgehog (SHH) signaling pathway. Individuals with Gorlin Syndrome are predisposed to developing SHH MB due to heterozygous germline mutations in the SHH receptor patched1 (*PTCH1),* or heterozygous germline nonsense mutations in the SHH pathway inhibitor suppressor of fused (*SUFU)* [1, 4, 26, 37]. Gorlin syndrome not only predisposes patients to MB but to other cancers, and can be characterized by macrocephaly and skeletal abnormalities [27]. Conversely, somatic mutations in *PTCH*, smoothened (*SMO)*, and *SUFU* in addition to amplifications of Glioma associated oncogene 1 (*GLI1)* and *GLI2* are responsible for sporadic SHH tumors [26]. Deletions in chromosome 9q are commonly seen in SHH-activated MB [2,26]. Accordingly, *PTCH* is located on chromosome 9q22 [2,26].

Briefly, SHH is a ligand for the transmembrane receptor PTCH, and when bound prevents PTCH from inhibiting SMO, a membrane G protein-coupled receptor [38, 39]. This results in the activation of GLI, a zinc finger transcription factor, by GSK3β as depicted in Figure 1.2 [39]. In the absence of SHH, GLI proteins, GLI1, GLI2, and GLI3 are sequestered by SUFU and

proteolytically cleaved in the cytosol (Figure 1.2). However, when GLI1 or GLI2 are phosphorylated they activate and translocate into the nucleus promoting the growth of granule cells in the cerebellum, also known as cerebellar granule neural precursors (CGNPs) [40]. Purkinje cells of the cerebellum secrete SHH during normal cerebellum development promoting *GLI1*, *CCND1*, *CCNE* and *MYC* gene expression and cell division (Figure 1.2) [39, 41]. This signal transduction demonstrates the critical role SHH signaling plays in regulating both stem cells and progenitors of the CNS [42].

Mutations in hedgehog-interacting protein (*HHIP)*, secreted frizzled related protein 1 (*SFRP1),* and focal amplifications *MYCN* are also found in SHH MBs. Moreover, C228T or C250T mutations in the *TERT* promoter are found in adult MB patients who exhibit a better prognosis [40]. Some tumors also exhibit chromosome 17p loss, 10q loss, gains of 3q, 20q and 21q [40]. Specifically, SHH *TP53*-mutants exhibit chromosomal tetraploidy, a classic feature of aggressive tumors [3].

1.1.4 c) Cell of origin

SHH-activated MBs are believed to originate from cells in the external granule layer (EGL) of the developing cerebellum [1, 4, 43]. During neural development, the rhombic lip generates the CGNPs of the EGL [44]. These CGNPs proliferate and migrate inward to establish the internal granular layer (IGL) during later stages of cerebellar development [44]. SHH signaling decreases as CGNPs proliferate, differentiate, and migrate into the IGL from the EGL [44]. SHH-activated tumors stain positively for classic EGL markers, ZIC1 and MATH1, but not IGL markers [45]. In 1997, Goodrich *et al.* demonstrated that heterozygous *Ptch1*$^{+/-}$ mouse models generated pre-neoplastic deposits in the cerebellum that resembled human SHH-activated MBs, due to overactivated SHH signaling [46]. Yang *et al.* have also shown that tumor deposits can form from

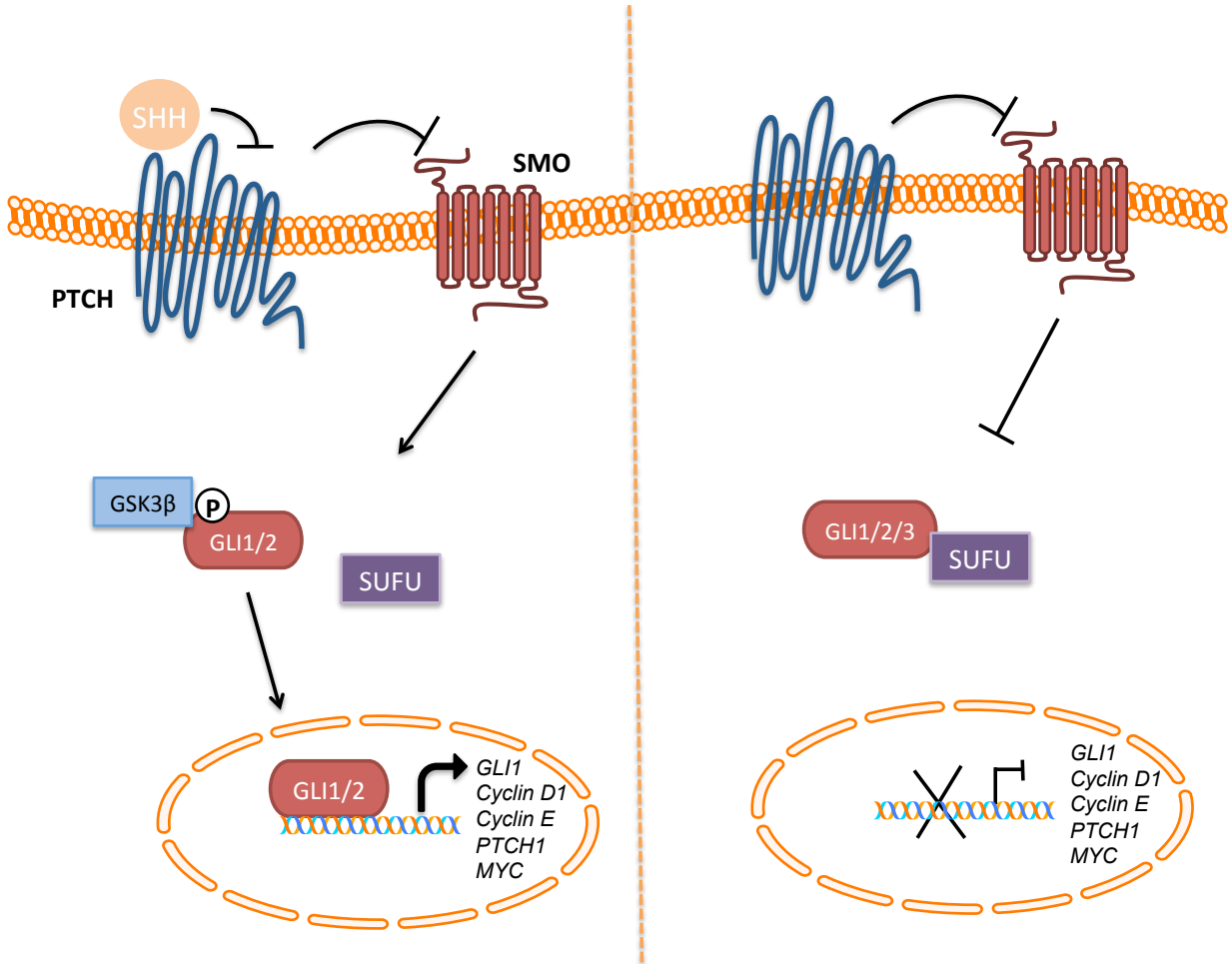

Figure 1.2: Normal SHH signaling.
In the presence of SHH the PTCH transmembrane receptor is inhibited from negatively regulating the downstream SHH signaling pathway. The G protein-coupled receptor, SMO, then is able to signal GLI proteins to translocate into the nucleus and turn on the expression of *GLI1, Cyclin D1*, *Cyclin E, PTCH1,* and *MYC*. In the absence of SHH, PTCH inhibits SMO from activating the intracellular complex, resulting in no gene expression. Adapted from Roussel *et al*., 2011.

both CGNPs and neural stem cells (NSCs) with *Ptch1* knockout, but only after the cells have commitment to a granule cell lineage [47]. Moreover, human SHH tumors have been shown to express markers of post-mitotic granule neurons, such as feminizing locus on X-3 (NeuN) and gamma- aminobutyric acid type A alpha6 subunit (GABRA6) [47]. Collectively, these studies suggest granule cells with SHH pathway mutations can predispose the developing cerebellum to SHH MB tumor initiation and/or progression.

1.1.4 d) Treatment options

Interestingly, SHH MB patients who undergo standard treatment demonstrate lower brain processing speed immediately after treatment [42] but uniquely exhibit less motor deficits post treatment despite tumors arising in the cerebellar hemispheres [48, 49]. Major research efforts have been made towards targeted SHH pathway therapies in hopes of improving treatment outcomes in SHH patients. For example, cyclopamine and vismodegib (GDC-0449) are two small molecule SHH pathway inhibitors that bind to SMO and prevent GLI activity [41, 50]. Cyclopamine has a relatively low binding affinity for SMO and patients have demonstrated treatment recurrence due to the resistance of prominin1 ($CD133^{+}$) stem cells to therapy [41]. Vismodegib initially demonstrated some therapeutic benefit however, patients in clinical trials also relapsed as a result of downstream *de novo* SHH mutations [50, 51]. Recent preclinical studies using Sonidegib (LDE225), a novel selective SMO inhibitor, demonstrated inhibition of *GLI1* and MB tumor regression when administered orally in $Ptch^{+/-}$ $p53^{-/-}$ and $Ptch^{+/-}$ $Hic1^{+/-}$ mice (Hypermethylated in Cancer-1 *(Hic1)* a frequent target of epigenetic gene silencing) [52].

In addition to mutations in the SHH signaling pathway, SHH tumors exhibit upregulation of signaling pathways such as, NOTCH and P13K. Accordingly, Hallahan *et al.* have demonstrated that γ-secretase, a NOTCH signaling inhibitor, decreases SHH MB cell

proliferation and increases apoptosis in xenograft models [53]. Other studies showed that loss of phosphatase and tensin homolog (*PTEN*) expression dramatically increases tumor onset in SHH mouse models and increases PI3K signaling [54]. To evaluate whether PI3K inhibition would improve vismodegib outcome in these SHH mouse models, a PI3K/mTOR inhibitor, GNE-317, was tested in combination with vismodegib and indeed demonstrated additional tumor regression [54]. Although some treatment options have increased overall survival, MB heterogeneity and treatment resistance continues to be an obstacle, suggesting combination therapies will have to be evaluated further to combat the disease.

1.1.5 GROUP 3

1.1.5 a) Incidence and demographics

The Group 3 subtype accounts for ~25% of MB cases and exhibits the worst prognosis with a ~50% 5-year survival rate [21, 26]. Metastatic dissemination is observed in 40-50% Group 3 MBs at the time of diagnosis and occurs in males more often than females (2:1) [25, 26]. Moreover, Group 3 MBs are found most frequently in children (3-16 years of age), and less frequently in infants [1]. Children have a 5-year survival rate of 58% and a 10-year survival rate of 50% [55], while infants with Group 3 MB have the worst prognosis with a 45% and 39% 5 and 10-year survival rate, respectively [26, 27, 55]. A high incidence of classic and LCA histology is seen in Group 3 MB patients [1, 3].

1.1.5 b) Genetic and molecular alterations

Advances in microarray and genomic sequencing technologies have enabled researchers to further characterized Group 3 and 4 MBs. Some chromosomal aberrations seen in Group 3 patients include, 17p deletion, gain of chromosome 1q, loss of chromosome 5q and 10q [21]. Cytogenetic isochromosome 17q occurs in 26% of Group 3 MB cases and is the most frequently

observed chromosomal aberration [21]. Molecular profiling has also demonstrated that the transcription factor, *MYC,* is amplified in ~15% of patients as a result of fusion between the promoter PVT1 and the second exon of *MYC* [40]. Moreover, studies have revealed that *MYC* status indicates a high risk of metastatic dissemination. Orthodenticle homeobox 2 (*OTX2)* is also overexpressed and/or amplified in 80% of Group 3 and 4 MB cases [26, 56, 57]. Specifically, *OTX2* amplifications occur between 7-21% of Group 3 cases and are mutually exclusive from *MYC* amplifications [3, 29, 56, 58]. Studies have shown that a number of polycomb gene promoters in Group 3 MB are maintained in a bivalent state by OTX2 mediated H3K27me3 maintenance [59]. Accordingly, mutations in enhancer zest homolog 2 (*EZH2)*, lysine demethylase 6A (*KDM6A*), chromodomain-helicase-DNA binding protein 7 *(CHD7)*, zinc fingers MYM type 3 (*ZMYM3)*, SWI/SNF-related, Matrix Associated, Actin Dependent Regulator Of Chromatin, Subfamily A, Member 4 (*SMARCA4)* and mixed lineage leukaemia 2 (*MLL3)* are commonly observed in Group 3 MB, in addition to chromatin disruptions around *OTX2*, *MYC* and *MYCN* [60, 61]. Lin *et al*. also reported frequent amplifications of TGFβ signaling genes in Group 3 MB patient samples [70]. Furthermore, genomic enhancer region rearrangements of proto-oncogenes, growth factor independent 1 (*GFI1)* and *GFI1B,* are highly prevalent in Group 3 MB [21, 61, 62]. These results suggest that dysregulation of the epigenetic landscape could be a critical contributor to MB pathogenesis.

Although Group 3 and 4 MB have many similarities, they do exhibit specific differences. For example, Group 3 MBs exhibit a phototransduction and GABAergic transcriptional profile while Group 4 does not [26, 40]. Previous studies have also suggested that natriuretic peptide receptor 3 (NPR3) could be a Group 3 immunohistochemistry marker [1, 4]; however, its functional relevance remains to be studied. Interestingly, tetraploidy is observed in 40-50% of Group 3 and

4 MBs [63]. Despite advances in transcriptional profiling, little is known about the functional relevance of these genomic aberrations; thus, a better understanding of the mechanisms contributing to Group 3 MB initiation, progression and metastasis continues to be integral.

1.1.5 c) Cell of origin

Despite limited knowledge of Group 3 MB tumor progression, studies suggested neural stem cells and/or CGNPs of the EGL are the cells of origin of *MYC* amplified Group 3 MBs. Orthotropic transplantation of cerebellar stem cells (Prominin1/CD133^{+}, Lineage^{-}) coupled with *MYC* overexpression and *TP53* inactivation generated tumors with similar molecular profiles and pathology to human Group 3 MB [64]. Kawauchi *et al*. also demonstrated that isolated atonal homologue 1 (*Atoh)-GFP* CGNPs from postnatal *Trp53*$^{-/-}$ mice transduced with *Myc* could generate aggressive tumor deposits with LCA histology [65, 27]. These tumor cells had similar gene expression profiles to embryonic stem cells supporting the existing evidence suggesting that Group 3 MB arise from neural stem-like cells or de-differentiated CGNPs. Furthermore, the same group recently showed that different cerebellar progenitors with *Myc* overexpression and *Trp53* inactivation were susceptible to transformation into Group 3-like MBs rather than a specific cell [66]. These models are informative; however, *TP53* mutations are rare in human Group 3 tumors, yet metastasis is frequently observed. Thus, better animal models recapitulating Group 3 tumor initiation and CSF dissemination are still needed.

Of note, since the oncogene *OTX2* is frequently overexpressed and/or amplified in Group 3 and 4 MB, Wortham and colleagues set out to produce a conditional *Otx2* overexpressing murine model to explore the oncogenic effects of *Otx2* in the hindbrain [67]. Interestingly they observed an accumulation of cerebellar white matter cells postnatal; however, *Otx2* overexpression was not able to fully transform the cells to generate tumor deposits [67]. Thus, other

genes are likely involved in Group 3 MB transformation and initiation, and will need to be explored in conjunction with OTX2.

1.1.6 GROUP 4

1.1.6 a) Incidence and demographics

Group 4 MBs account for 35% of MB cases and exhibit an intermediate prognosis similar to SHH MB [21, 26]. The metastatic frequency of Group 4 MBs is between 30-40% and the gender distribution is 2:1 between males and females [27]. Group 4 MBs account for 50% of MBs observed in children [27] and 25 % of MBs in adults [21], and commonly carry a classic histology [1, 3].

1.1.6 b) Genetic and molecular alterations

Isochromosome 17q is found in 60-80% of Group 4 MBs and 17q chromosome deletion occurs in 73% of cases [21, 27]. Group 4 subtypes exhibit *MYCN* amplifications as opposed to *MYC*. However, *OTX2* amplification and/or overexpression is commonly observed in Group 3 and Group 4 MB, while forkhead box G1 (*FOXG1B)* and cyclin-dependent kinase 6 (*CDK6*) amplification are commonly observed in only Group 4 tumors [26, 68]. The most common genetic mutation occurs in *KDM6A* [60]. *KDM6A* is expressed on chromosome X and is responsible for the demethylation of H3K27me3 marks. Interestingly, the loss of one X chromosome copy is seen in 80% of Group 4 MB females [60]. In addition*, ZMYM3* is found on chromosome X and is often mutated [61].

Large scale transcriptome studies have revealed a Group 4 MB gene signature which includes expression of semaphorin pathway genes, cyclic adenosine monophosphate, G protein–coupled receptors, and β-adrenergic signaling genes [1]. Published data also suggests potassium voltage-gated channel subfamily A member 1 (KCNA1) could act as an immunohistochemical marker for Group 4 tumors [4,61].

1.1.6 c) Cell of origin

There are no highly reliable murine models for Group 4 tumors to date; however, neural stem cells have recently been suggested as the cell of origin. It has been reported that upper rhombic lip progenitor transcription factor markers lim homeobox transcription factor 1 alpha (LMX1A), eomesdermin (EOMES), and lim homeobox 2 (LHX2) are exclusively expressed in Group 4 MBs [69]. LMX1A is essential in upper rhombic lip cell fate specification and demonstrates a master regulatory role in the transcriptional profile of Group 4 MB [69]. As a result, research groups have begun to develop Group 4 mouse models from upper rhombic lip progenitors. Swartling and colleagues generated transgenic mice expressing *MYCN* and a firefly luciferase gene in cerebellar and brainstem neural stem cells using a tetracyclin inducible system [70, 71]. These data demonstrated that *MYCN* transduced P0 cerebellar NSCs and E14 lower rhombic lip NSCs generated tumors with LCA histology similar to human Group 4 MB [71]. Despite this, our understanding of the cell of origin for Group 4 MB remains poor.

1.1.6 d) Treatment options for Group 3 and 4 MB

The lack of Group 3 and 4 MB murine models has made it difficult to develop therapies targeted at the aggressive MB subtypes that frequently exhibit metastatic dissemination at the time of diagnoses. However, Morfouace *et al*. recently demonstrated that pemetrexed and gemcitabine, two FDA approved drugs, have antiproliferative effects in Group 3 patient derived xenografts (PDX) *in vivo* [24]. Pemetrexed is a multitargeted antifolate that disrupts DNA synthesis, while gemcitabine creates single strand breaks, disrupts DNA synthesis and induces apoptosis [24]. Both are in phase II clinical trials for patients with non-small cell lung cancer [72]. Importantly, mice with SHH MB which were administered the two drugs did not respond to the therapy suggesting the drugs have *MYC*-driven specificity [24]. Bromodomain and extraterminal

domain family (BET) proteins that specifically suppress MYC-related transcriptional activity have also recently shown success in preclinical models targeting *MYC*-driven MB [21]. However, since OTX2 is amplified and overexpressed in 80% of Group 3 and 4 MBs, it and its downstream effectors are attractive targets for treatment. In 2010, all-*trans* retinoic acid (ATRA) was tested on OTX2 positive MB cells and was able to decrease *OTX2* expression and reduce cell proliferation while increasing neural differentiation; however cell lines quickly became resistant to the therapy [73]. Moreover, subsequent testing with ATRA and other retinoic acids was ineffective in stem cell-enriched tumorsphere conditions and in intracranial transplant models [73].

The above successes and subsequent failures underscore the need for more specialized MB treatments. MB is a disease of dysregulated cerebellar development with a stem/progenitor cell of origin regardless of subtype. In order to find novel therapies, we need to have a good understanding of stem/progenitor cell regulation during normal development. Thus, we turn to the normal cerebellum for answers.

1.2.0 CEREBELLAR DEVELOPMENT AND MOLECULAR REGULATION OF STEM/ PROGENITOR CELLS

1.2.1 Cerebellum structure and function

The cerebellum accounts for 10% of the brains volume and contains about 80% of the brain's total neurons when fully developed [44, 74]. It has long been known for its control over fine movements and coordination of the body [75], interpreting ascending signals, and commanding descending signals to make body movements more adaptive and accurate. However, new evidence suggests the cerebellum can control higher cognitive functions including attention, language, and emotions [75-77] as damage to the cerebellum in premature children also predicts long-term cognitive impairments [78, 79]. The cerebellum is composed of two hemispheres and a

central vermis with extensive lobulations and foliations [80, 81]. It has an outer cerebellar gray matter layer, also known as the cerebellar cortex, and an inner layer of white matter, containing the cerebellar nuclei within [80, 81]. The gray matter is further divided into 3 layers of neural cells including the inner most granule layer that contains neuronal Golgi cells, unipolar brush cells, Lugaro cells and 5 x 10^{10} granule cells [78]. The granule layer holds the only glutamatergic neurons of the cerebellum [44, 82, 83]. The middle Purkinje layer contains the Purkinje cells, Bergmann glia and candelabrum cells [78]. Purkinje cells are the main GABAergic neurons of the cerebellum and are amongst of the largest neurons in the CNS with extensive dendritic branching [78, 84]. While the outer most molecular layer, contains the dendritic trees of the Purkinje cells, along with the inhibitory stellate and basket cells [78]. Briefly, the granule cells receive input signals from neurons outside the cerebellum that project onto the Purkinje cell dendrites sending inhibitory signals to the deep cerebellar nuclei [78, 66]. Output signals are further projected through the superior cerebellar peduncles on to the vestibular and red nuclei to coordinate motor function [78, 66]. Many of the clinical symptoms MB patients present with are a result of impaired neural connectivity between the cerebellum, cortex, and peripheral nervous system.

1.2.2 Human cerebellum development

Initial fate mapping experiments have established how morphogens, transcription factors, and signaling molecules control the specification of the central nervous system (CNS) and its neuroepithelial regions [81, 85]. The forebrain (prosencephalon), midbrain (mesencephalon), and hindbrain (rhomobencephalon) of the CNS form from the anterior portion of the neural tube and can be distinguished within 28 days after fertilization [86]. At this time, the “anlage” or cerebellar bulge begins to form as well [78, 87]. The cerebellum develops from dorsal rhomobomere 1 [78]. Specifically, the two hemispheres of the cerebellum originate from the isthmus and

rhomobomere 1, while the vermis from the roof plate of the isthmus and rhomobomere 1, and the alar plate of the isthmus (Figure 1.3) [78, 88]. The expression of gastrulation brain homeobox 2 *(Gbx2)* and fibroblast growth factor 8 (*Fgf8*) in rhomobomere 1 inhibit the expression of *Otx2* and homeobox A2 (*Hoxa2)* in the hindbrain and direct the development of the cerebellar primordium [78, 89, 80]. Both GBX2 and OTX2 continue operating antagonistically against each other while generating the midbrain-hindbrain boundary [78], also known as the isthmic organizer or isthmus [78, 89]. The expression of *Fgf8,* Engrailed 1 *(En1), En2, Wnt1, Pax2*, Iroquas (*Irxs), Shh*, and transforming growth factor beta *(Tgf-β)* in murine models have been shown to further guide neurogenesis and cell- type specification in the midbrain and hindbrain (Figure 1.4) [90,81, 91-93]. Eventually both *Otx2* and *Gbx2* expression disappears in the isthmus [78, 81, 89]. Studies also suggest that FGF8 is necessary for vermis development since in the absence of *Fgf8* expression, *Otx2* increases and inhibits vermis formation [81].

The progenitor cells, which guide cerebellum development, originate from the ventricular zone (primary neurogenic zone) lining the fourth ventricle and the rostral rhombic lip (secondary neurogenic zone) [94]. Briefly, at about E10.5, neural progenitors begin to migrate from the ventricular zone of the developing brain to the future dentate nucleus of the cerebellar nuclei generating the Purkinje neurons of the gray matter along the way [44, 78]. Next, the upper rhombic lip progenitors expressing *Atoh/Math* extend rostral over the developing cerebellar bulge [81]. Much of this migration is guided by axon guidance molecules such as, ephrin receptor B4 (ERBB4), UNC5H, and netrin which will be discussed in more detail in the thesis discussion [96]. This forms the EGL [81]. The cerebellar anlages then fuse at the midline and begin developing primary fissures, while *Atoh1*$^{+}$ CGNP cells in the EGL amplify in response to SHH release by the Purkinje neurons (Figure 1.5) [42, 94]. The EGL is quiet stable until 2 months postnatal at which

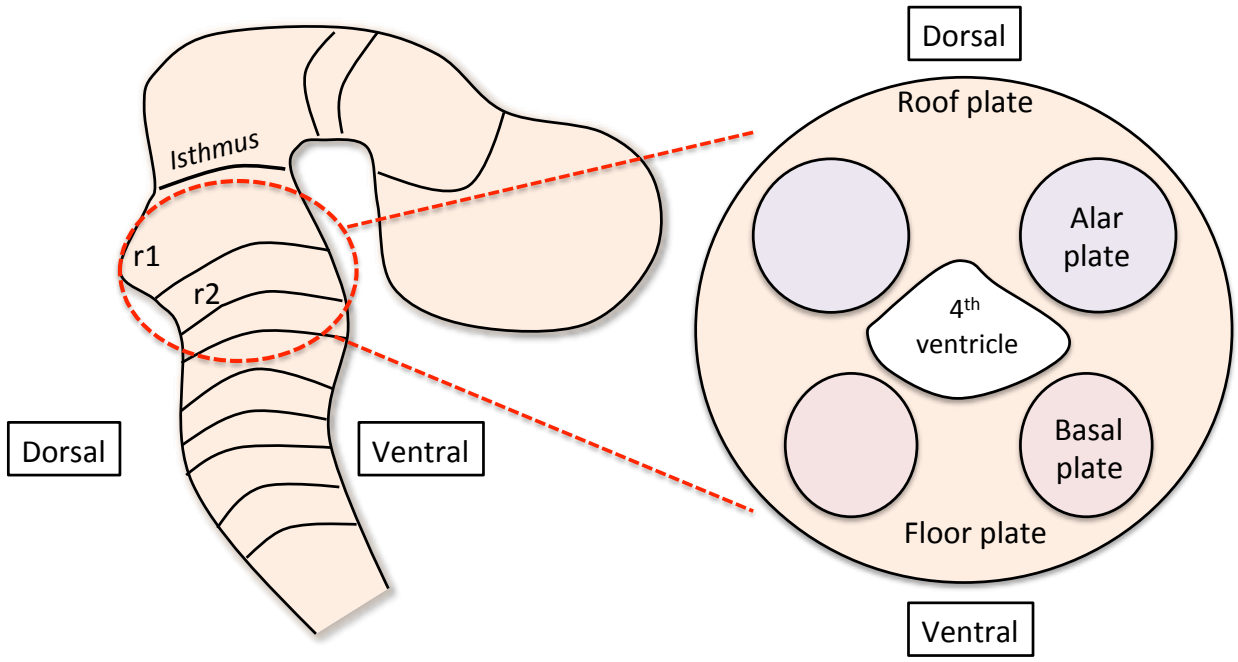

Figure 1.3: Nervous system and cerebellum development.
Progenitors from the ventricular zone and rhombic lip generate the cell lineages of the cerebellum. The progenitors move from the dorsal end of the isthmus and rhombomere 1 along the alar plate and roof plate during development. Adapted from Bally-Cuif *et al.,* 1999 [95].

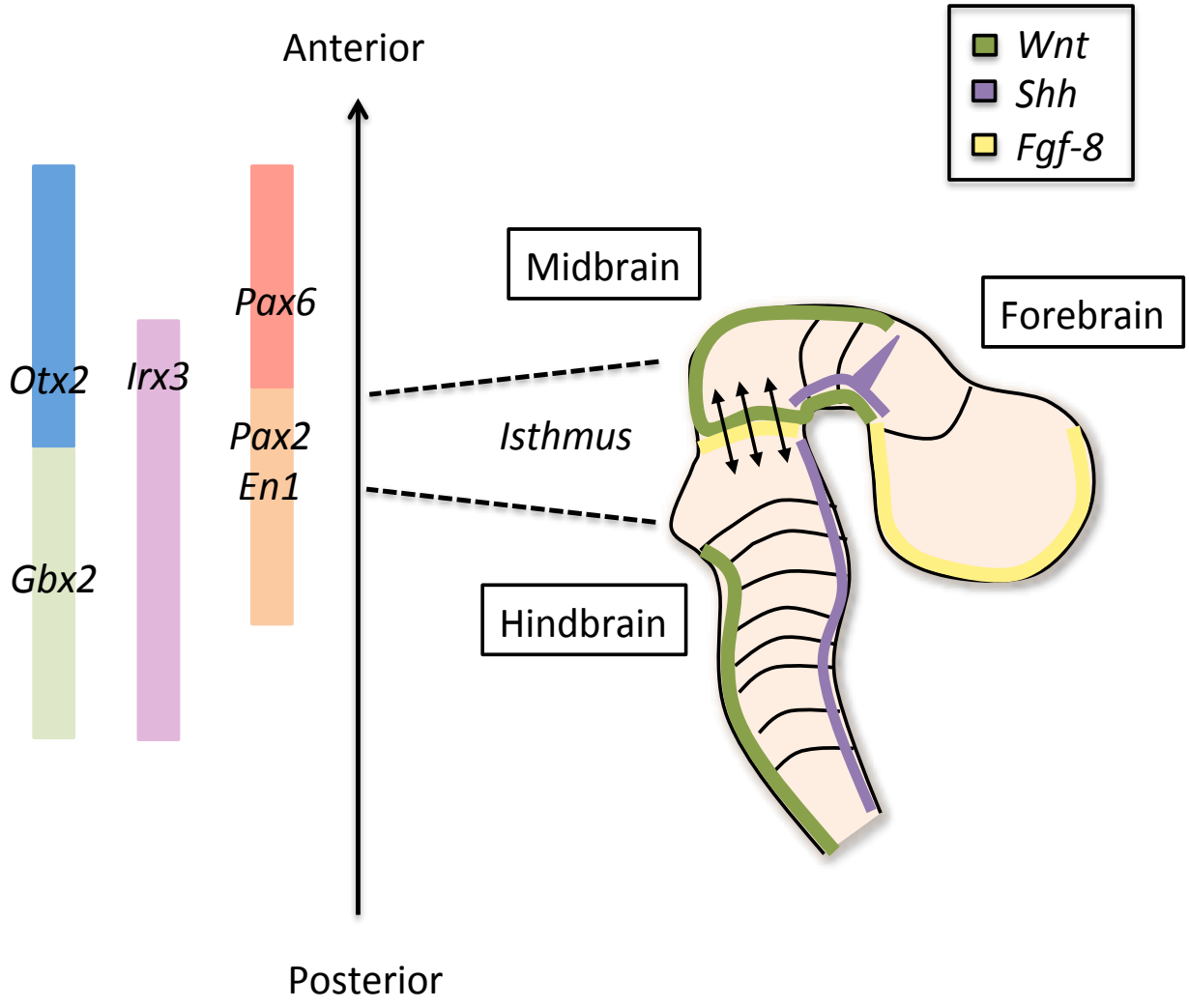

Figure 1.4: Midbrain-Hindbrain boundary.
The isthmic organizer of the midbrain-hindbrain boundary and the expression of genes above and below the boundary that drive the spatial organization, and cell lineage specification of the cerebellum. *Otx2* and *Gbx2* expression leads the creation of the isthmic organizer. Adapted from Carlson, 2014.

time the CGNPs exit the cell cycle, differentiate and migrate inward towards the IGL along the processes of the Bergmann glia (Figure 1.5) [44, 97]. During this time, Purkinje neurons begin to grow more rapidly until about 2 years postnatal [44, 98, 99].

Cerebellum development and gene expression profiling have provided insight towards which cerebellar progenitors initiate MB. Originally, MB tumors were believed to originate from cells according to their anatomical region. In recent years, studies have demonstrated that the cell of origin is subtype specific. For instance, experiments with conditional overexpression of *Shh* in either CGNP cells expressing *Math* or neural stem cells expressing *Gfap* demonstrated tumor initiating capacity only once committed to the granule cell lineage, concluding that transformation within CGNPs was a determinant to SHH-activated initiation [100]. Moreover, WNT MBs are known to infiltrate the dorsal brainstem and studies show that *WNT1* is expressed during the expansion of cerebellar stem cells in the ventricular zone and rhombic lip of the developing nervous system [101]. Accordingly, Gibson *et al.* determined lower rhombic lip progenitors with *Ctnnb1* mutations accompanied by a *Trp53* mutation could initiate WNT-like MB tumors in the dorsal brain stem [5, 101, 102]. These data, underscore the idea that the knowledge of normal cerebellum development can be exploited for the discovery of MB subtype-specific cells of origin.

Similarly, the critical roles for OTX2 during early embryogenesis and cerebella development have ignited interest into studying the underlying functions of this transcription factor in regulating MB pathogenesis. In particular, its overexpression and/or amplification in Group 3 and 4 MB tumors is of high interest and needs to be more thoroughly elucidated, specifically in stem cell conditions. This is not only due to the MB stem/progenitor cells of origin but also the fact that these primitive cells are major contributions to treatment resistance,

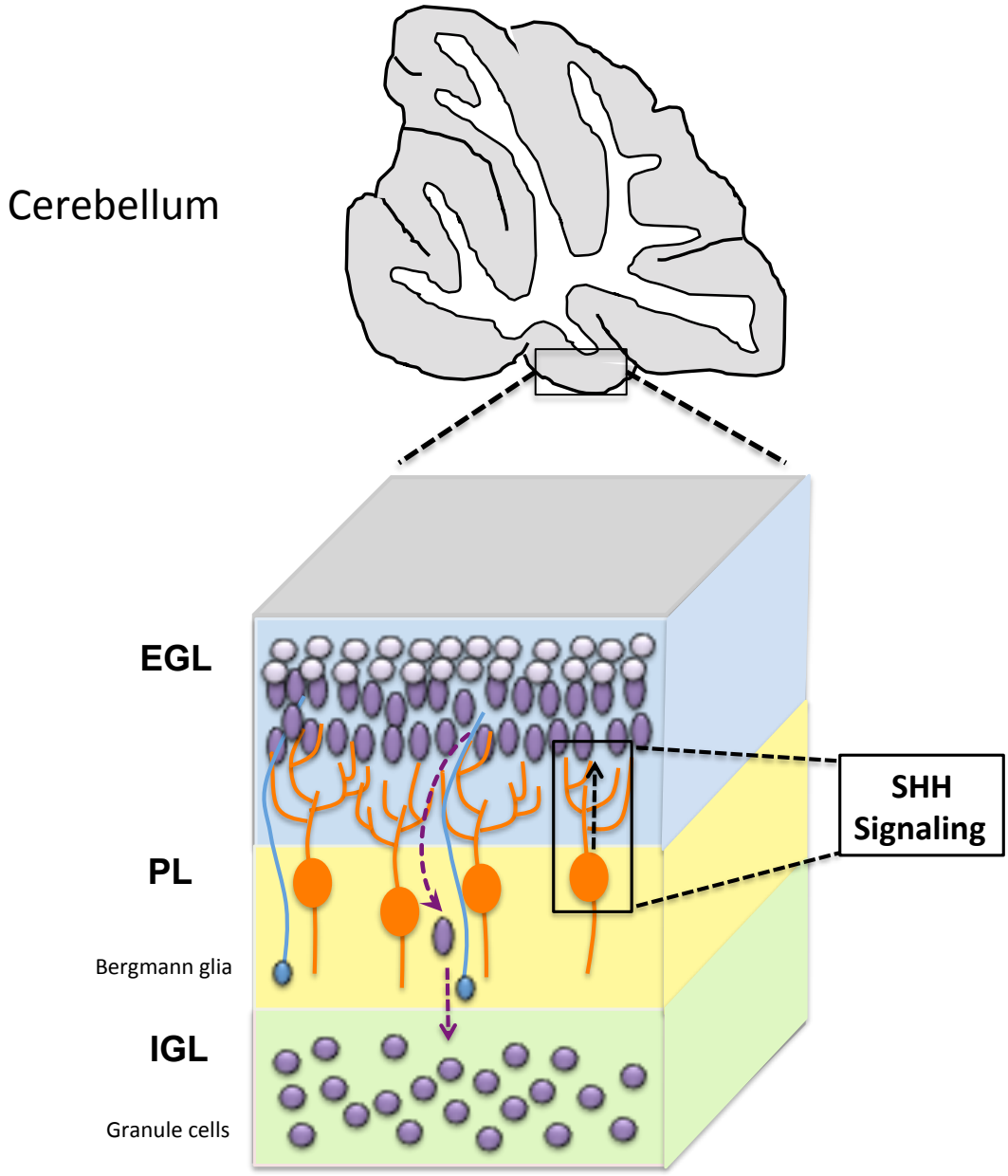

Figure 1.5: The gray matter of the cerebellum during development.
The proliferation and migration of cerebellar granule neural precursor cells in the EGL into the IGL along Bergmann glia signaled by SHH secreted by the Purkinje cells in the middle layer. EGL: external granule layer, PL: Purkinje layer, IGL: internal granule layer. Adapted from Butts *et al*., 2014.

recurrence and ultimately poor prognosis. As my thesis focuses on the role of OTX2 in Group 3 and Group 4 MB, I will first extensively describe the specific roles of this transcription factor during normal neurodevelopment.

1.3.0 OTX2

1.3.1 OTX2 and its role in the developing nervous system.

OTX2 is a homeodomain bicoid transcription factor that has multiple roles in human embryo, brain and eye development [56]. Homeodomain transcription factors are responsible for anterior-posterior body axis patterning. The *OTX2* gene is encoded on human chromosome 14q22.3 and is composed of 5 exons, of which the first 2 are noncoding. *OTX2* undergoes alternative splicing events that result in 2 isoforms; one isoform being 297 (NP_068374.1) amino acids long and the other more abundant form being 289 (NP_758840.1) amino acids long. Of note, the rodent OTX2 protein shares identical amino acid sequence to human OTX2 [10, 103], and spatial-temporal expression of *Otx2* in the rodent fetal brain is in accordance with human *OTX2* expression patterns [104]. OTX2 binds with high affinity to the DNA sequence: 5'-TAATCC-3' through its homeodomain and turns target gene expression on or off (Figure 1.6) [10, 105, 106]. Specifically, it can act as a repressor by binding to Groucho co-repressor proteins via its conserved SIWSPA motif [10, 107].

Otx2 is initially expressed across the entire murine blastula but becomes restricted to the rostral end of the fetus during gastrulation [10]. As gastrulation proceeds, OTX2 regulates forebrain, midbrain and rostral hindbrain formation [105, 108]. Studies have demonstrated that *Otx2* expression in the early stages of anterior mouse brain development guides endodermal cells to the anterior visceral endoderm (AVE) [89, 109]. As previously mentioned, *Otx2* progressively becomes limited to the anterior plate while the expression of *Gbx2* becomes limited to the

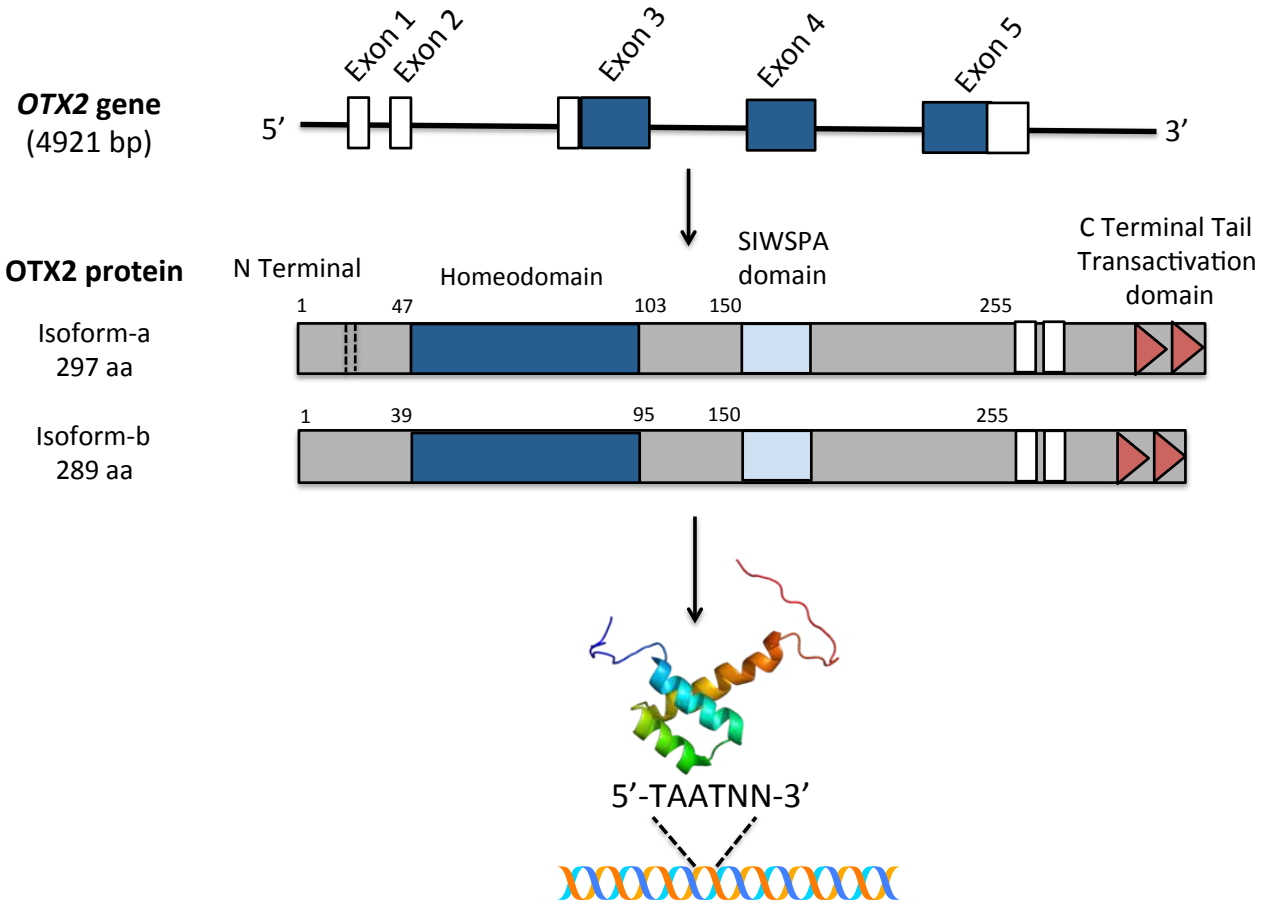

Figure 1.6: The OTX2 gene and protein.
The *OTX2* gene is composed of 5 exons, the first 2 exons being noncoding. There are 5 transcriptional splice variants that encode two protein isoforms: isoform-a and isoform-b. OTX2 binds the conserved DNA sequence: YTAATNN or TAATCC. The *OTX2* gene structure is adapted from Beby *et al.*, 2013 and protein structure is adapted from https://en.wikipedia.org/wiki/Orthodenticle_homeobox_2.

posterior neural plate [89]. The anterior neural plate generates the forebrain and midbrain, while the posterior plate generates the hindbrain and spinal cord [89]. *Wnt1* is expressed in the isthmic organizer of the midbrain-hindbrain boundary along with *Otx2*, while *Fgf8* is expressed in the hindbrain along with *Gbx* [89]. OTX2 is integral for the positioning of the isthmic organizer, *Otx2* inactivation studies reveal anteriorly shifted isthmic organizers [105], while caudal *Otx2* knock-in studies demonstrated more posteriorly positioned isthmus organizers and caudally extended inferior colliculi [89]. Moreover, conditional deletion of *Otx2* throughout the dorsal midbrain reveals disruptions in the differentiation of midbrain cell types and cerebellar development in the dorsal midbrain [110]. Complete deletion of *Otx2* is embryonic lethal due to the loss of the rostral neuroectoderm and is known as the "headless phenotype"; whereas, *Otx2* heterozygotes display various craniofacial abnormalities as mentioned above [56, 111]. These data demonstrate the critical role *Otx2* plays during head development, especially when guiding the AVE [56].

Later in human cerebellar development, *OTX2* is expressed in the progenitor cells of the EGL but is not detected post-natally similar to findings in the rodent cerebellum [112, 113]. This supports MBs embryonic origin and provides further support for OTX2 as an attractive therapeutic target. Specifically, expression of OTX2 is present in EGL precursors of 23+ week human fetal cerebella, while at 26 weeks, OTX2 is detected in cells of the IGL, and in the cytoplasm of dentate nuclei neurons and Purkinje cells [112]. However, in the postnatal cerebellum, OTX2 levels are lost as expression is restricted to choroid plexus, pineal gland and retinal pigment epithelium in adult tissues [112]. Thus, alongside its function in brain patterning, OTX2 studies have demonstrated that the transcription factor is also required for dopaminergic neurogenesis, glutamatergic differentiation, choroid plexus, pineal gland, and retinal photoreceptor development, each of which will be discussed in more detail below.

1.3.2 OTX2 and dopaminergic neurons

During neural progenitor specification, transcription factors such as OTX2 are, in part, responsible for progenitor cell fate both in the anterior-posterior and dorsal-ventral direction of nervous system development. Mesencephalic dopaminergic progenitors rely not only on *Otx2* but morphogens such as, FGF8, SHH, and WNT1 to signal proliferation and/or dopaminergic differentiation [114, 115]. Dose-dependent *Otx2* overexpression in the ventral mesencephalon has been shown to induce an expansion of mesencephalic dopaminergic progenitors and neurons in the anterior-posterior direction [115]. Embryos overexpressing *Otx2* in this study exhibited increases in proliferation, Ki67 detection and *CCND1* expression [115], while $En1^{cre/+}$; $Otx2^{flox/flox}$ mutants in other studies displayed decreased expression of *Shh*, NK6 homeobox 1 (*Nkx6.)1* and *Nkx2.2* alongside reduced numbers of dopaminergic progenitors in the mesencephalon [107]. Similarly, in addition to increased cell proliferation, Omodei *et al.* observed increases in *Wnt1* expression with *Otx2* overexpression [107], while with a lack of *Otx2* expression decreased proliferation of sex determining region Y-box 2 ($SOX2^+$) mesencephalic dopaminergic progenitors and defected nuclear receptor related-1 ($NURR^+$) post-mitotic mesencephalic dopaminergic precursor differentiation were observed [115].

After progenitor neurogenesis in the midbrain, OTX2 demonstrates a role in neuronal axon guidance. Axon tracts have been shown to develop within zones of high *Otx2* expression in the zona limitans intrathalamica (ZLI) in mouse forebrains and midbrains [116]. Fibroblast cells transfected with *Otx2* under strong promoters have even shown to produce more neurite growths compared to controls [116]. In *Drosophila,* altered *Otd* (homolog of vertebrate *Otx2* gene) expression in the developing embryonic brain can generate defects in axonal pathways along the ventral midline [117]. Accordingly, reduced *Otx2* expression induces a selective loss of axonal

projections in post-mitotic dopaminergic neurons of the dorsal midbrain [114]. Chung and colleagues have also revealed differences in *Otx2* expression between A9 and A10 dopaminergic neurons and their axonal projections [114]. In fact, overexpression of *Otx2* in A9 dopaminergic neurons increases the expression of A10 dopaminergic axon guidance cues, such as neuropilin 1 (*Nrp1), Nrp2*, and *Slit2*, while *Otx2* knockdown (KD) decreases their gene expression [114]. *Otx2* conditional knock-out mice, $En1^{cre/+};Otx2^{flox/flox}$, also lose A10 dopaminergic projections while A9 dopaminergic projections are spared of any defects in the dorsolateral striatum [114].

1.3.4 OTX2 and glutamatergic progenitor of the thalamus

Glutamatergic progenitors arise from the dorsal telencephalon and thalamus of the human brain [118]. Studies suggest a genetic program suppresses GABAergic differentiation during specification of glutamatergic progenitors. In fact, conditional *Otx2* knockout mice exhibit an increase in GABAergic differentiation and a loss of glutamatergic differentiation in the thalamus [119]. Puelles *et al*. have observed that in the absence of *Otx2,* GABAergic fate increases alongside achaete-scute family BHLH transcription factor 1 (*Mash1)* expression, while Neurogenin 2 (*Ngn2)* expression is repressed [119] concomitant with activation of the GABAergic transcription factors *Pax3, Pax7*, and *Lhx1* [119]. Analysis of cell cycle activity revealed increases in the frequency of cells in the S and M phases in $OTX2^-$ progenitors. Collectively, these data underscore the notion that the regulatory role of OTX2 is both temporally and cell-type dependent.

1.3.5 OTX2 choroid plexus

At later embryonic stages, OTX2 plays a critical role in choroid plexus development. Conditional *Otx2* knockout studies demonstrate complete and partial dependence of *Otx2* early and late in the development of each choroid plexus [120]. $Gdf7\text{-}Cre/Otx2^{flx/flx}$ mice exhibit

decreased hindbrain choroid plexus development and a 2-fold increase in annexin V staining in choroid plexus cells [120]. Johansson *et al*. have also observed altered CSF composition in the choroid plexus and increased WNT4 and transglutaminase 2 (TGM2, a Wnt modulator) levels in the CSF due to *Otx2* deletion [120]. Transcript analysis revealed increases in target WNT signaling genes such as *Cyclin D1*, with no changes in *Shh, Fgf* or *Tgf-β* pathway genes [120]. Accordingly, these data suggests OTX2 regulates not only proliferation and development of the choroid plexus, but the composition of signaling molecules in the CSF as well.

1.3.6 OTX2 and its role in pineal gland and eye development

Although *Otx2* is highly expressed in the developing brain, it becomes restricted to retinal photoreceptors and pinealocytes in the adult brain [121]. The optic vesicles in the eye contain photoreceptors, bipolar cells, amacrine cells, and horizontal cells [122]. In 2003, Nishida *et al*. demonstrated how both retinal photoreceptor cells and pinealocytes were dependent on *Otx2* expression during development [121]. *Otx2* conditional knockout mice revealed an absence of rhodopsin+ photoreceptor cells and an increase in Pax6+ amacrine cells [123]. Loss of bipolar cells and horizontal cells in the retina, and pinealocytes in the pineal gland was also observed [123]. OTX2 induced cone-rod homeobox (*Crx*) gene expression and accordingly supported previous studies which demonstrate CRX is required for differentiation and maturation of photoreceptor cells and the pineal gland [121, 124, 125, 109]. Conversely, retroviral gene transfer resulted in increased photoreceptor cell fate from retinal progenitors [123]. Thus, it is not surprising that *OTX2* mutations in humans are associated with micropthalmia (small eye) and anophthalmia (absence of an eye) [121].

Beyond retinal development, *Otx2* is expressed in the retinal pigment epithelium (RPE) where it represses *Ffg8* and *Sox2* expression from the neural retina for RPE homeostasis [122]. *Otx2*

ablation studies in the retina (*Otx2*$^{+/-}$; *Crx*$^{-/-}$) reveal dramatic photoreceptor degeneration and decreased bipolar cell maturation [126], suggesting OTX2 is required for both photoreceptor and bipolar cell maturation and maintenance. Fossat *et al.* in fact demonstrated that OTX2 is required for maintenance of photoreceptor and bipolar cells through life [127-129]. Demonstrating once again that OTX2s role in the nervous system is cell-type specific.

1.3.7 OTX2 and its role in medulloblastoma

Due to advances in digital karyotyping and gene expression analysis, *OTX2* amplification and/or overexpression is now associated with Group 3 and Group 4 MB classification. In 2005, Boon *et al.* found that 8 of 42 primary tumors examined exhibited *OTX2* copy number amplification. In addition, they found that *OTX2* expression was higher in primary tumor tissue than in normal cerebellar tissue [58]. Adamson and colleagues went on to confirm these trends in 201 primary tumors and 11 MB cell lines revealing single gene focal gains of *OTX2* in 21% of tumors and *OTX2* overexpression in 74% of primary tumors [56]. The authors also associated *OTX2* amplifications with double minute chromosomal gains [56]. Notably, high *OTX2* expressing MB tumors are more commonly located in the vermis of the cerebellum, associated with worse patient outcomes as well as classic or LCA histology, all features of Group 3 and 4 MB [112].

This characteristic amplification and/or overexpression of OTX2 found in the most aggressive MB subtypes, suggest that OTX2 plays an oncogenic role in MB initiation, progression and maintenance. In 2010, Adamson *et al.* transfected MHH-1 MB cells with *OTX2* and observed increased proliferation in the *OTX2* expressing cells compared to controls [56]. High *OTX2* expressing kidney epithelial cells injected into the cerebral hemispheres of mice demonstrated higher numbers of Ki67 positive cells compared to controls as well [56]. Moreover, developmental studies demonstrate an OTX2 pro-proliferative effect in neuronal progenitors.

Ectopic overexpression of *Otx2* in the mouse hindbrain results in accumulation of proliferative cells in the cerebellar white matter and dorsal brainstem of postnatal mice [67]. Interestingly, OTX2 is expressed at low levels in SHH MB, yet our lab has recently shown that when *OTX2* is overexpressed in this subtype, a decrease in self-renewal and cell growth is observed [11]. This functional dichotomy is also evident in neural tissues in which *Otx2* expression inhibits proliferation in thalamic progenitors while inducing proliferation in progenitors of the dorsal brain stem [119]. These data suggest that OTX2 regulates proliferation and/or differentiation in a region-specific manner.

In addition, studies to date have demonstrated that OTX2 maintains MB cells in a higher proliferative state. Bunt and colleagues showed that *OTX2* KD in Group 3 MB cell lines decreased cell growth while inducing morphological changes consistent with increased neuritic outgrowths, and elevated expression of neural developmental genes [130]. Interestingly, Bai *et al*. demonstrated how OTX2 expression is mutually exclusive from the expression of myogenic marker, desmin, in medullomyoblastoma [131]. MYC amplification is also observed alongside *OTX2* amplification in Group 3 MB [1]. ChIP analysis by Bunt *et al.* showed that MYC and OTX2 bind to the transcriptional start sites of their target genes in close proximity, suggesting they work together in regulating gene expression [132]. Epigenetics studies have also revealed that OTX2 maintains Group 3 and 4 MB gene target promoters and embryonic stem cells in a bivalent state by controlling histone methylation and acetylation [59, 133]. Specifically, *OTX2* expression is associated with increased H3K27me3 marks in OTX2-bound promoters as well as increased H3K4me3 and H3K9ac marks [59]. Interestingly, polycomb genes such as, *EZH2* decrease in expression while demethylase enzymes such as, *KDM6A* increase in expression when OTX2 is knocked down in Group 3 and 4 MB cell lines [59].

To date, existing OTX2 studies have demonstrated that this transcription factor contributes to MB tumor progression by regulating cell cycle gene expression and tumor growth [59, 132]. However, these data were collected from studies performed in adherent or serum containing cultures, not accounting for the MB primitive stem/progenitor cell of origin. As OTX2 plays pivotal roles during the early stages of neurodevelopment, including those primitive cells belonging to the cerebellar lineages, our laboratory set out to explore the function of OTX2 in MB stem cell populations. We discovered that when Group 3 and Group 4 MB cells are grown in stem cell-enriched conditions, OTX2 KD results in a decrease in both self-renewal capacity or stem cell function and cell growth [11]. However, the molecular mechanisms by which OTX2 regulates MB stem cells were not identified. Therefore, the focus of this thesis is to delineate how OTX2 maintains MB cells in an undifferentiated state and whether it has a role in suppressing neural differentiation. This requires a general understanding of the basic principles of stem cell biology and how stem cell function is assessed both *in vitro* and *in vivo*. These concepts, as they apply to putative cancer stem cells or CSCs, are briefly described below.

1.4.0 CANCER STEM CELLS

1.4.1 The cancer stem cell theory

MB is a highly heterogeneous cancer with a complex ecosystem of cells. The cancer stem cell (CSC) theory proposes that a small subset of self-sustaining cells called CSCs can self-renew, differentiate, and establish heterogeneous populations of tumor cells in a wide variety of cancers [134] . Self- renewal is the division of a stem cell that produces either two daughter cells that can also self- renew (a symmetric division), or one daughter cell that can self-renew and one that cannot (an asymmetric division) [135]. Asymmetric division generates the differentiated cells, which make up our different organs and the heterogeneous populations of cells in multiple

cancer types. Moreover, some CSC populations are quiescent and cycle slowly, enabling them to escape current cancer treatments such as chemotherapy, targeted at actively dividing cells (Figure 1.7) [134]. This interpretation on cycling is adopted from observations in normal stem cells that demonstrate active cycling during development but become more quiescent during adult homeostasis [136]. Some CSC theories suggest CSCs arise from normal stem/progenitors that acquire specific mutations enabling them to take on CSC features, while other theories suggest CSCs arise from tumor cells that acquire additional mutations that impart stem-like characteristics.

1.4.2 The first cancer stem cells: assays

The first CSCs identified were in acute-myelogenous leukemia (AML) [137]. Previous studies demonstrated that AML tumors contained a larger, faster dividing subset of cells and a smaller, slower dividing subset of cells similar to normal hematopoietic stem cells [138]. It was believed that these slower dividing CSCs were refractory to conventional cancer therapy and were the cause of relapse. In 1994, AML cells exhibiting the cell surface marker expression profile cluster of differentiation (CD) $CD34^+/CD38^-$ were identified as CSCs. Importantly, $CD34^+/CD38^-$ cells sorted by flow cytometry and transplanted into severe combined immuno-deficient (SCID) mice demonstrated leukemia initiating capacity [137].

For many years, it was believed that solid tumors did not contain CSCs; however in 2003, Al Hajj *et al.* identified a distinct population of cells with tumorigenic CSC potential in human breast cancer [139]. They demonstrated that isolated $CD44^+CD24^-$ human breast cancer cells exhibited tumor initiating capacity in SCID mice [140]. Tumors developed with as few as 200 $CD44^+CD24^-$ transplanted cells, while other tumor cells, even at higher doses, displayed no tumorigenic potential [140]. Singh and colleagues also discovered a putative CSC population in

brain tumors. They revealed that the classic neural stem cell marker $CD133^+$ selected for glioblastoma and MB CSCs, or brain tumor propagating cells [141]. These $CD133^+$ tumor cells could initiate tumor growth with karyotypically abnormal cells *in vivo* [141]. However, more recent studies have shown that $CD133^-$ cells are also tumorigenic after transplantation in a manner similar to $CD133^+$ cells [142]. Work towards identification of better cell surface markers has led to the discovery that stage-specific embryonic antigen 1 (SSEA1)/$CD15^+$ MB cells also possess tumor progenitor or stem-like characteristics [143-145]. Moreover, in 2015, our laboratory showed that the cell surface marker CD271 selected for a lower self-renewing stem/progenitor cell population, specifically in SHH MB [142]. In addition to the cell surface markers mentioned above, other common CSC markers used in oncology research today include CD44, CD24, CD29, CD90, CD133, epithelial surface antigen (ESA), and aldehyde dehydrogenase (ALDH1) [140, 141]. It is likely that for each CSC phenotype, multiple markers will be required for higher quality sorting, molecular characterization and subsequent therapeutic targeting.

Testing the CSC theory required a robust assay to measure the tumor propagating potential of specific cell surface markers. As a result, standard stem cell assays were developed to isolate the best CSC markers. A CSC marker must be able to be utilized for isolation of tumor cells that: 1. Give rise to new secondary tumors that recapitulate the original patient tumor phenotype after xenotransplantation and 2. Be able to re-establish tumorspheres *in vitro* through serial passaging in the sphere-forming assay (Figure 1.8) [146, 135]. The sphere-forming assay is the current gold-standard *in vitro* measure of self-renewal [146]. Primary patient samples and cell lines are plated on low attachment plates at clonal density (1-20 cells/µl) in serum-free media over multiple passages. In this thesis we employed both *in vivo* xenotransplantation with cell lines and *in vitro* sphere-forming assays to explore the molecular mechanism by which OTX2 enhances

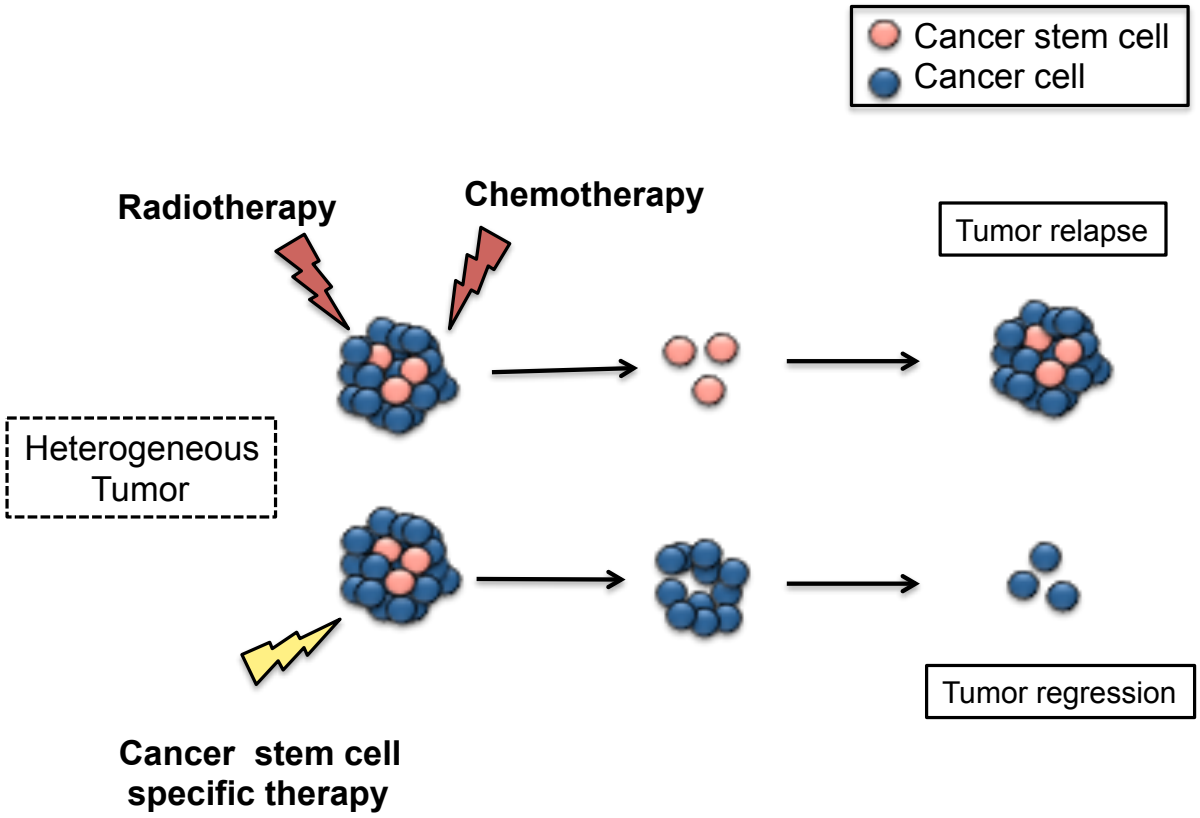

Figure 1.7: Cancer stem cell survival with conventional chemotherapy.
Cancer stem cells are typically resistant to conventional chemotherapy targeted at actively dividing cells and are able to regenerate the tumor despite some tumor cell death. Targeted cancer stem cell therapies are hypothesized to abolish tumor relapse by eliminating the CSCs. Adapted from Dick, 2008.

self-renewal and inhibits differentiation in Group 3 and 4 MB stem/progenitor cell populations. Continued research efforts evaluating MB cell lines or primary patient samples in stem cell enriched conditions will help identify key properties which will render CSC populations sensitive to novel therapies. Using these model systems as a basis, my overarching goal is to characterize how OTX2, the amplified and/or overexpressed transcription factor in Group 3 and Group 4 MB stem/progenitor cells is contributing to MB pathogenesis.

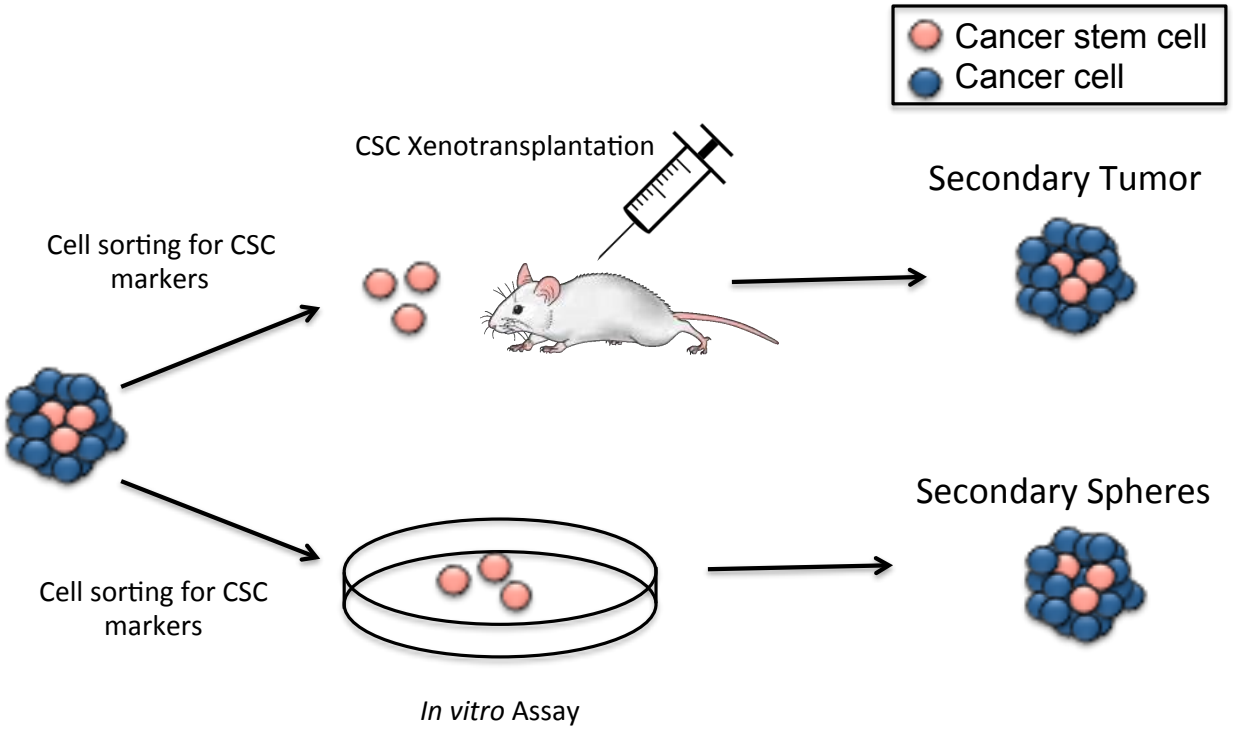

Figure 1.8: Cancer stem cell isolation.
Cancer stem cells are isolated using staining for specific cell surface markers. A given cell population is defined as having cancer stem cell properties if it is exhibits *in vivo* self-renewal capacity after xenotransplantation as well as self-renewal capacity at clonal density in serum free conditions *in vitro*.

CHAPTER 2: RATIONALE AND HYPOTHESIS

2.1 RATIONALE

As MB is believed to originate from stem and progenitor cell populations that exist transiently during normal cerebellar development, targeting tumor cells with stem/progenitor molecular signatures that persist beyond the early developmental stages represents a therapeutic strategy that may have less toxic effects on the nervous systems of young MB patients. Yet, surprisingly little is known about the role of subtype-specific genes in MB stem cell-like populations. Moreover, since OTX2 is amplified and/or overexpressed in 80% of Group 3 and Group 4 MB, the two least studied and most aggressive subtypes, understanding how OTX2 modulates tumorigenesis by enhancing self-renewal and suppressing differentiation in these subtypes will be critical to move forward with drug discovery platforms.

2.2 HYPOTHESIS AND RESEARCH AIMS

We hypothesize that OTX2 maintains MB cells in a state of higher self-renewal by transcriptionally inhibiting neural differentiation. I also predict that increasing the expression of downstream neural differentiation OTX2 target genes will shift cells towards a differentiated, less aggressive phenotype in Group 3 and 4 MB.

To test this hypothesis, we set 3 main objectives:

AIM 1: To validate the effects of OTX2 on self-renewal/differentiation following OTX2 knockdown.

AIM 2: To determine the relationship between OTX2 and select neural differentiation genes in regulating cell function *in vitro.*

AIM 3: To investigate the downstream pathways known to modulate the effects of select neural

differentiation genes following OTX2 knockdown in Group 3 and Group 4 MB stem/progenitor cells.

CHAPTER 3: MATERIALS AND METHODS

3.1 Cell culture

D283 and D341 cells were purchased from the American Type Culture Collection (ATCC, Rockville, MD, USA). The D283 cell line [147, 148] exhibits features of both Group 3 [149, 150] and Group 4 MB [148], and D341 is a Group 3 MB cell line (Table 1.0) [151]. D425 [152] Group 3 cells were obtained from Dr. Magimairajan Vanan (University of Manitoba, Winnipeg, Manitoba). D283 cells were cultured in Eagle's minimum essential media (EMEM) (ATCC) containing 10% FBS (ThermoFisher Scientific, Ottawa, ON, Canada) on tissue culture plates (Table 1.0). D341 and D425 cells were cultured in StemPro® Neural Stem Cell Serum Free Medium (Life Technologies, Burlington, ON, Canada) as tumorspheres on ultra low-attachment plates. Recently derived MB3W1 cells [153] were cultured in Stem Cell Media consisting of Dulbecco's modified Eagle's medium (DMEM)/F12 supplemented with 1% N2 (Gibco, Burlington, ON, Canada), 1% B27 (Gibco), 20 ng/ml epidermal growth factor (EGF; R&D Systems, Minneapolis, MN, USA), 20 ng/ml basic fibroblast growth factor (bFGF; R&D Systems), and 4% penicillin-streptomycin 10,000 U/mL (Life Technologies) on tissue cultures plates grown in suspension (Table 1.0). Recently derived HD-MB03 cells [154] were cultured in RPM1 1640 media (Corning Life Sciences, VWR, Radnor, PA, USA) containing 10% FBS (ThermoFisher Scientific) media on tissue culture plates (Table 1.0). Upon reaching confluence, all cells were dissociated in Accutase (Invitrogen, Burlington, ON, Canada) and passed 1:10.

Table 1.0: Properties of cell lines used.

	D283	D341	D425	MB3W1	HD-MB03
Organism	Human	Human	Human	Human	Human
Tissue	Peritoneum tissue	Cerebellum	Cerebellum	Pleural effusions	Vermis/ Fourth ventricle
Gender	Male (6 year old)	Male (3.5 year old)	Female (5 year old)	Male (22 months)	Male (3 year old)
Culture Properties	Semi-adherent	Suspension	Suspension	Suspension	Semi-adherent
Karyotype	Hypodiploid	Hyperdiploid	Diploid	Tetraploid	Hypodiploid
Source	ATCC	ATCC	Dr. Magimairajan Vanan	Dr. Matthias Wölfl	Dr. Till Milde

3.2 Tumorsphere assays

Tumorsphere assays were performed as previously described [11, 142, 155]. Briefly, D283 cells were dissociated and plated at clonal density between 1-20 cells/µl onto 24-well ultra low-attachment plates in Neural Proliferation Media consisting of Dulbecco's modified Eagle's medium (DMEM)/F12 supplemented with 1% N2 (for the growth of post-mitotic neurons and neuronal tumor cells) (Gibco), 1% B27 (supports low or high-density growth of CNS neurons) (Gibco), 20 ng/ml epidermal growth factor (EGF; R&D Systems), and 20 ng/ml basic fibroblast growth factor (bFGF; R&D Systems). MB3W1 were cultured in Stem Cell media while, D341, D425, and HD-MB03 cells were all cultured in StemPro media and plated at clonal density as described above. All tumorspheres were counted and dissociated after 5-6 days, re-plated at clonal density for secondary tumorsphere formation and counted again after 5-6 days (Figure 3.1). For transfections and semaphorin protein treatment, recombinant human L1CAM (R&D Systems), SEMA4D (R&D Systems), and NRP1 (ACRO Biosystems, Newark, DE, USA) Fc chimera proteins were added to D283 tumorsphere cultures (50-1000 ng/ml) at day 0 for both primary and secondary passage.

3.3 Small interfering RNA

OTX2, SEMA4D, L1CAM and NRP1 levels were knocked down in D283, D341, D425, MB3W1, and/or HD-MB03 cells using Silencer select siRNAs (Life Technologies), while a non-silencing (scramble) siRNA was used as a negative control. OTX2 was knocked down using three independent siRNAs (s9931, s9932, s9933), while the SEMA genes were knocked down using 2 independent siRNAs for SEMA4D (s51388, s20598), L1CAM (s8036, s8038), and NRP1 (s16843, s16844). All sequences were used at a concentration of 30 nM and combined with Lipofectamine RNAiMAX (Life Technologies) as detailed under manufacture's

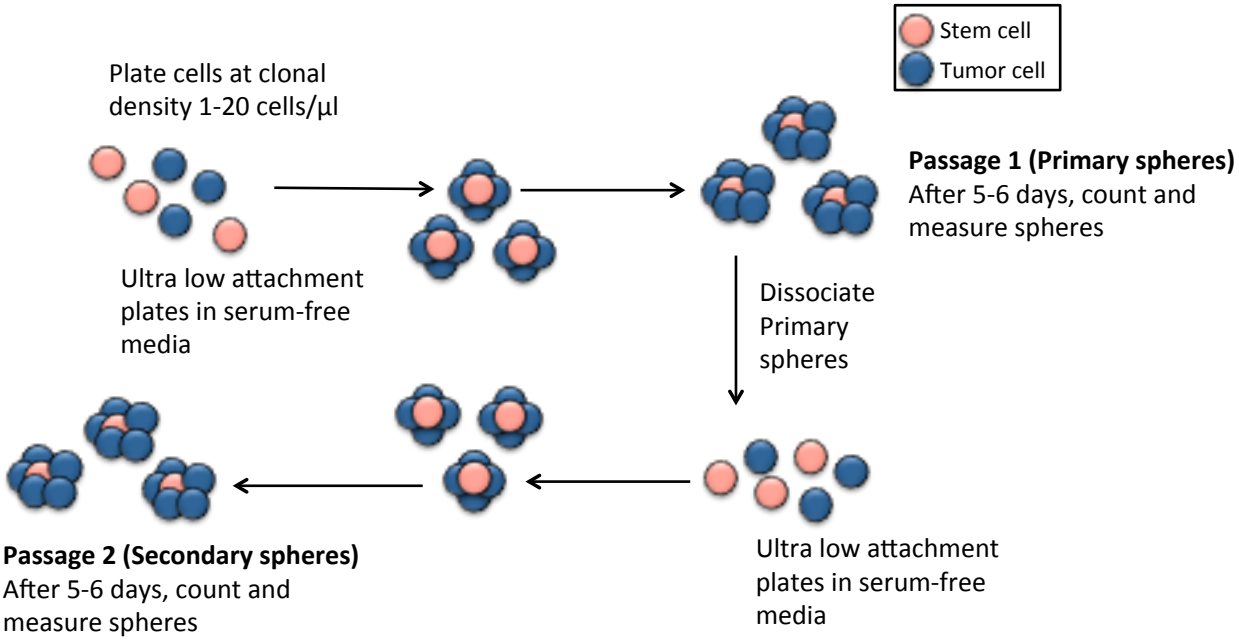

Figure 3.1: Tumorsphere assay.
Tumorspheres are plated at clonal density in ultra low attachment plates in serum-free media. After 5-6 days, tumorspheres are counted and dissociated, then re-plated at clonal density for secondary tumorsphere formation and counted again after 5-6 days.

instructions. For each gene, knockdown was evaluated by Western blot.

3.4 Gene expression profiling and analyses

Extracted RNA from D283 scramble control and OTX2 KD tumorspheres (siRNA 9931) (N=3 biological replicates for each) was subjected to GeneChip 3′ oligonucleotide microarray hybridization and processing performed by Stem Core Laboratories at the Ottawa Hospital Research Institute. Analysis was performed by the Ottawa Bioinformatics Core Facility, Ottawa Hospital Research Institute. HuGene 2.0 st microarray RMA expression values were generated by the Affymetrix Expression Console. Gene symbol annotations were based on Affymetrix provided HuGene-2_0-st-v1.na35.hg19 transcript cluster annotations, assigning each transcript cluster identifier to the first provided gene symbol in the annotation. Fold change and significance for transcript cluster identifiers between conditions were determined using the R limma package. Differentially expressed pathways were analyzed using Ingenuity Pathway Analysis (IPA; Redwood City, CA, USA). Transcripts differentially expressed at least 2-fold (up- or downregulated) and with a value of $p<0.05$ were considered significant. Downstream effects analysis was conducted using the Z-score algorithm to predict the expected causal effects between differentially expressed genes and cell function. A Z-score ≥ 2 indicates that the function is significantly increased; whereas, a Z-score ≤ -2 indicates that the function is significantly decreased. Gene Set Enrichment Analysis (GSEA) [156] was also performed on expression data comparing D283 OTX2-KD to scrambled control tumorspheres (Affymetrix HuGene 2.0st). GSEA results were explored using the Reactome [157, 158] and KEGG [159-161] databases to identify pathways significantly enriched in the expression sets.

3.5 Chromatin immunoprecipitation sequencing

Chromatin immunoprecipitation was performed as previously described [11]. D283

tumorspheres were crosslinked for 10 minutes in 1% formaldehyde and quenched by 0.125M glycine for 5 minutes. Using 500 µl of sonification buffer [50 mM HEPES, pH 7.9, 140 mM NaCl, 1 mM EDTA, 1% (w/v) Triton X-100, 0.1% (v/v) sodium deoxycholate, 1% (w/v) SDS and protease inhibitors] cell pellets were resuspended and sonicated into ~400 bp with a bioruptor. Samples were incubated with protein A-Dynabeads ovalbumin and salmon sperm DNA for 1 hour at 4°C to preclear the chromatin. OTX2 antibody (Abcam (ab21990)) was coupled to protein A-Dynabeads with protein A (rabbit antibody) in immunoprecipitation buffer. The precleared-chromatin and antibody bound beads were incubated overnight at 4°C. Unbound chromatin was washed away while the bound chromatin was eluted in 400 µl of elution buffer and reverse crosslinked with 5 M NaCl (0.2 M final) and 4 µl of RNAse A (1 mg/ml) overnight at 55°C. Samples were treated with proteinase K (20 µg/µl), DNA was extracted using phenol:chloroform and suspended in 50 µl elution buffer [11]. ChIP-seq data were generated on a NextSeq 2500 and mapped to the GRCh38 human genome model using bowtie2 v2.2.4. Peaks were called using MACS2 v2.1.0.20140616. Peaks called were masked for ENCODE blacklist peak locations.

3.6 Immunofluorescent staining

D283 and D425 tumorspheres were washed with phosphate buffered saline (PBS) and fixed in 10% formalin for 2-3 hours. Fixed tumorspheres were washed 2X with PBS and incubated in fresh, ice cold 15% sucrose followed by 30% sucrose each for 2-3 hrs at 4°C. Samples were embedded in OCT, frozen, cut in 10 µm-thick sections, washed in Tris-buffered saline (TBS 1X) for 10 min and incubated with blocking solution (1% BSA and 5% serum in TBS) for 45 minutes at room temperature. Sections were stained with Mouse Anti-Neuron-specific βIII- tubulin Monoclonal Antibody (1:100) (Catalog # MAB1195, R&D Systems) and

incubated at room temperature for 2 hours. Slides were then washed with TBS 3 x 5 min, followed by secondary antibody incubation (Alexa flour 488 goat anti-mouse IgG) (1:200) (Cat#: A-11001, Thermo fisher) for 1 h at room temperature. Slides were then washed 3 x 5 min with TBS and counterstained with prolong gold anti-fade mountant with DAPI (Molecular Probes, Life Technologies, Cat #: P36935).

3.7 Western Blot

Protein was isolated from all cells and their respective controls using either the All-In-One Purification Kit (Norgen Biotek) according to manufacturer's instructions or isolated using IP-Lysis Buffer (975 µl Lysis Buffer 10 µl 50X protease inhibitor and 5 µl orthovanadate). Twenty micrograms of protein was loaded onto 10% Tris-glycine gels (10% resolving buffer, 4% separating buffer).

Protein was transferred using a semi-dry transfer apparatus to a nitrocellulose membrane (BioRad). Membranes were blocked in 2.5% non-fat milk in Tris Buffered Saline with Tween 20 (TBST) and then incubated at 4°C overnight with antibodies to β-actin (Abcam Inc. (ab8226), Toronto, ON, Canada, 1:1000), SEMA4D (Abcam (ab134128), 1:500), L1CAM (Gene Tex (GTX23200), Irvine, CA, USA, 1:500), NRP1 (Abcam (ab81321), 1:500), βIII-Tubulin (R&D Systems (MAB1195), 1:1000). OTX2 (Abcam (ab21990) 1:500), pERK/Total ERK (Cell Signaling Technology (4370/4695), 1:500), p38/Total p38 (Cell Signaling Technology (3316/3042), 1:500), Rho (Thermo Fisher (1862332), 1:500) antibodies were diluted in Super-signal primary antibody buffer and membranes were treated with enhancer buffer for 10 min prior to blocking with 2.5 % non-fat milk. Membranes were washed several times with TBST before application of goat anti-rabbit horseradish peroxidase (HRP), donkey anti-rabbit HRP (Jackson ImmunoResearch Laboratories Inc. (711-035-152), Baltimore, PA, USA, 1:5000) or

goat anti-mouse HRP secondary antibodies (Abcam (ab6789), 1:5000). Membranes were developed using SuperSignal West Pico (Fisher Scientific).

3.8 Real Time-qPCR

Total RNA was extracted from D283, D341, and D425 tumorspheres using the Norgen All in one kit (Norgen Biotek, Thorold, ON, Canada) or the Norgen RNA extraction kit (Norgen Biotek) according to manufacturer's instructions for mammalian cultured cells. First-strand cDNA was synthesized as previously described using the Superscript III First Strand Synthesis System (Life Technologies) [11]. GoTaq qPCR Master Mix (Fisher Scientific) was used for sample preparation and analysis was performed on a Mx3000P (Stratagene, Santa Clara, CA, USA) qPCR system. Glyceraldehyde 3-phosphate dehydrogenase (*GAPDH*) was used to normalize all values and specific primer sequences for each gene evaluated are listed in Table 1.1. The following qPCR conditions were used: 50°C for 2 minutes, 95°C for 2 minutes, and 40 cycles of 95°C for 15 seconds and 60°C for 30 seconds.

3.9 Lentiviral transduction

Stable knockdown of OTX2 was performed as previously described [11] using two shRNAmir lentiviral constructs (Open Biosystems, GE Dharmacon) consisting of a dual-expression system with GFP as a transduction marker and puromycin resistance for selection. A non-silencing (scramble) shRNA sequence was used as a negative control. Cells were seeded in 6- well plates at $2x10^5$ cells/well in serum free media 24 hours prior to transduction.

3.10 Rho pulldown

Rho activity was measured in D283 and HD-MB03 scramble control and OTX2 KD tumorsphere derived cells using the Active Rho Pull-Down and Detection kit according to manufacturer's instructions (ThermoFisher Scientific). For each treatment, 12-18 wells of

Table 1.1: List of primer sequences used for Real Time qPCR.

Gene	Forward sequence	Reverse sequence
GAPDH	3'-GAAATCCCATCACCATCTTCCAGG-5'	3'-GCAAATGAGCCCCAGCCT TCTC-5'
OTX2	5'-GAGGTGGCACTGAAAATCAAC-3'	5'-TCTTCTTTTTGGCAGGTCTCA-3'
TUJ1	5'-GGCCTTTGGACATCTCTTCA-3'	5'-TCGCAGTTTTCACACTCCTTC-3'
MAP2	5'-ATTCTGGCAGCAGTTCTCAAA-3'	5'-TGCTTCCTCGGTTAGAGACAA-3'
SEMA4D	5'-CGTCATGGTTGATGGAGAACT-3'	5'- AGCCAAGGGATTGCATATTCT-3'
L1CAM	5'-AAATGGCTGTGAAGACCAATG-3'	5'-GATGAAGCAGAGGATGAGCAG-3'
NRP1	5'-CGATTTGGAGGACAGAGACTG-3'	5'-GGGGCTATCTTTCCACAGAAC-3'
SEMA6A	5'-TTTGTTCAAGCCGTGGATTAC-3'	5'-GCCACTCTTGGGAAAACTACC-3'
PLXNA2	5'-ACCATCACACAGGTCAAGGAG-3'	5'-CACTCCAAGTCCATGTCCACT-3'
SLIT2	5'-TGAATTTACCGTGTTGGAAGC-3'	5'-CAGATGCTCCTTCAAATGCTC-3'
DCC	5'-TACTGGACCACCTTCCAACTG-3'	5'-CCTCACATGAAGAGAGCTTGG-3'
EPHA3	5'-GGAAGAGATCAGTGGTGTGGA-3'	5'-TTTTGACTGTGGTCCATGACA-3'
EPHA5	5'-ACAAAGGAAGCCAAATCACCT-3	5'-GGTAGAAACCCAAAGGCAGAC-3'
EPHB2	5'-GACTCCACTACAGAGACTGCT-3'	5'-TCTCATCGTAGCCACTCACCT-3'

tumorspheres were pooled, washed with ice cold TBS and resuspended in 0.5ml Lysis buffer [25mM Tris HCl, pH 7.2, 150mM NaCl, 5mM $MgCl_2$, 1% NP-40 and 5% glycerol and 10 µl 50X protease inhibitor]. Briefly, samples were mixed with glutathione resin agarose beads bound with GST-Rhotekin-RBD, incubated for 1hr at 4°C, washed and eluted. The samples and total lysates were evaluated for Rho activity by Western blot.

3.11 Group 3 and Group 4 MB patient sample analysis

Fully annotated Affymetrix Gene 1.1 ST Array datasets [162, 163] were used to compare transcript levels of axon guidance genes in a total of 234 Group 3 and Group 4 patient samples. The following axon guidance genes were not part of this published micro-array dataset: *GNG3, EFNA4, ARPC1B, TUBB4A, MIR27B* and *ITGA4*. A Pearson correlation co-efficient was calculated for OTX2 and each of the axon guidance genes. The FDR correction was used to adjust for multiple comparisons (FDR < 0.1). Survival was compared in patients with SEMA gene expression (>80th percentile) to patients with low SEMA gene expression (<20th percentile) and the associated p-value was calculated.

3.12 Intracerebellar transplantation

The University of Manitoba Animal Care Committee approved all procedures and protocols. Dissociated tumorspheres from D283 scramble controls and stable OTX2 KD were injected into the cerebellum of 5-7 week old NOD-SCID mice. Animals were anesthetized with isoflurane and injected with $2X10^5$ (N=8 scramble, N=7 OTX2 KD), $1X10^5$ (N=3 scramble, N=3 OTX2 KD), and $5X10^4$ (N=4 scramble, N=4 OTX2 KD) MB cells. Animals lost ~20% of their weight at 42 days, at which time they were anesthetized with isoflurane, perfused with formalin (VWR International, Mississauga, Ontario, Canada) and the brains extracted. Brains and associated tumors were placed in 10% formalin for up to 7 days, embedded in paraffin and

sectioned at 5 μm. Sections were de-waxed in xylene, rehydrated through a graded series of alcohol concentrations and stained with Hematoxylin and Eosin. Slides were imaged using an EVOS xl core microscope (AMG, Seattle, WA, USA).

For Ki67 staining, sectioned paraffin embedded samples were rehydrated in tap water. Antigen retrieval was conducted by boiling in citrate buffer (pH 6.0) for 20 min followed by a 30 min cool down. Samples were washed before and after exogenous peroxidase treatment for 10 min followed by blocking for 1 hour at room temperature with 10% sheep serum in PBS. Primary antibody (Ki67 Cell Signaling Technology 9449S) was diluted 1:800 in 1% sheep serum in PBS and applied overnight at 4°C. Secondary Biotinylated anti-mouse antibody (Jackson ImmunoResearch 515-065-003) was diluted 1:500 and samples were incubated for 2 hours at room temperature. Straptavidin (Jackson ImmunoResearch 016-030-084) was diluted 1:400 and applied for 30 minutes at room temperature followed by 2 minutes in DAB. Samples were counterstained with Hematoxylin, dehydrated and mounted with Permount.

3.13 Statistical tests

All statistical analyses were performed using Prism 5 software (GraphPad Software, La Jolla, CA, USA). One-way ANOVAs and Tukey's tests for multiple comparisons were used to determine statistical significance for all OTX2 siRNA tumorsphere data, and to determine whether there was a significant difference between each siRNA. All analyses were checked for homogeneity of variances using a Brown-Forsythe test. Tumor data were analyzed using an independent sample one-tailed *t* test with Welch's correction. Subsequent recombinant Fc L1CAM, SEMA4D and NRP1 protein tumorsphere data and dual OTX2/SEMA gene KD data were analyzed using a one-way ANOVA followed by a Dunnett's test for multiple comparisons. Normalized ROCK inhibitor data were analyzed using a repeated measures 2-way ANOVA

followed by a Dunnett's test for multiple comparisons. All data are reported as a mean ± standard error of the mean (SEM). A p-value less than 0.05 was considered significant.

CHAPTER 4: RESULTS

4.1 AIM 1: To validate the effects of OTX2 on self-renewal/differentiation following OTX2 knockdown

4.1.1 OTX2 knockdown decreases MB self-renewal in both well-established and recently derived cell lines *in vitro*

Our lab previously showed that OTX2 KD decreases self-renewal capacity in the Group 3 and 4 MB cells lines D283 [147] and D341 [151] grown in neural precursor media [11]. To further validate this effect on self-renewal, we knocked down OTX2 in D283, D341 and D425 [152] Group 3 tumorspheres as well as the recently established HD-MB03 and MB3W1 Group 3 tumorspheres [147, 154] using 3 independent siRNA sequences (Figure 4.1A). OTX2 KD in all five cell lines resulted in a significant decrease in tumorsphere formation and self-renewal capacity when grown in stem cell-enriched conditions relative to scramble (controls) tumorspheres (Figure 4.1B-I). These results extend our previous findings in Group 3 and 4 MB established cell lines and reveal that OTX2 KD also decreases self-renewal capacity in recently derived Group 3 MB cells.

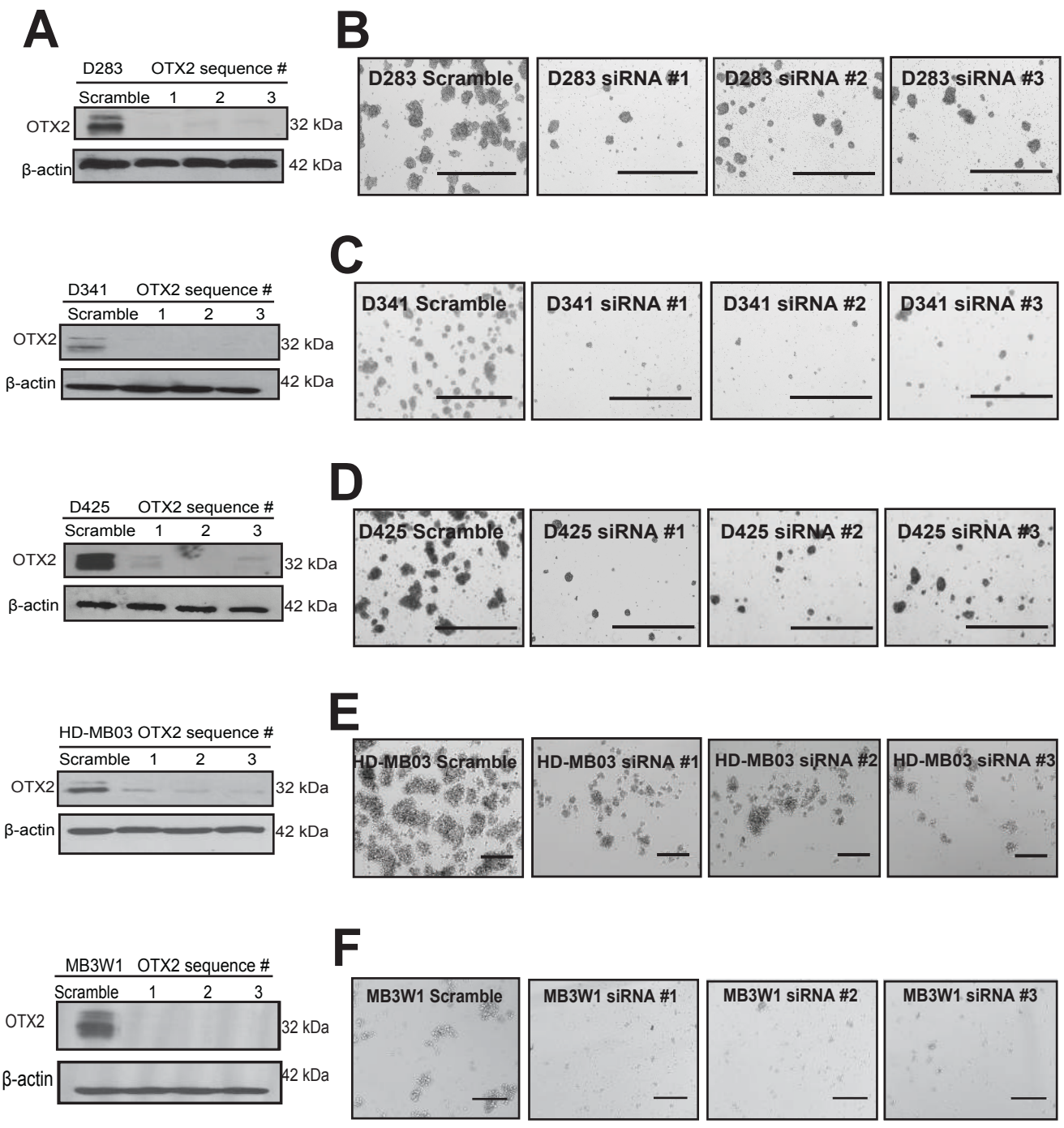
A
D283 OTX2 sequence #
Scramble 1 2 3
OTX2
32 kDa
β-actin
42 kDa
B
D283 Scramble
D283 siRNA #1
D283 siRNA #2
D283 siRNA #3
C
D341 OTX2 sequence #
Scramble 1 2 3
OTX2
32 kDa
β-actin
42 kDa
D341 Scramble
D341 siRNA #1
D341 siRNA #2
D341 siRNA #3
D
D425 OTX2 sequence #
Scramble 1 2 3
OTX2
32 kDa
β-actin
42 kDa
D425 Scramble
D425 siRNA #1
D425 siRNA #2
D425 siRNA #3
E
HD-MB03 OTX2 sequence #
Scramble 1 2 3
OTX2
32 kDa
β-actin
42 kDa
HD-MB03 Scramble
HD-MB03 siRNA #1
HD-MB03 siRNA #2
HD-MB03 siRNA #3
F
MB3W1 OTX2 sequence #
Scramble 1 2 3
OTX2
32 kDa
β-actin
42 kDa
MB3W1 Scramble
MB3W1 siRNA #1
MB3W1 siRNA #2
MB3W1 siRNA #3

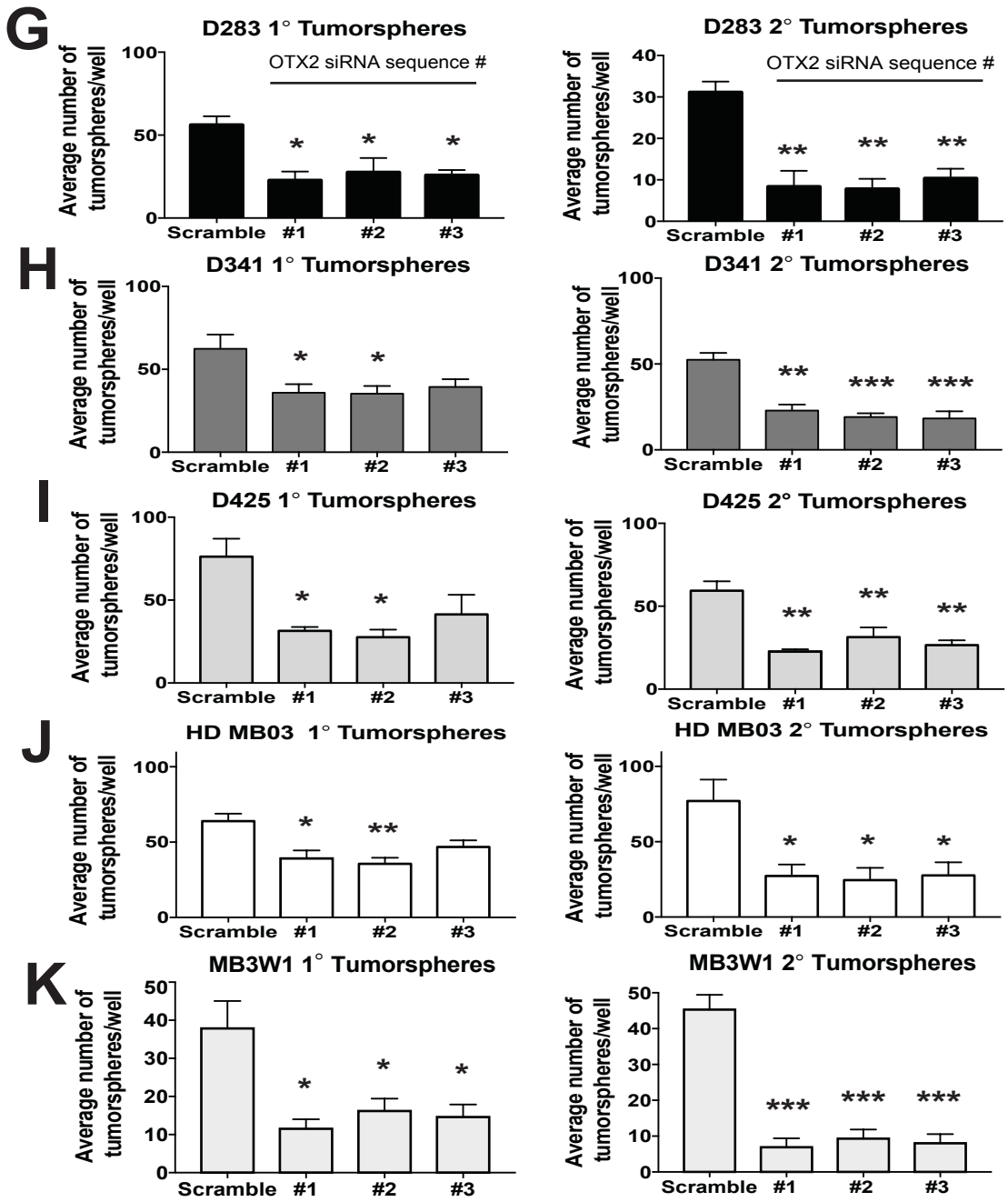

Figure 4.1: Knockdown of OTX2 in Group 3 and Group 4 MB tumorspheres decreases self-renewal.

(**A**). Western Blot validation of OTX2 knockdown in tumorspheres from D283, D341, D425 MB cell lines and recently derived HD-MB03, and MB3W1 cell lines using 3 independent siRNA sequences relative to scramble siRNA. β-actin serves as a loading control. (**B-E**). Representative images of tumorspheres at secondary passage following OTX2 knockdown in D283 (**B**), D341 (**C**), D425 (**D**), HD-MB03 (**E**) and MB3W1 (**F**) cells. Scale bar: 1000 μm. (**G-K**). Quantification of primary (left) and secondary (right) tumorsphere number in D283 (**G**), D341 (**H),** D425 (**I**), HD-MB03 (**J**) and MB3W1 (**K**) tumorspheres following OTX2 knockdown. Error Bars: s.e.m. $p<0.05$*, $p<0.01$**, $p<0.001$***. N=3 or N=4 biological replicates or independent transfections and between n=10-20 technical replicates for each siRNA performed.

4.1.2 OTX2 knockdown increases differentiation in both well-established and recently derived MB cell lines *in vitro*

Our lab previously demonstrated that OTX2 KD decreases cell growth and viability in tumorsphere culture [11]; however, we did not determine whether this was also accompanied by an increase in differentiation. To explore whether the decrease in self-renewal capacity results in increased differentiation, we evaluated the expression of the classic neuronal differentiation markers, βIII-tubulin and MAP2, following OTX2 KD by qPCR and/or immunofluorescence staining (IF). βIII-tubulin or *TUJI* and *MAP2* transcript levels were strongly upregulated in D283 tumorspheres following OTX2 KD by qPCR (Figure 4.2A-B). Similarly, βIII-tubulin was upregulated by IF in D283 and D425 tumorspheres following OTX2 KD (Figure 4.2C-D). These results reveal that OTX2 KD increased neuronal differentiation in Group 3 and 4 MB cell lines in stem cell-enriched conditions and that OTX2 is important for regulating the balance between self-renewal and differentiation in highly aggressive MB cells.

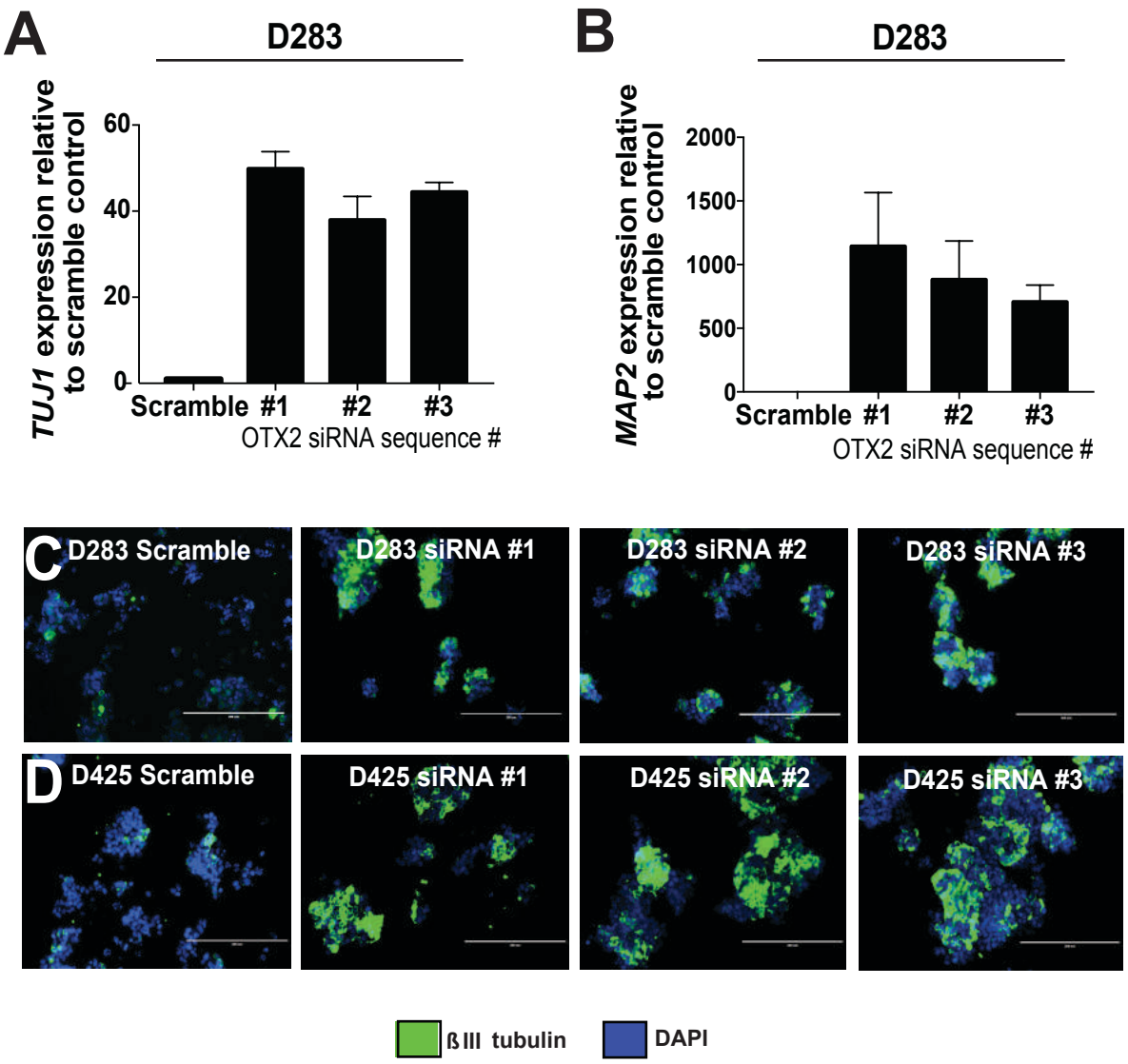

Figure 4.2: Knockdown of OTX2 in Group 3 and Group 4 MB tumorspheres increases neural differentiation.
(**A-B**). *TUJ1* (**A**) and *MAP2* (**B**) expression following OTX2 knockdown using 3 siRNAs in D283 tumorspheres by qPCR. Error Bars: s.e.m. N=3 biological replicates and n=9 technical replicates performed. Contributions from Dr. Ravinder Kaur. (**C-D**). Immunofluorescent staining of D283 (**C**) and D425 (**D**) tumorspheres for ßIII-tubulin following OTX2 knockdown using 3 siRNAs. Scale bar: 200 μm. Courtesy of Nazanin Tatari.

4.1.3 OTX2 knockdown inhibits tumor growth and decreases tumor initiating capacity from D283 tumorspheres *in vivo*

Since OTX2 KD decreases MB self-renewal capacity *in vitro*, we wanted to further explore the effect of OTX2 KD on MB tumorspheres by evaluating both tumor growth and tumor-initiating capacity, a feature associated with cancer stem cell function, *in vivo*. To examine this, we generated stable D283 OTX2 KD cells using 2 shRNA sequences (Figure 4.3A), and injected $2x10^5$ cells derived from tumorspheres for both D283 scramble (N=8) and D283 OTX2 KD (sequence #2) cells (N=7) into the cerebellum of NOD SCID mice. Tumors derived from OTX2 KD tumorspheres (0.7 ± 0.3 mm^2) were significantly smaller than those derived from scramble controls (3.6 ± 1.4 mm^2) (Figure 4.3B-C). Importantly, limiting dilution analysis comparing tumor growth from $2x10^5$, $1x10^5$, and $5x10^4$ D283 scramble relative to D283 OTX2 KD tumorsphere cells revealed a decrease in tumor initiating capacity following OTX2 KD (Figure 4.3D). D283 scramble tumorspheres displayed retention of tumor-initiating capacity with decreasing cell numbers injected, while tumor initiation from D283 OTX2 KD tumorspheres declined with decreasing cell numbers, as only small nests of tumor cells were observed, if any, following injection of $5x10^4$ cells (Figure 4.3D). This was supported by Ki67 staining for tumor cell proliferation that revealed a decrease in Ki67 levels in D283 OTX2 KD tumors (Figure 4.3E). Taken together, these results demonstrate that OTX2 contributes to both tumor growth and tumor-initiating capacity from MB stem/progenitor cells *in vivo*.

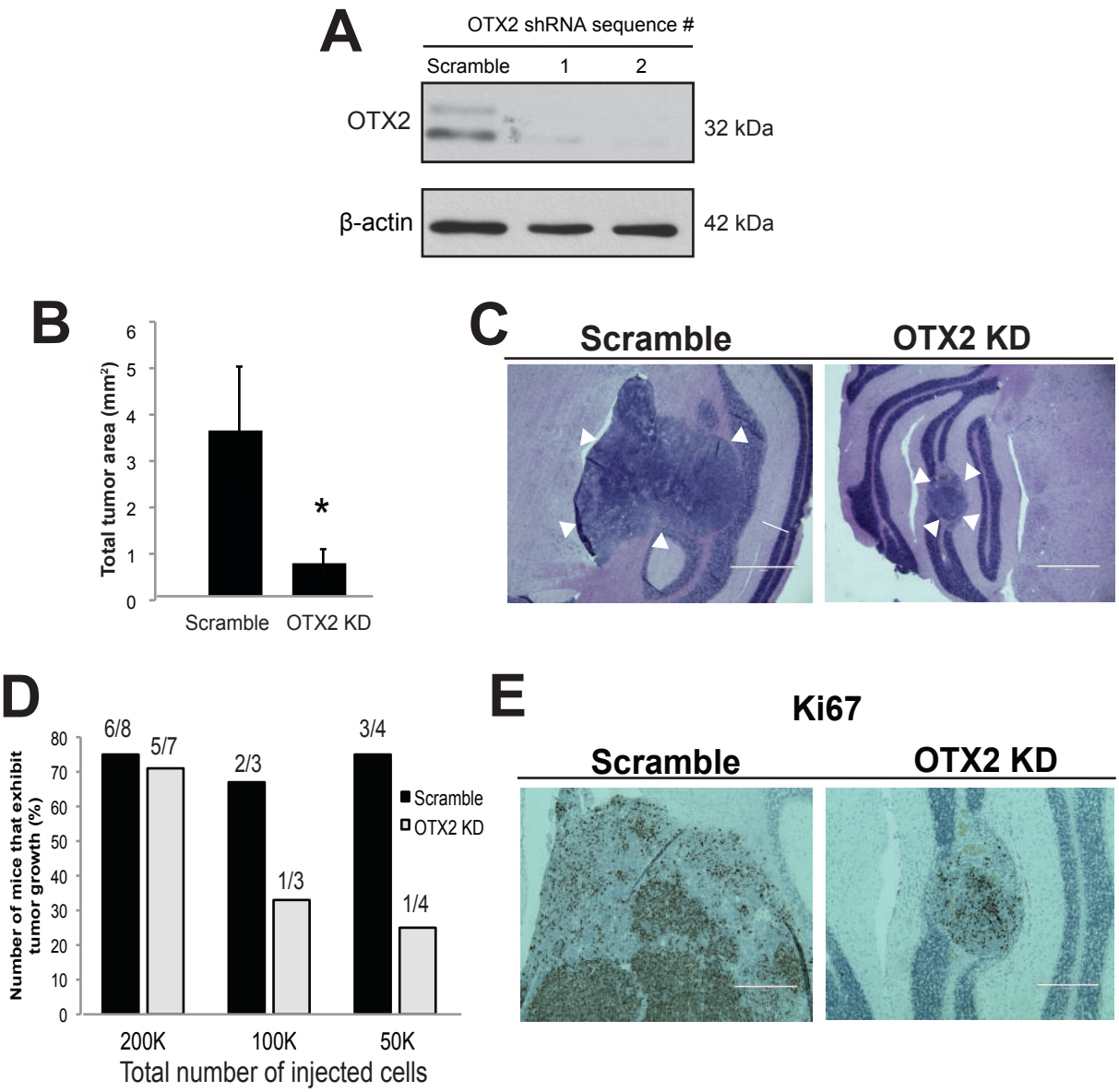

Figure 4.3: OTX2 knockdown decreases tumor growth and tumor initiating capacity *in vivo*.

(**A**). Western blot validation of stable OTX2 knockdown in D283 cells using 2 shRNA sequences relative to scramble control. ß-actin serves as a loading control. (**B**). Quantification of tumor area following intracerebellar injection of $2x10^5$ D283 scramble (N=8) or OTX2 knockdown (N=7) tumorsphere cells. Error bars: s.e.m. $p<0.05$ *. (**C**). Representative images of tumors derived from D283 scramble or D283 OTX2 knockdown cells following injection into the cerebellum of NOD SCID mice. Scale bar: 1000 μm. Arrows denote intracerebellar tumors from each. Surgeries performed by Nazanin Tatari. (**D**). Limiting dilution analysis of tumors derived from D283 scramble relative to D283 OTX2 knockdown tumorspheres following intracerebellar injection. Lower number of animals displaying evidence of tumor growth with OTX2 knockdown cells as compared to scramble cells. (**E**). Representative images of Ki67 staining in tumors derived from D283 scramble or D283 OTX2 knockdown cells following injection into NOD SCID mice. Scale bar: 400 μm. Courtesy of Ludivine Morrison.

4.2 AIM 2: To determine the relationship between OTX2 and select neural differentiation genes in regulating cell function in vitro.

4.2.1 Global gene expression analysis and ChIP-sequencing reveal a negative correlation between OTX2 and expression of a large cohort of axon guidance genes in MB cells

Our results demonstrate that OTX2 regulates the balance between self-renewal and differentiation in MB cells. Next, we sought to evaluate the molecular mechanisms contributing to these effects by characterizing the OTX2-regulatory network in MB stem/progenitor cells. The dramatic increases in *TUJI* and *MAP2* levels following OTX2 KD prompted us to investigate whether a larger cohort of neurodevelopment genes were differentially expressed. Therefore, we performed global gene expression analysis using Human Gene 2.0 microarrays to compare the molecular profiles of D283 OTX2-expressing scramble tumorspheres relative to OTX2 KD tumorspheres generated by siRNA (Figure 4.1A). Of the 3614 significantly and differentially ($p<0.05$ and ± 2-fold) expressed transcripts in D283 scramble control relative to OTX2 KD tumorspheres, Ingenuity Pathway Analysis (IPA) revealed that those pathways associated with cell cycle and neuronal differentiation/axon guidance, such as ephrin, netrin, slit and semaphorin (SEMA) signaling, represented the top dysregulated networks (Figure 4.4A-B; Tables S1-S2). This was further supported by GSEA that demonstrated an enrichment of genes associated with cell cycle in the D283 high OTX2-expressing scramble tumorspheres (Figure 4.4C); whereas, enrichment of genes associated with neuronal differentiation and axon guidance (Figure 4.5D-E; Table S3) was observed in the D283 OTX2 KD tumorspheres. IPA downstream effects analysis confirmed these findings with 85 of 252 differentially expressed neural development genes exhibiting measurement directions consistent with an increase in neuronal differentiation (Z-score: 3.2) (Table S1). Of the 90 axon guidance gene transcripts that were significantly and

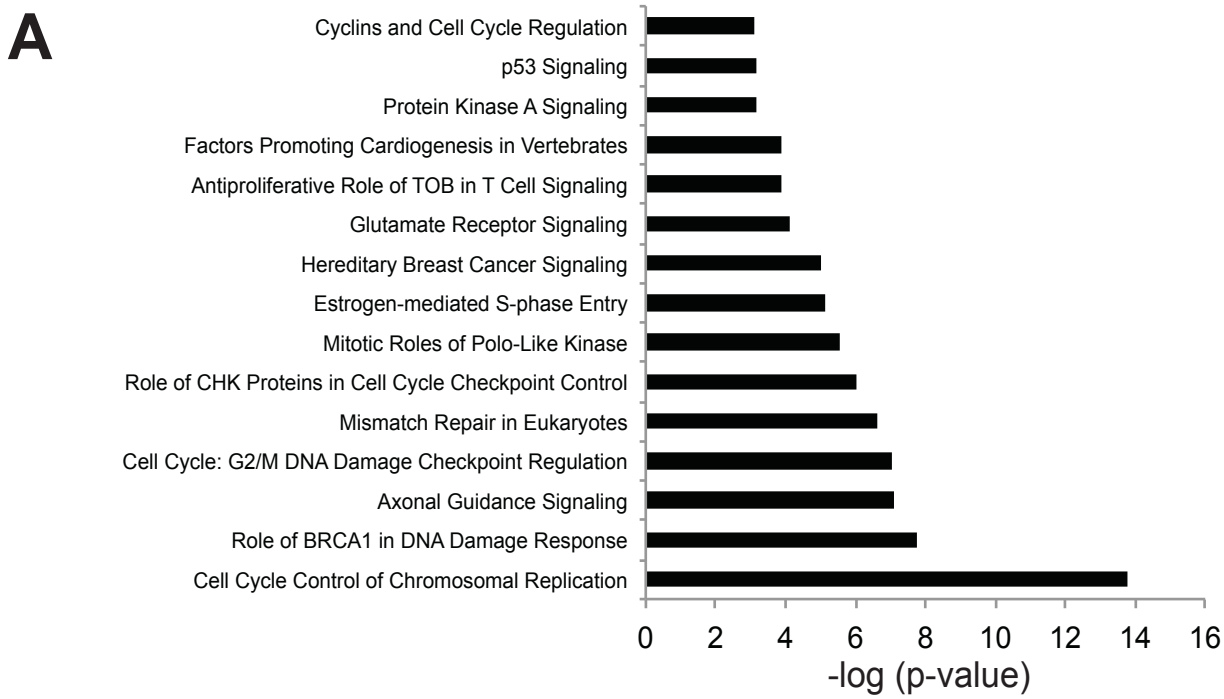
A
Cyclins and Cell Cycle Regulation
p53 Signaling
Protein Kinase A Signaling
Factors Promoting Cardiogenesis in Vertebrates
Antiproliferative Role of TOB in T Cell Signaling
Glutamate Receptor Signaling
Hereditary Breast Cancer Signaling
Estrogen-mediated S-phase Entry
Mitotic Roles of Polo-Like Kinase
Role of CHK Proteins in Cell Cycle Checkpoint Control
Mismatch Repair in Eukaryotes
Cell Cycle: G2/M DNA Damage Checkpoint Regulation
Axonal Guidance Signaling
Role of BRCA1 in DNA Damage Response
Cell Cycle Control of Chromosomal Replication
0 2 4 6 8 10 12 14 16
-log (p-value)

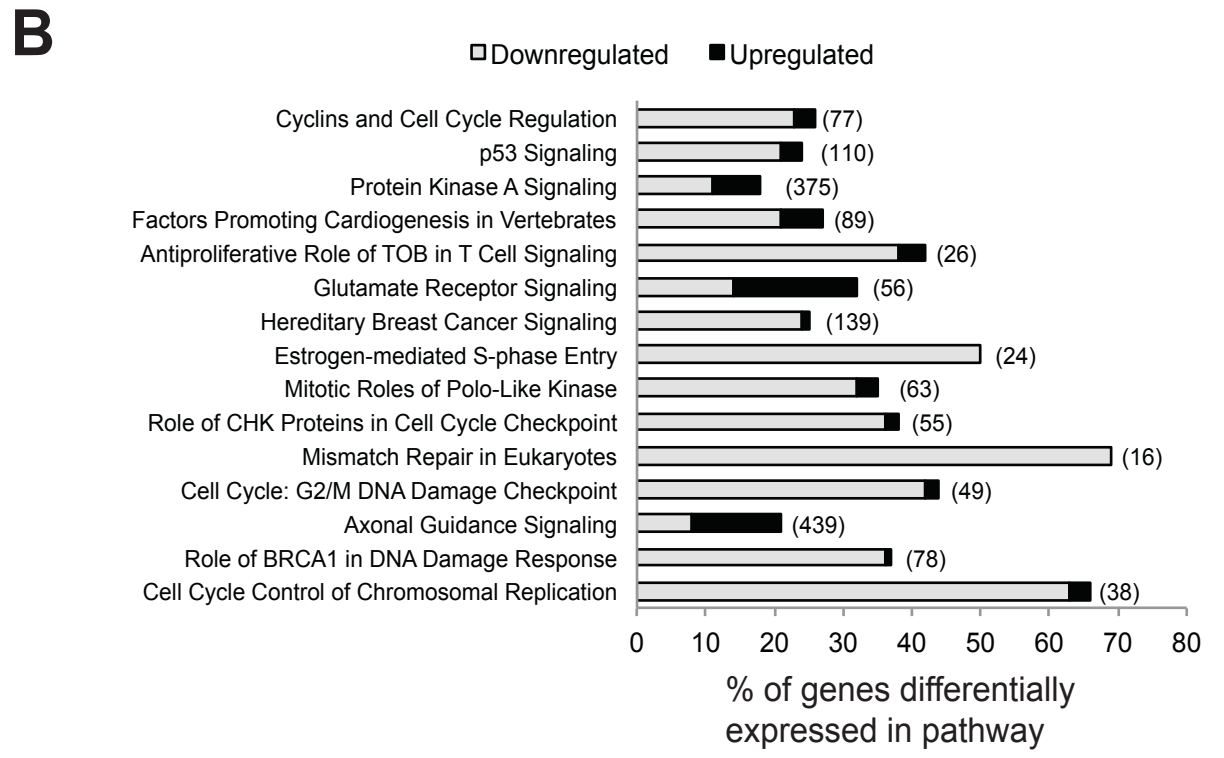
B
Downregulated
Upregulated
Cyclins and Cell Cycle Regulation (77)
p53 Signaling (110)
Protein Kinase A Signaling (375)
Factors Promoting Cardiogenesis in Vertebrates (89)
Antiproliferative Role of TOB in T Cell Signaling (26)
Glutamate Receptor Signaling (56)
Hereditary Breast Cancer Signaling (139)
Estrogen-mediated S-phase Entry (24)
Mitotic Roles of Polo-Like Kinase (63)
Role of CHK Proteins in Cell Cycle Checkpoint (55)
Mismatch Repair in Eukaryotes (16)
Cell Cycle: G2/M DNA Damage Checkpoint (49)
Axonal Guidance Signaling (439)
Role of BRCA1 in DNA Damage Response (78)
Cell Cycle Control of Chromosomal Replication (38)
0 10 20 30 40 50 60 70 80
% of genes differentially expressed in pathway

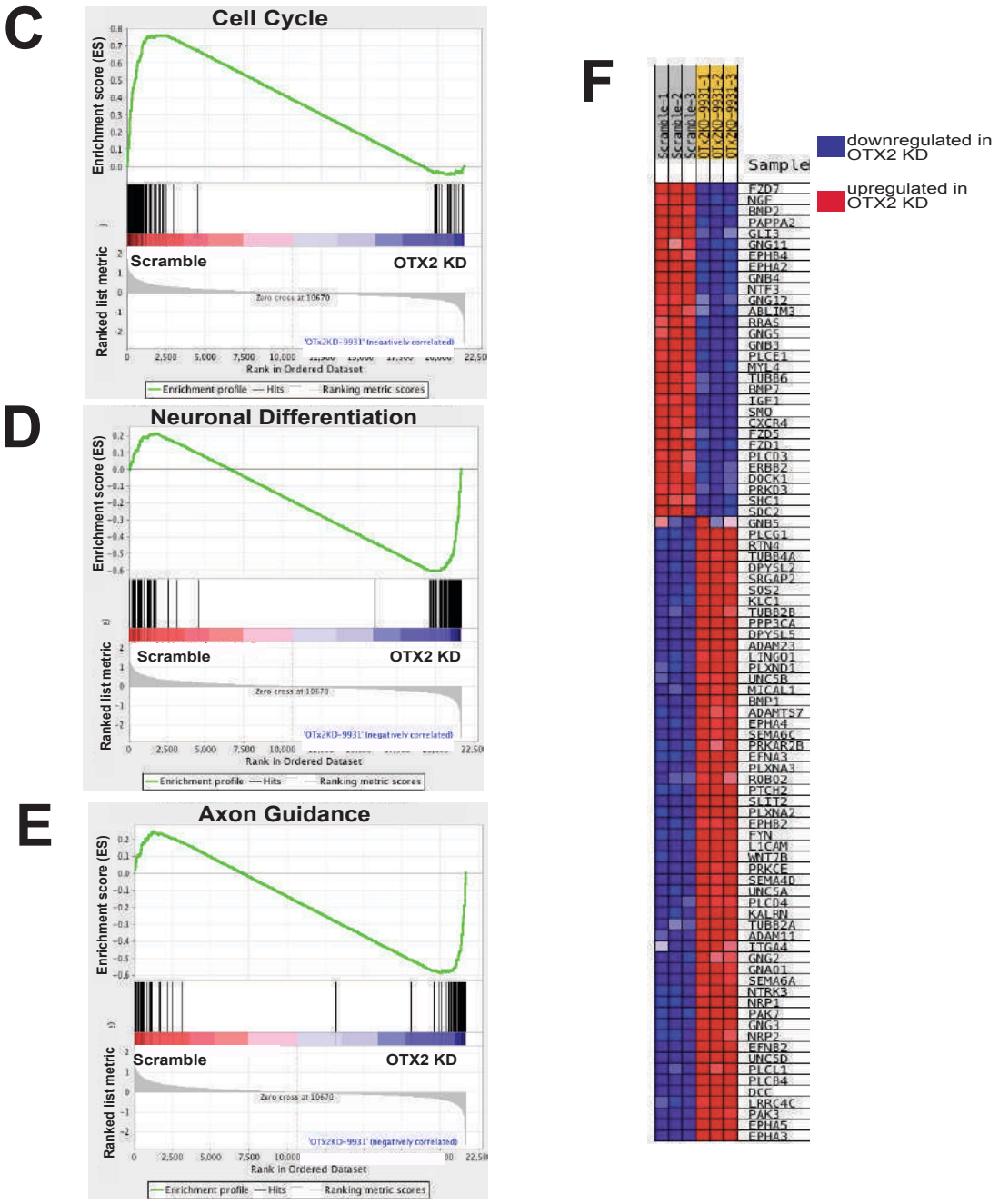

Figure 4.4: OTX2 knockdown increases expression of neuronal differentiation and axon guidance genes.

(**A-B**). IPA analysis showing major pathways (**A)** affected by OTX2 knockdown in D283 tumorspheres and the frequency of genes within these pathways (**B**) that are upregulated (black) and downregulated (grey). (**C**). Gene set enrichment analysis (GSEA) demonstrating enrichment of genes associated with cell cycle in the control scramble D283 tumorspheres. (**D-E**). GSEA demonstrating that neuronal differentiation and axon guidance genes are enriched in gene sets that are downregulated in the scramble and upregulated in the OTX2 knockdown D283 tumorspheres. (**F**). Representative heat map of genes that are significantly downregulated (blue) and upregulated (red) following OTX2 knockdown in D283 tumorspheres. Note that the majority of genes are upregulated following OTX2 knockdown. GSEA and representative heat map courtesy of Gareth Palidwor.

differentially expressed, 57 (or 63%) were upregulated following OTX2 KD (Figure 4.4F; Table S2, Table 1.2). The family of genes that regulate axon guidance has been found to play prominent roles in tumor progression [164], but to our knowledge, has never been associated with stem/progenitor cell populations in highly aggressive MB.

To determine whether axon guidance genes are directly or indirectly regulated by OTX2, chromatin immunoprecipitation (ChIP) sequencing (ChIP-Seq) was performed on high OTX2-expressing D283 tumorspheres. A clear, statistically significant association was observed between differential expression of axon guidance genes and the presence of one or more OTX2 binding peaks within -5kb to +2kb of the transcription start site (TSS) for each gene (Fisher Exact test; $p < 2.2e-16$) (Table 1.2). SEMA signaling was the most overrepresented pathway. SEMA genes are classically known as inhibitory axon growth cone guidance cues, but have also been found to play prominent roles in tumor cell proliferation, survival, cell adhesion, angiogenesis, and migration in other cancers [165, 166]. The SEMA ligands are membrane-bound or secreted proteins that mediate their effects mainly through plexin (PLXN) receptors with neuropilins (NRPs) often serving as co-receptors [166]. The transmembrane protein L1CAM interacts with NRP1 and is also a co-receptor [167]. Of the 9 SEMA ligands or receptors negatively correlated with OTX2 expression, 5 genes exhibited OTX2 overlaps/binding peaks and 2 genes (*NRP1* and *SEMA6C*) display OTX2-binding motifs (TAATCT and/or TAATCC) within the region of the TSS we investigated. As expression of all SEMA pathway genes was upregulated following OTX2 KD, our results suggest that in Group 3 and 4 MB, OTX2 may serve as a direct or indirect repressor of SEMA signaling. Moreover, our data reveal a novel role for SEMA pathway genes in the most aggressive MB subtypes.

Table 1.2: Axon guidance pathway genes that were significantly and differentially expressed following OTX2 knockdown and the number of OTX2 binding peaks/overlaps within -5kb-+2kb of their transcriptional start sites.

Gene Assignment	Fold change	Overlaps/OTX2-binding peaks
UNC5B	2.599856508	5
SLIT2	3.365945926	4
EFNB2	8.458995374	3
*SEMA6A**	5.542465942	3
PLXNA2	3.436757362	3
LRRC4C	3.696844429	3
KLC1	2.163857258	3
IGF1	0.467094383	3
SHC1	0.486217368	3
FZD5	0.456667281	3
GNG12	0.30012554	3
GNG3	6.14369672	2
NRP1	4.525936467	2
SEMA6C	2.811277756	2
FZD1	0.411479558	2
EPHA4	2.713058833	2
PLCE1	0.340932018	2
PLCD3	0.392306551	2
SRGAP2	2.107118816	2
NRP2	5.392071649	2
PLCL1	4.499103846	2
RRAS	0.324050897	2
GNG11	0.367793953	2
EPHA5	29.7964111	1
DCC	19.9143847	1
FZD7	0.082085886	1
EPHA3	35.96546453	1
UNC5D	8.093918561	1
PLCB4	9.425849634	1
SLIT1	13.04052457	1
GNB3	0.257122066	1
KALRN	4.807760401	1
EPHA2	0.185952064	1
BMP2	0.166236374	1
CXCR4	0.350026972	1
GNB4	0.294242592	1
EFNA3	3.293833584	1

PPP3CA	2.488226239	1
NGF	0.220082042	1
PTCH2	3.165072031	1
UNC5A	3.648270412	1
MYL4	0.356958518	1
WNT7B	3.035941518	1
DPYSL5	2.223862104	1
TUBB6	0.284219872	1
EFNA4	0.178674171	1
PLCD4	3.266598176	1
SDC2	0.492339251	1
SOS2	2.033516927	1
BMP7	0.414541181	1
MICAL1	2.42543301	1
GNG5	0.405713159	1
PRKD3	0.45951462	1
GNB5	2.131834339	1
ERBB2	0.438769353	1
ARPC1B	0.46707323	1
L1CAM	5.106598619	0
PAPPA2	0.14758633	0
GNAO1	5.746351854	0
PLXNA3	3.432025645	0
PAK3	5.539728734	0
PAK7	4.687338552	0
SEMA4D	3.456588028	0
ADAM23	2.299033785	0
EPHB2	2.728741378	0
SMO	0.422761137	0
BMP1	2.389216627	0
ADAM11	4.631441635	0
DPYSL2	2.284545748	0
LINGO1	2.15434803	0
ADAMTS7	2.484673007	0
EPHB4	0.273709611	0
TUBB4A	2.125011035	0
RTN4	2.057498911	0
PLXND1	2.284524635	0
DOCK1	0.465017957	0

*Semaphorin signaling genes highlighted in red.

4.2.2 Axon guidance genes are negatively correlated with OTX2 expression in tumorspheres from established and recently derived MB cell lines as well as Group 3 and Group 4 patient samples

We next validated the negative correlation between OTX2 and SEMA gene expression at the transcript and/or protein levels in established and recently derived MB cell lines as well as Group 3 and Group 4 patient samples. Several members of other axon guidance gene families (*SLIT2, EFNB2, EPHA3, EPHA5, DCC*) (Figure 4.5A-B), as well as select SEMA pathway genes, including SEMA ligands (*SEMA4D*, *SEMA6A*) and receptors *(NRP1*, *L1CAM*, *PLXNA2*) (Figure 4.6A-B) were evaluated in scramble and OTX2 KD tumorspheres from multiple MB cell lines by qPCR. OTX2 expression was negatively correlated with all axon guidance gene transcript levels (Figure 4.5A-C, Figure 4.6A-B).

Importantly, significant correlations between OTX2 and axon guidance pathway genes were also observed in patient samples. Using fully annotated Affymetrix Gene 1.1 ST Array datasets [168], transcript levels of axon guidance genes in those Group 3 and 4 tumors that exhibit amplification or overexpression of *OTX2* and those that do not were compared using a Pearson correlation co-efficient and a FDR<0.1. Next, 234 patient samples were interrogated, and 40 axon guidance genes showed a significant correlation with *OTX2* expression (Table 1.3). Of these 40 genes, 27 (68%) were negatively correlated with *OTX2* expression (Table 1.3). Interestingly, SEMA signaling was also the most overrepresented pathway in this dataset with 5 genes (*SEMA6A, SEMA4D, NRP1, NRP2* and *L1CAM*) all exhibiting a negative correlation with *OTX2* expression (Table 1.3). Importantly, lower expression of the SEMA ligand *SEMA4D* was associated with poor outcome (Figure 4.7A), suggesting a novel role for this gene as a Group 3 and 4 prognostic indicator.

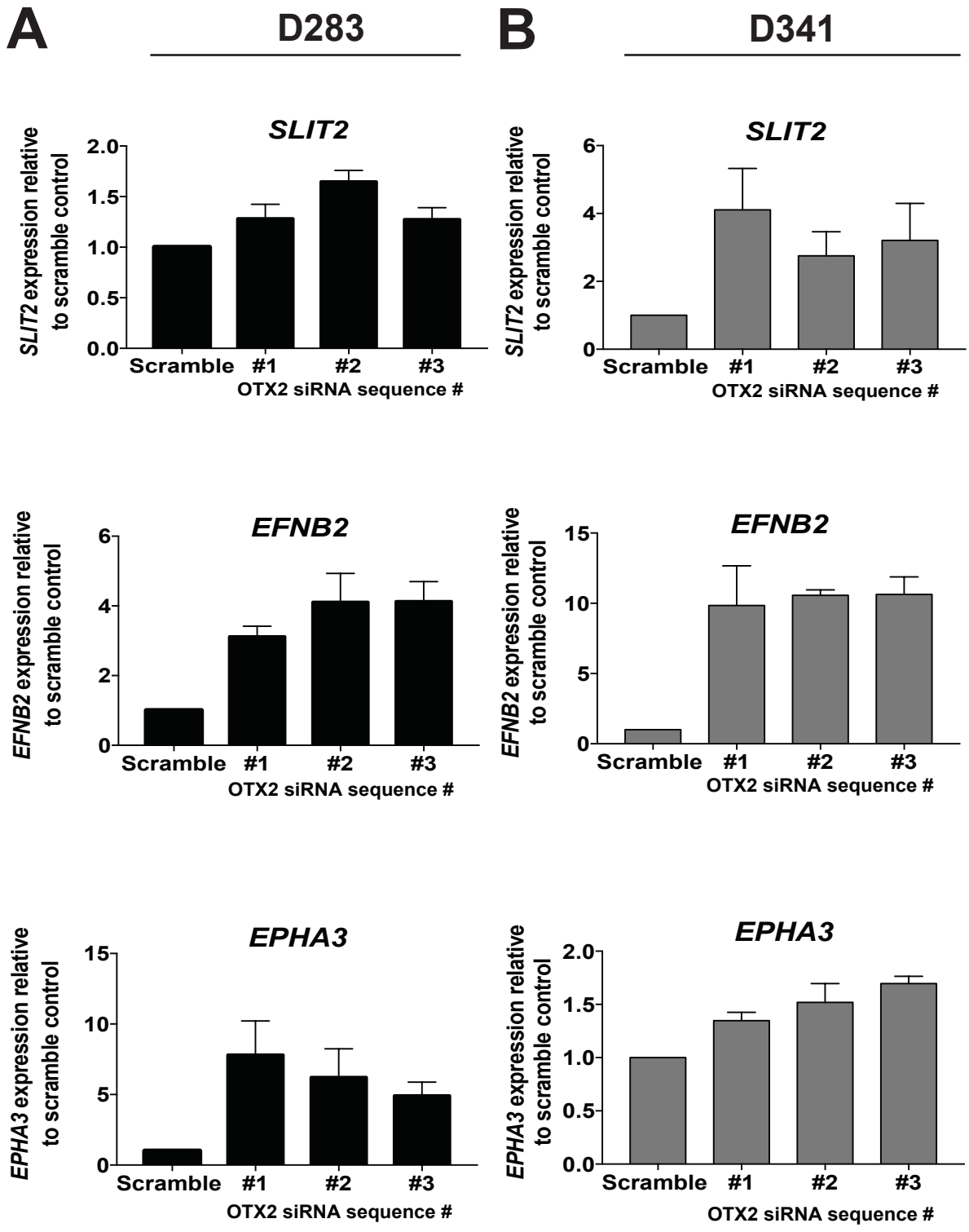
A
D283
B
D341
SLIT2
SLIT2 expression relative to scramble control
2.0
1.5
1.0
0.5
0.0
Scramble
#1
#2
#3
OTX2 siRNA sequence #
SLIT2
SLIT2 expression relative to scramble control
6
4
2
0
Scramble
#1
#2
#3
OTX2 siRNA sequence #
EFNB2
EFNB2 expression relative to scramble control
6
4
2
0
Scramble
#1
#2
#3
OTX2 siRNA sequence #
EFNB2
EFNB2 expression relative to scramble control
15
10
5
0
Scramble
#1
#2
#3
OTX2 siRNA sequence #
EPHA3
EPHA3 expression relative to scramble control
15
10
5
0
Scramble
#1
#2
#3
OTX2 siRNA sequence #
EPHA3
EPHA3 expression relative to scramble control
2.0
1.5
1.0
0.5
0.0
Scramble
#1
#2
#3
OTX2 siRNA sequence #

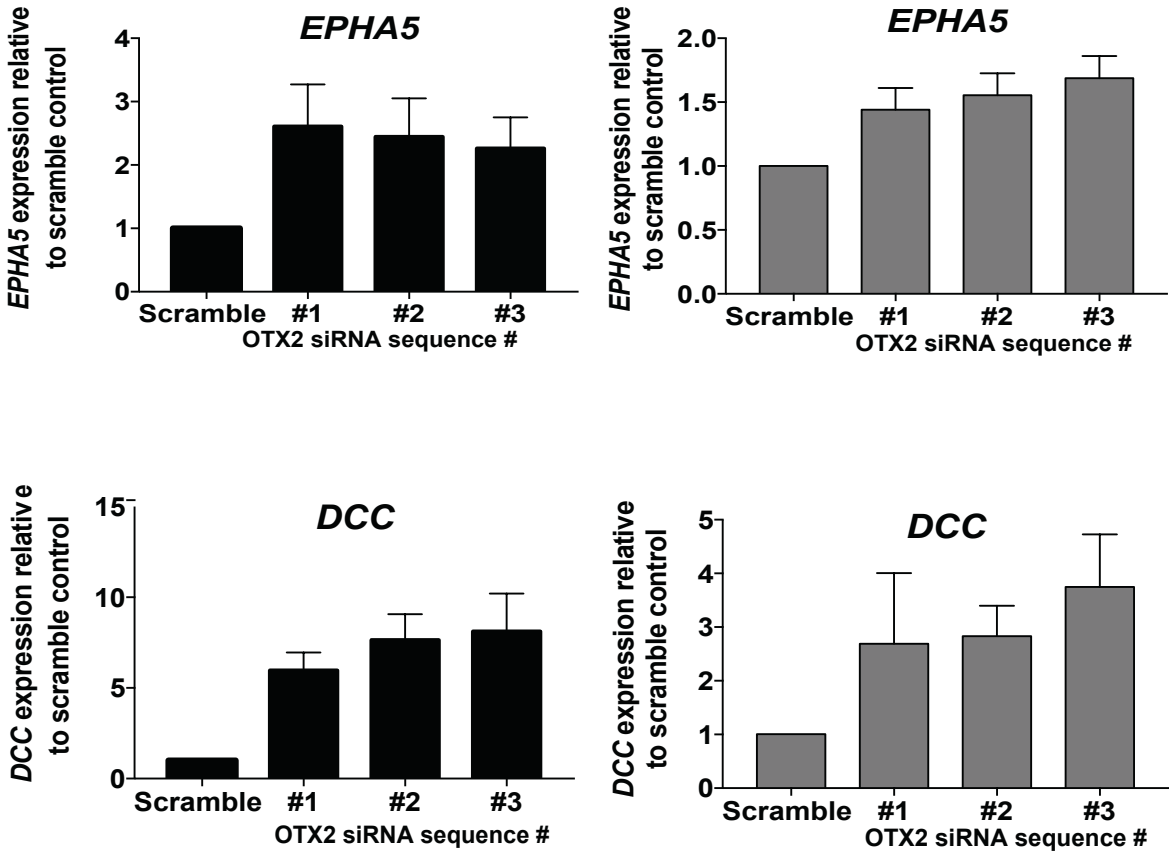

Figure 4.5: Axon guidance genes are negatively correlated with OTX2 expression in D283 and D341 MB cell lines.

(**A-B**). Expression of select axon guidance pathway genes, *SLIT2, EFNB2, EPHA3, EPHA5*, and *DCC* in D283 (**A**) and D341 (**B**) MB tumorspheres following OTX2 knockdown using 3 siRNAs by qPCR. Error bars: s.e.m. N=3 biological replicates and n=9 technical replicates performed.

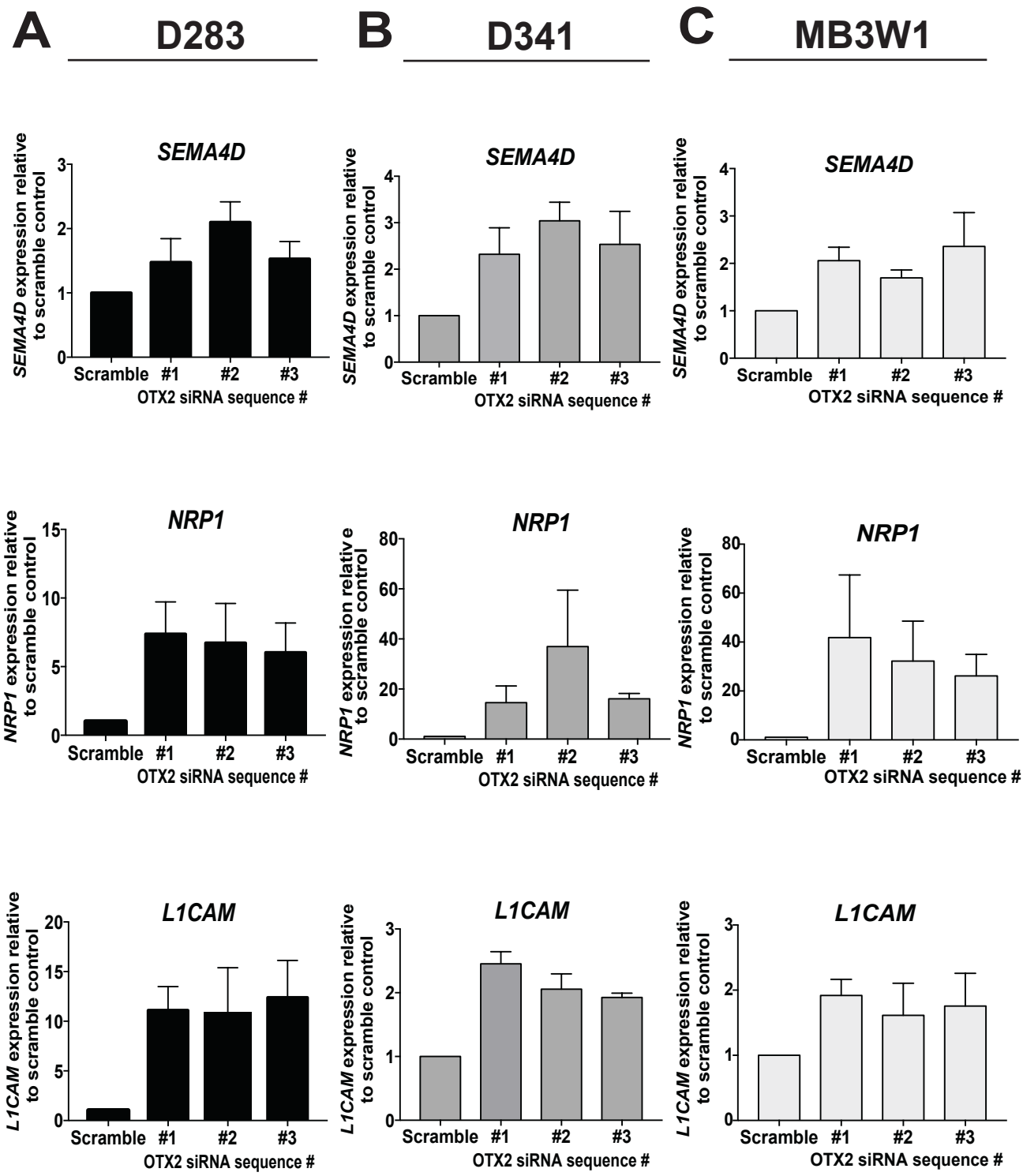
A
D283
B
D341
C
MB3W1
SEMA4D
SEMA4D expression relative to scramble control
Scramble #1 #2 #3
OTX2 siRNA sequence #
NRP1
NRP1 expression relative to scramble control
L1CAM
L1CAM expression relative to scramble control

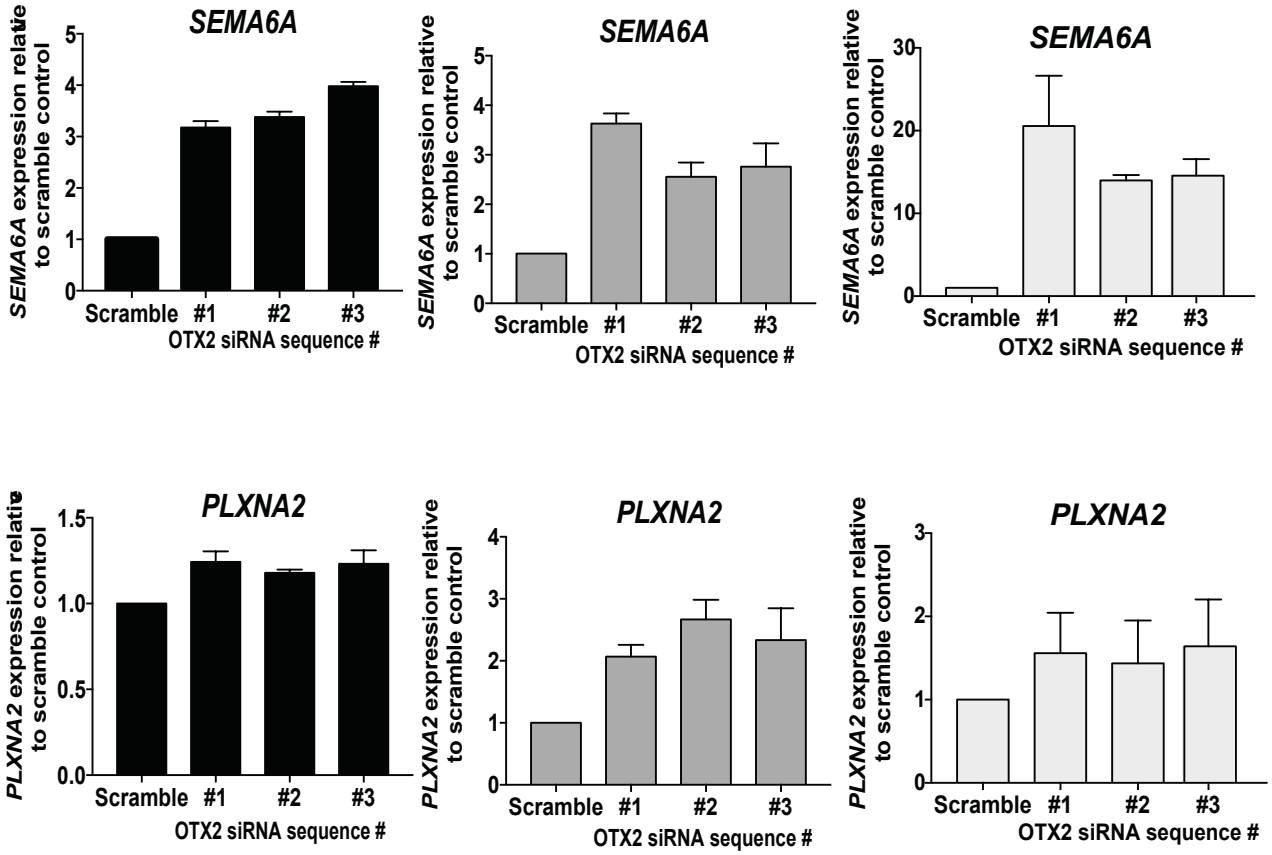

Figure 4.6: Semaphorin genes are negatively correlated with OTX2 expression in D283, D341 and MB3W1 MB cell lines.

(**A-C**). Expression of select semaphorin pathway genes, *SEMA4D, NRP1, L1CAM, SEMA6A,* and *PLXNA2* in D283 (**A**), D341 (**B**) and MB3W1 (**C**) MB tumorspheres following OTX2 knockdown using 3 siRNAs by qPCR. Error bars: s.e.m. N=3 biological replicates and n=9 technical replicates performed.

Table 1.3: Correlation between OTX2 and expression of axon guidance genes in Group 3 and 4 MB patient samples.

Gene Assignment	Pearson coefficient[A]	Pearson P-value	Pearson Q-value
GLI3	-0.552	0	0
MICAL1	-0.385	0	0
ROBO2	-0.375	0	0
ABLIM3	-0.374	0	0
DPYSL2	-0.329	0	0
PAK7	-0.321	0	0
SEMA6A	**-0.281**	**0**	**0**
CXCR4	-0.272	0	0
NRP1	**-0.269**	**0**	**0**
GNB4	-0.267	0	0
SRGAP2	-0.26	0	0
SHC1	-0.254	0	0
NRP2	**-0.254**	**0**	**0**
LINGO1	-0.245	0	0.001
EPHB4	-0.234	0	0.001
ADAM23	-0.227	0	0.002
ADAM11	-0.223	0.001	0.002
BMP2	-0.215	0.001	0.003
PLCB4	-0.198	0.002	0.006
PLCL1	-0.179	0.006	0.015
UNC5A	-0.173	0.008	0.02
SEMA4D	**-0.163**	**0.013**	**0.03**
EPHA5	-0.147	0.025	0.053
NGF	-0.14	0.033	0.065
LRRC4C	-0.14	0.033	0.065
L1CAM	**-0.14**	**0.033**	**0.065**
EPHA3	-0.133	0.042	0.079
SMO	0.136	0.038	0.074
GNG5	0.152	0.02	0.043
GNB5	0.162	0.013	0.031
EPHA2	0.185	0.005	0.012
KLC1	0.199	0.002	0.006
UNC5D	0.218	0.001	0.002
PAPPA2	0.224	0.001	0.002
PRKAR2B	0.228	0	0.002
PRKD3	0.229	0	0.002
ERBB2	0.239	0	0.001
FZD1	0.268	0	0
SOS2	0.314	0	0
GNB3	0.32	0	0

[A] Pearson coefficient; measure of linear correlation between OTX2 and the axon guidance genes.

Of the 5 SEMA pathway genes negatively correlated with OTX2 expression in Group 3 and Group 4 patient samples, *L1CAM* and *NRP1* were most strongly upregulated following OTX2 KD in tumorspheres (Figure 4.7B), and SEMA4D was associated with prognosis (Figure 4.7A). Thus, we chose these 3 genes for additional analyses at the protein level. Upon OTX2 KD, we observed an increase in L1CAM, NRP1 and SEMA4D protein concomitant with an increase in the neuronal marker ßIII tubulin by Western blot in D283 tumorspheres (Figure 4.7B). This was also observed in tumorspheres derived from the recently established MB3W1 Group 3 cell line [153] (Figure 4.7C). Collectively, these results provide further support for the idea that axon guidance genes, particularly those belonging to the SEMA signaling pathway, are putative tumor suppressors in Group 3 and Group 4 MB.

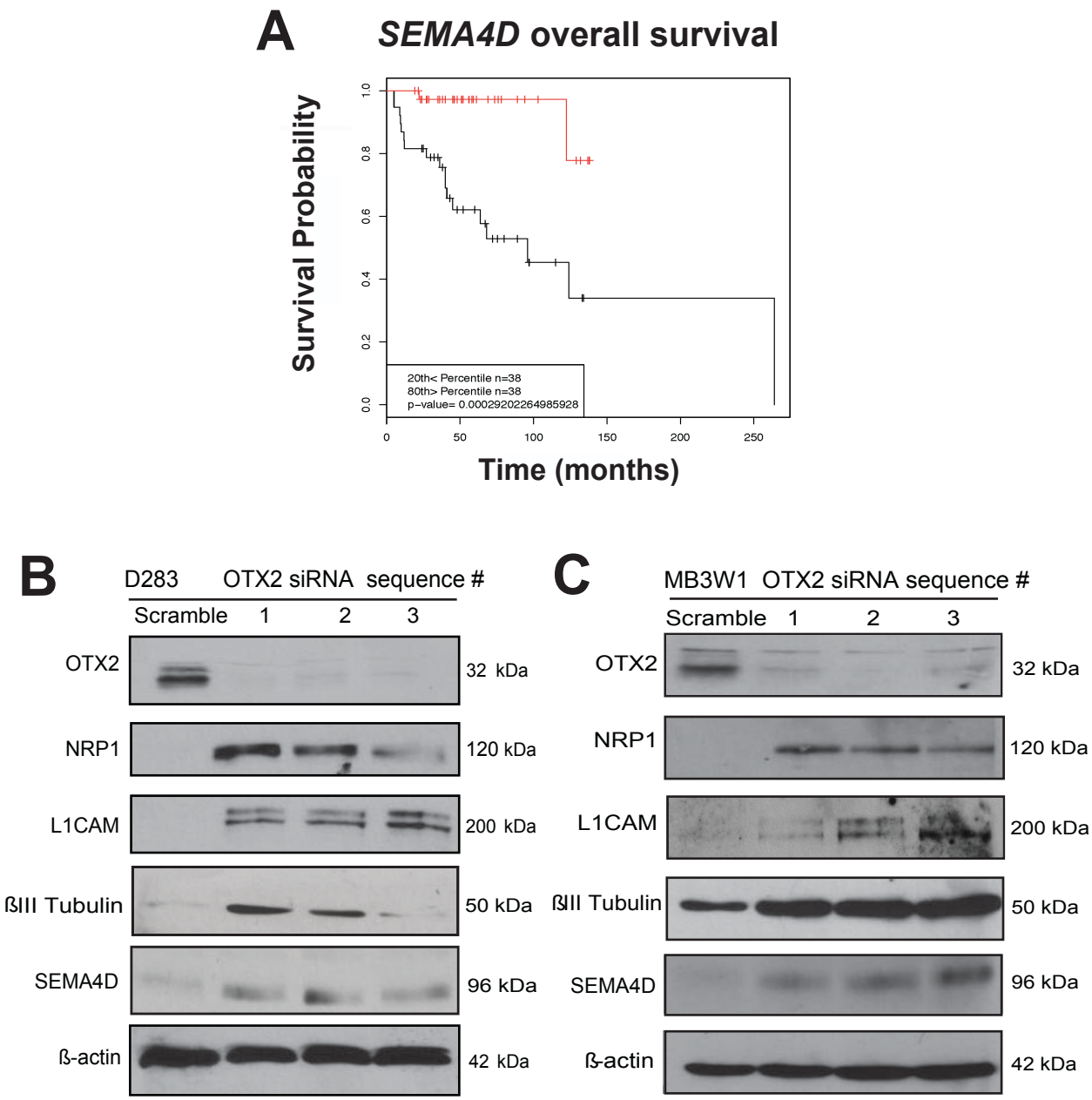

Figure 4.7: Semaphorin genes are negatively correlated with OTX2 expression in established and newly derived cell lines as well as patient samples.
(**A**). Kaplan-Meier curves of Group 3 and Group 4 patients with high (red) and low (black) *SEMA4D*. (**B**). Western blots depicting increases in NRP1, L1CAM, SEMA4D, and ßIII tubulin protein levels following OTX2 knockdown in D283 tumorspheres. β-actin serves as a loading control. (**C**). Western blots depicting increases in NRP1, L1CAM, SEMA4D and ßIII tubulin protein levels following OTX2 knockdown in recently derived MB3W1 tumorspheres. β-actin serves as a loading control. N=3 biological replicates.

4.2.3 Increased semaphorin levels are inversely correlated with tumorsphere formation, self-renewal and growth in MB tumorspheres

To further explore the relationship between OTX2 and SEMA pathway genes in regulating cell function *in vitro,* we employed biochemical and genetic approaches to test how modulation of OTX2 and SEMA pathway gene expression affects MB self-renewal and growth. Recombinant human L1CAM (Figure 4.8A-C), SEMA4D (Figure 4.9A-C), and NRP1 (Figure 4.10A-C) Fc chimera proteins were added to D283 tumorsphere cultures (50-1000 ng/ml) and evaluated over passage. Increasing concentrations of recombinant SEMA4D Fc, L1CAM Fc, and NRP1 Fc chimera resulted in a dose-dependent decrease in both primary and secondary tumorsphere formation (Figure 4.8A-C, 4.9A-C, 4.10A-C), without affecting growth and viability (Figure 4.11A-F); however, only the highest concentration (1000 ng/ml) was significant. These results suggest that increased levels of SEMA pathway proteins are associated with a decrease in self-renewal capacity in Group 3 and 4 MB tumorspheres.

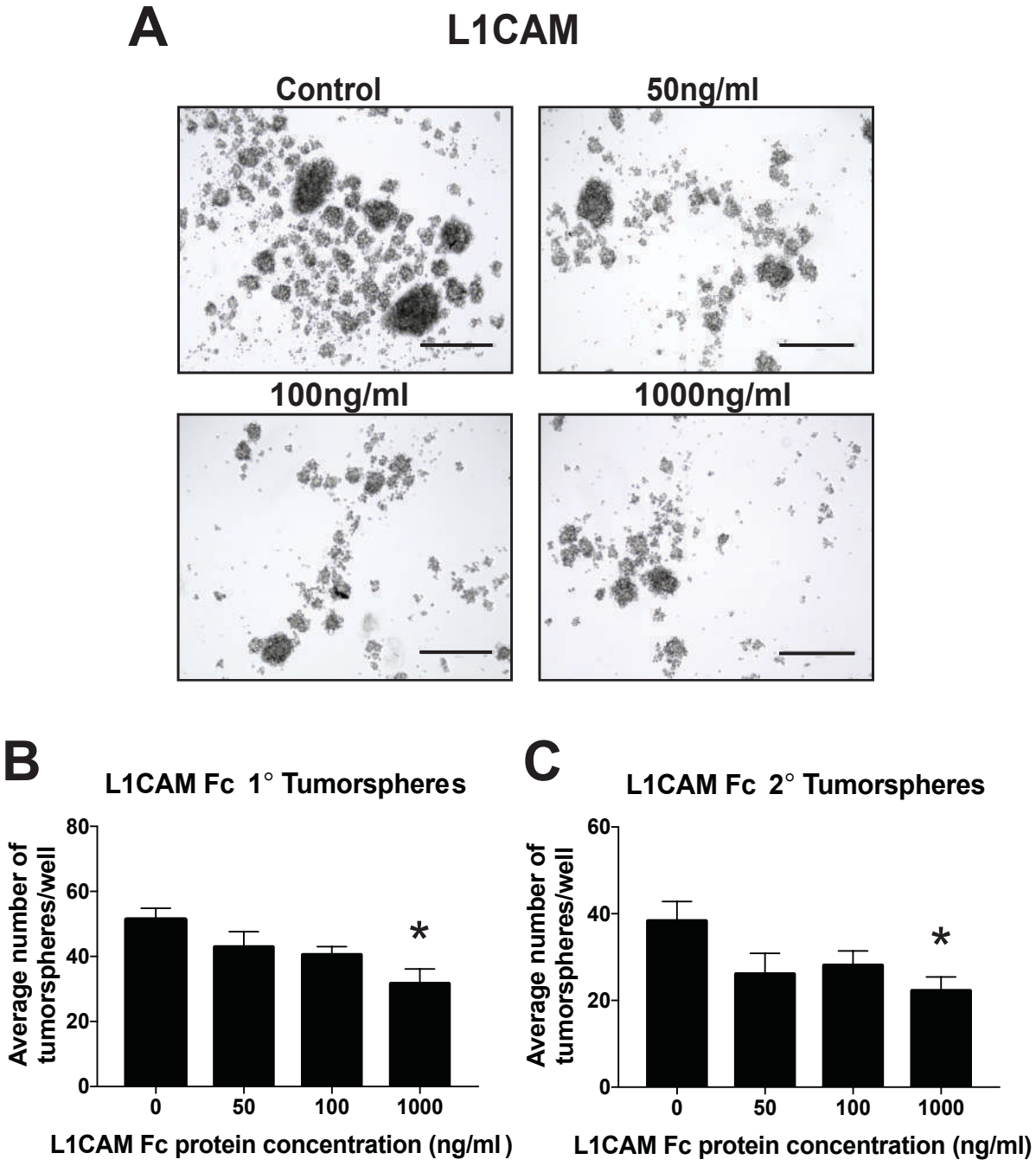

Figure 4.8: Recombinant L1CAM Fc treatment decreased self-renewal.
(A). Representative images of D283 tumorspheres following 5-day treatment with recombinant L1CAM Fc (**A**) chimera protein. (**B-C**). Total number of primary (left) (**B**) and secondary (right) (**C**) tumorspheres following 5-day treatment with L1CAM Fc. Error bars: s.e.m. $p<0.05$ *. Scale bar: 400 μm. N=4 biological replicates and n=20 technical replicates were performed.

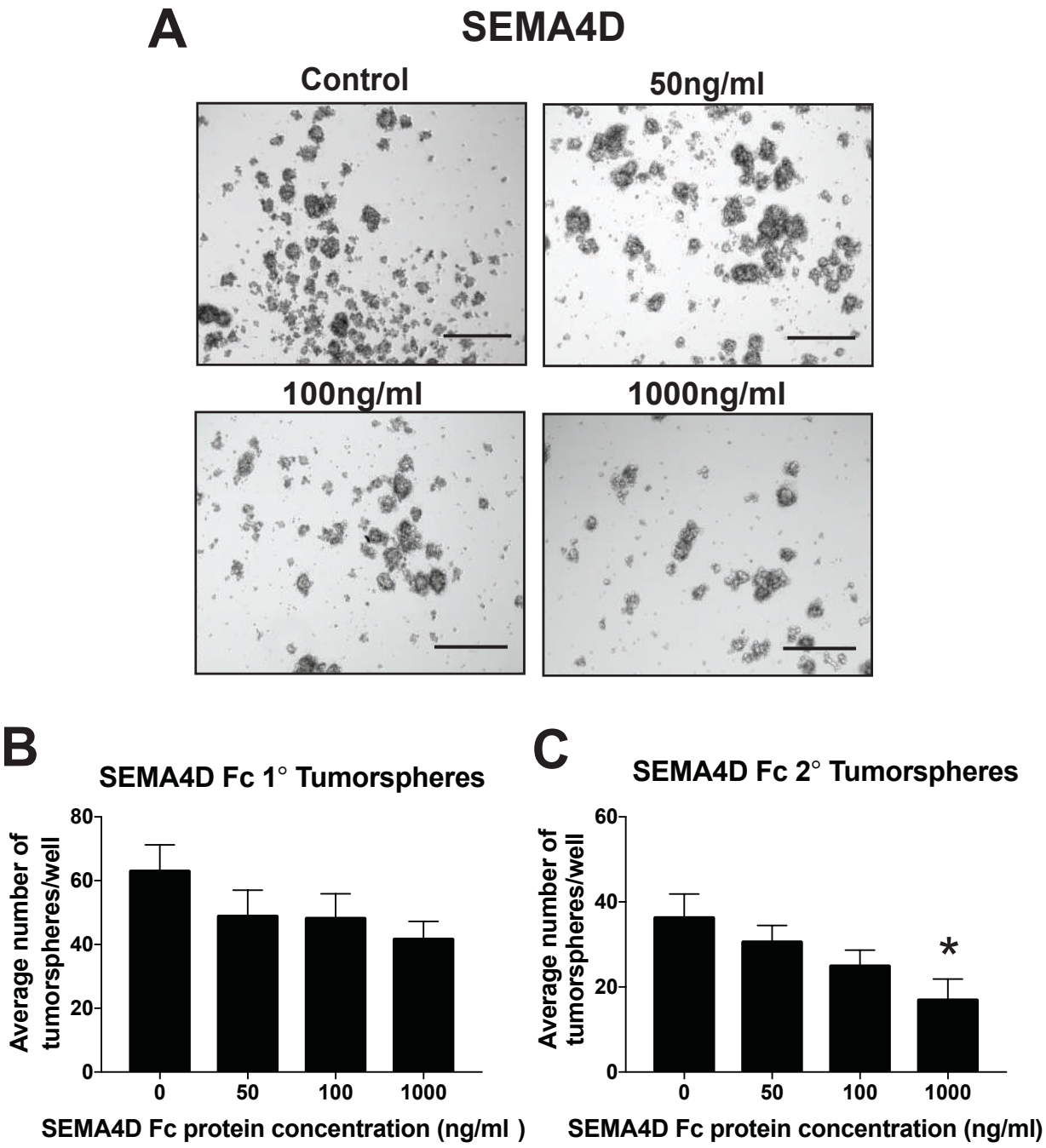

Figure 4.9: Recombinant SEMA4D Fc treatment decreased self-renewal.
(**A**). Representative images of D283 tumorspheres following 5-day treatment with recombinant SEMA4D Fc (**A**) chimera protein. (**B-C**). Total number of primary (left) (**B**) and secondary (right) (**C**) tumorspheres following 5-day treatment with SEMA4D Fc. Error bars: s.e.m. $p<0.05$ *. Scale bar: 400 μm. N=4 biological replicates and n=18 technical replicates were performed.

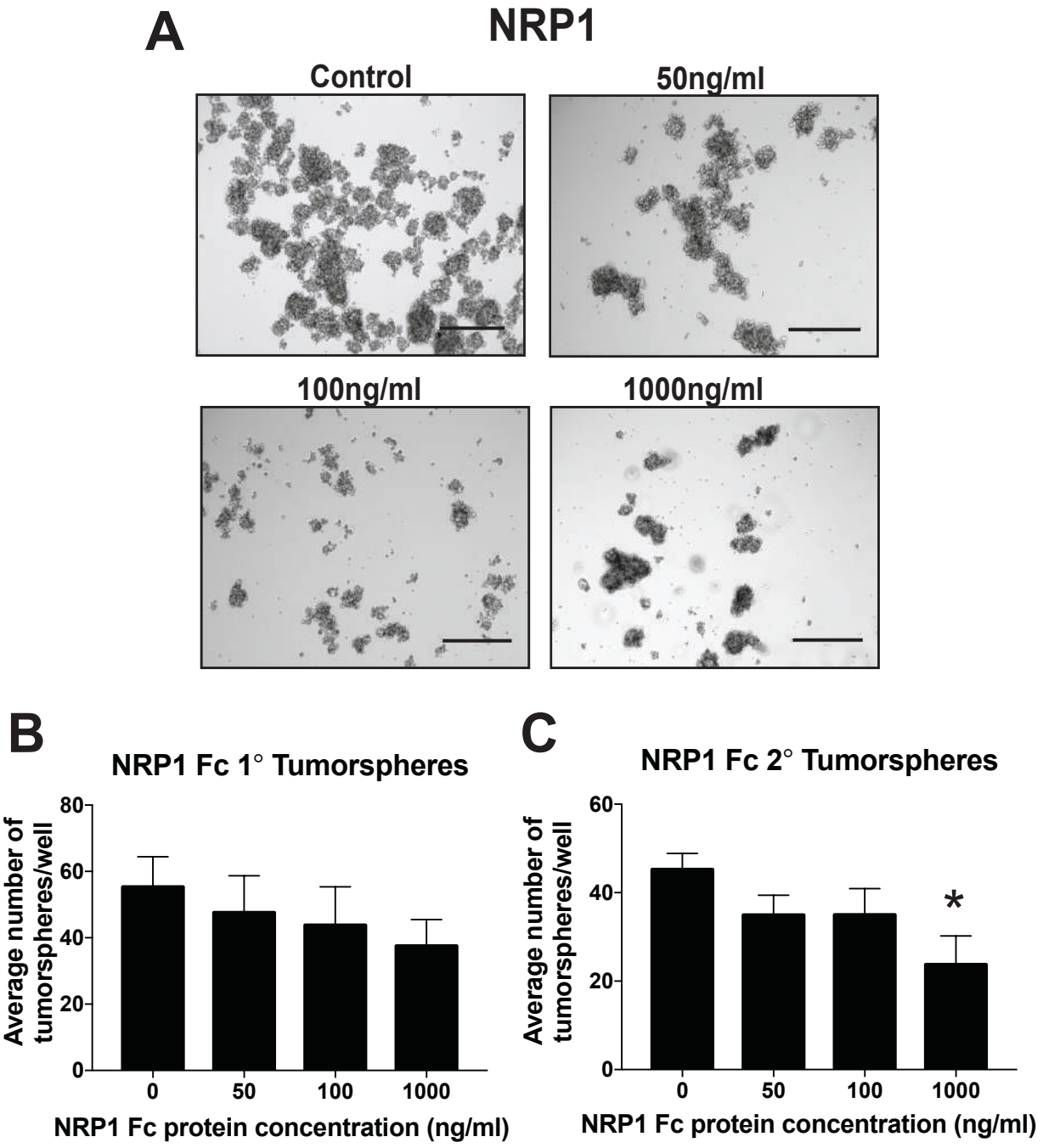

Figure 4.10: Recombinant NRP1 Fc treatment decreased self-renewal.
(A). Representative images of D283 tumorspheres following 5-day treatment with recombinant NRP1 Fc (**A**) chimera protein. (**B-C**). Total number of primary (left) (**B**) and secondary (right) (**C**) tumorspheres following 5-day treatment with NRP1 Fc. Error bars: s.e.m. $p<0.05$ *. Scale bar: 400 μm. N=4 biological replicates and n=18 technical replicates were performed.

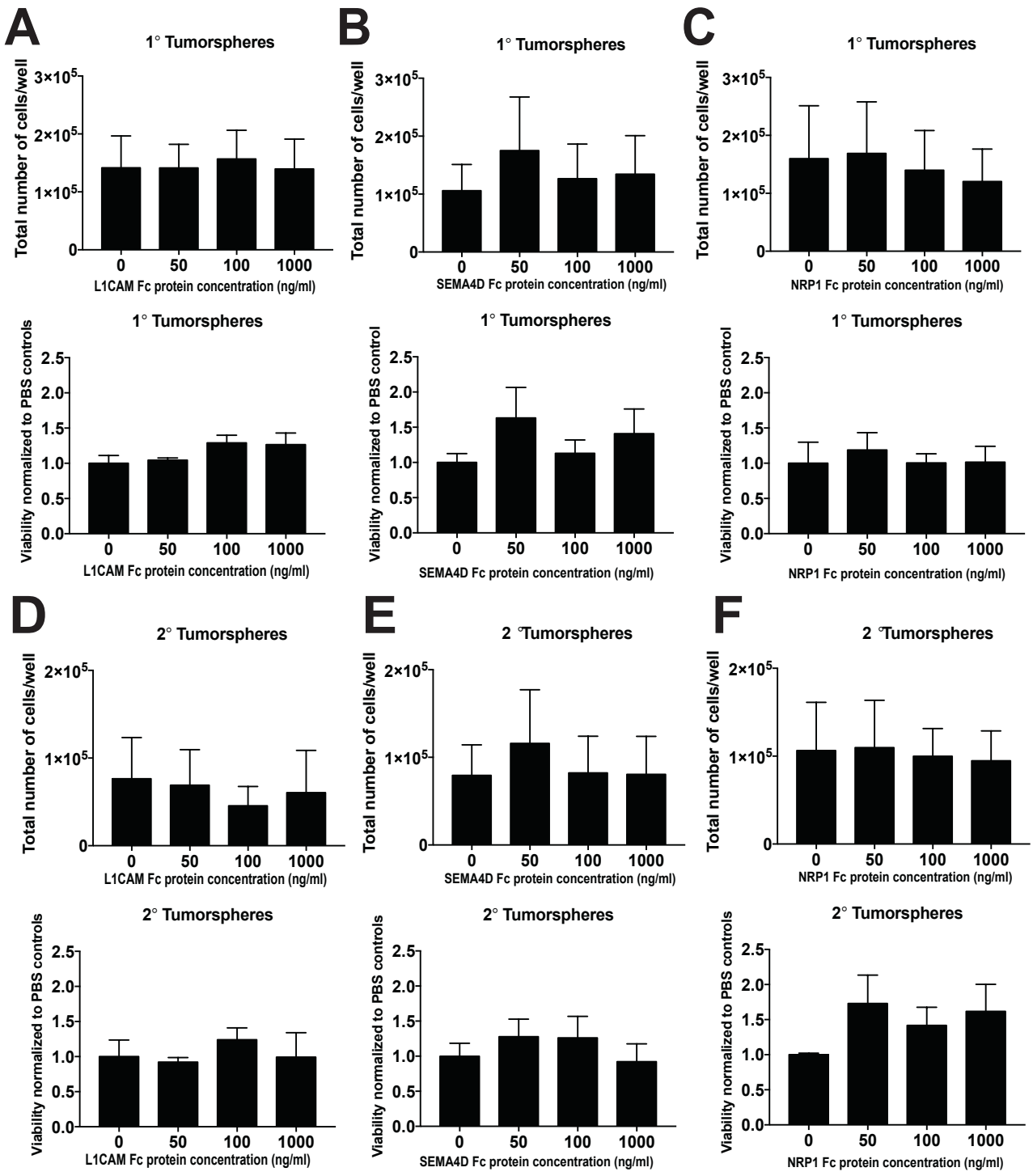

Figure 4.11: Recombinant semaphorin protein treatment does not significantly affect cell number or viability of D283 tumorspheres.

(A-C). Total number of cells (upper) and viability (lower) in primary D283 tumorspheres following 5-day treatment with recombinant L1CAM Fc (**A**), SEMA4D Fc (**B**) or NRP1 Fc (**C**) chimera proteins. N=4 biological replicates. Error bars: s.e.m. (**D-F**). Total number of cells (upper) and viability (lower) in secondary D283 tumorspheres following 5-day treatment with L1CAM Fc (**D**) SEMA4D (E) or NRP1 (**F**) chimera proteins. Error bars: s.e.m. N=4 biological replicates.

In addition to evaluating the effects of increased SEMA gene levels, we also asked whether downregulation of L1CAM, SEMA4D, and NRP1 reverses the OTX2-KD phenotype in Group 3 and 4 MB cells by increasing self-renewal and growth. To accomplish this, we performed dual OTX2/SEMA gene KD experiments in D283 tumorspheres. OTX2 was knocked down using 1 of our validated siRNA sequences at day 0 (s9931 or s9932, as these resulted in the most significant phenotypic change (Figure 4.1A), and then at day 2, cells were treated with either 2 independent *SEMA4D*, *NRP1* or *L1CAM* siRNA sequences or a non-silencing scramble siRNA (negative control). Dual KD was successful for L1CAM at the protein level (Figure 4.12A-B), but no rescue in tumorsphere formation or cell number was evident in OTX2 KD/L1CAM KD tumorspheres (Figure 14.12B-D). Dual KD was successful for SEMA4D at the protein level (Figure 4.13A-B), and we observed a partial rescue in both tumorsphere formation and cell number for OTX2 KD/SEMA4D KD (Figure 4.13C-D). The dual KD was also successful for NRP1 at the protein level (Figure 14A-B), while again only a partial rescue in both tumorsphere formation and cell number for OTX2 KD/NRP1 KD tumorspheres was observed (Figure 4.14C-D). The most significant increase in tumorsphere number was observed following dual OTX2/SEMA4D KD (28% and 30% increase in tumorsphere number using SEMA4D Seq#1 and Seq#2 respectively relative to OTX2 KD alone) (Figure 4.13C), and the most significant increase in cell number was seen in dual OTX2/NRP1 KD tumorspheres (56% and 43% increase in the average number of cells/well using NRP1 Seq#1 and Seq#2 respectively relative to OTX2 KD alone) (Figure 4.14D). Similar results were obtained for MB3W1 tumorspheres in which a small increase in sphere number and a significant increase in cell number were observed following dual OTX2/SEMA4D or OTX2/NRP1 KD (Figure 4.15). For both D283 and MB3W1 tumorspheres, there was no significant change in viability as measured

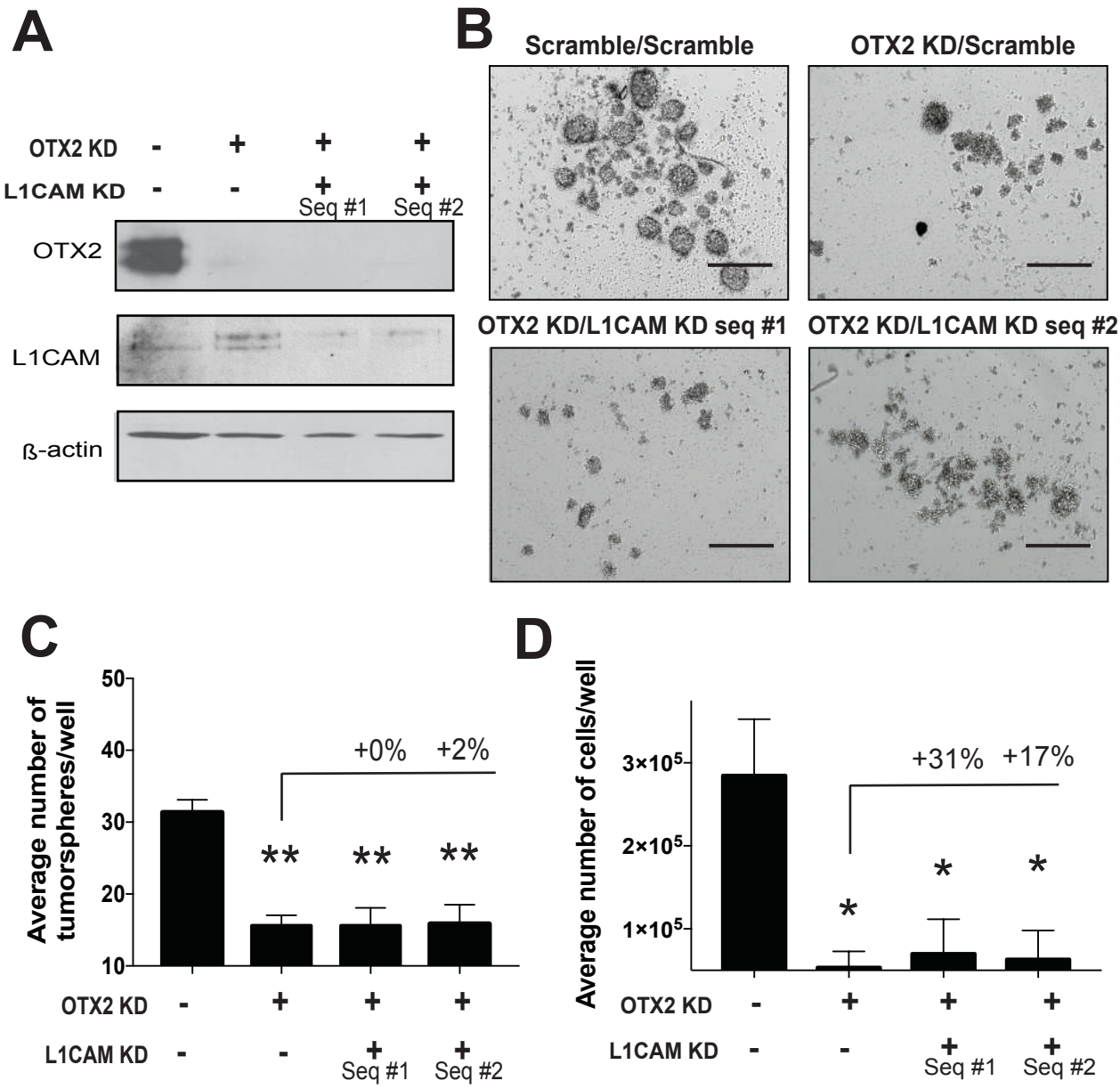

Figure 4.12: Decreased levels of L1CAM in OTX2 knockdown cells results in no rescue of tumorsphere formation and growth.

(**A**). Western blots depicting OTX2 and L1CAM protein levels following dual OTX2 and L1CAM knockdown in D283 tumorspheres over 5 days. β-actin serves as a loading control. (**B**). Representative images of D283 tumorspheres following dual OTX2 and L1CAM knockdown. Scale bar: 400 µm. (**C**). Quantification of tumorsphere number following dual OTX2 and L1CAM knockdown in D283 tumorspheres over 5 days. Error Bars: s.e.m. $p<0.01$**. N=3 biological replicates and n=12 technical replicates. (**D**). Quantification of total cell number following dual OTX2 and either L1CAM knockdown in D283 tumorspheres over 5 days. Error Bars: s.e.m. $p<0.05$*. N=3 biological replicates.

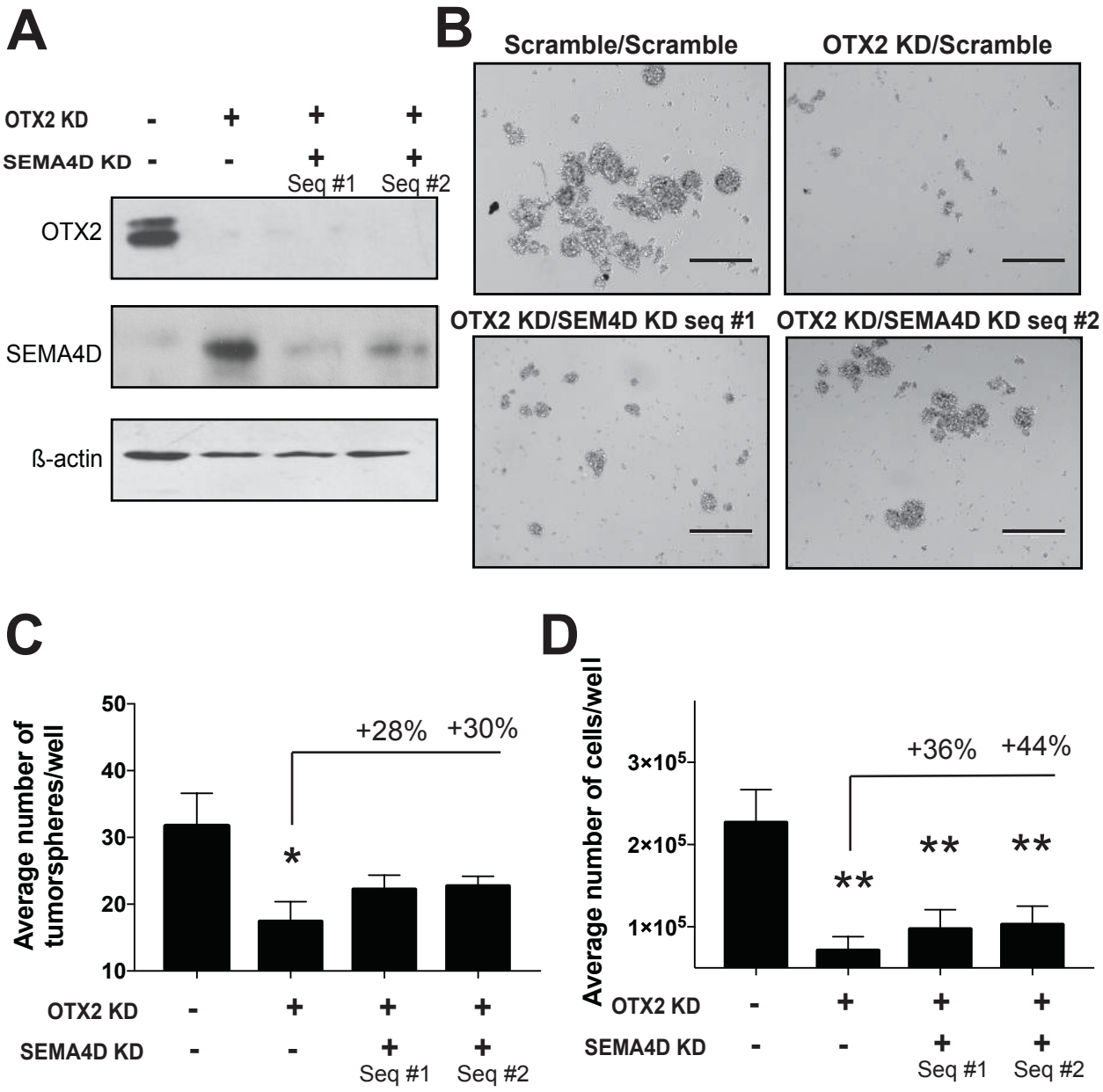

Figure 4.13: Decreased levels of SEMA4D in OTX2 knockdown cells results in a partial rescue of tumorsphere formation and growth.
(**A**). Western blots depicting OTX2 and SEMA4D protein levels following dual OTX2 and SEMA4D knockdown in D283 tumorspheres over 5 days. β-actin serves as a loading control. (**B**). Representative images of D283 tumorspheres following dual OTX2 and SEMA4D knockdown. Scale bar: 400 µm. (**C**). Quantification of tumorsphere number following dual OTX2 and SEMA4D knockdown in D283 tumorspheres over 5 days. Error Bars: s.e.m. $p<0.05$*. N=4 biological replicates and n=12 technical replicates. (**D**). Quantification of total cell number following dual OTX2 and either SEMA4D knockdown in D283 tumorspheres over 5 days. Error Bars: s.e.m. $p<0.01$**. N=8 biological replicates.

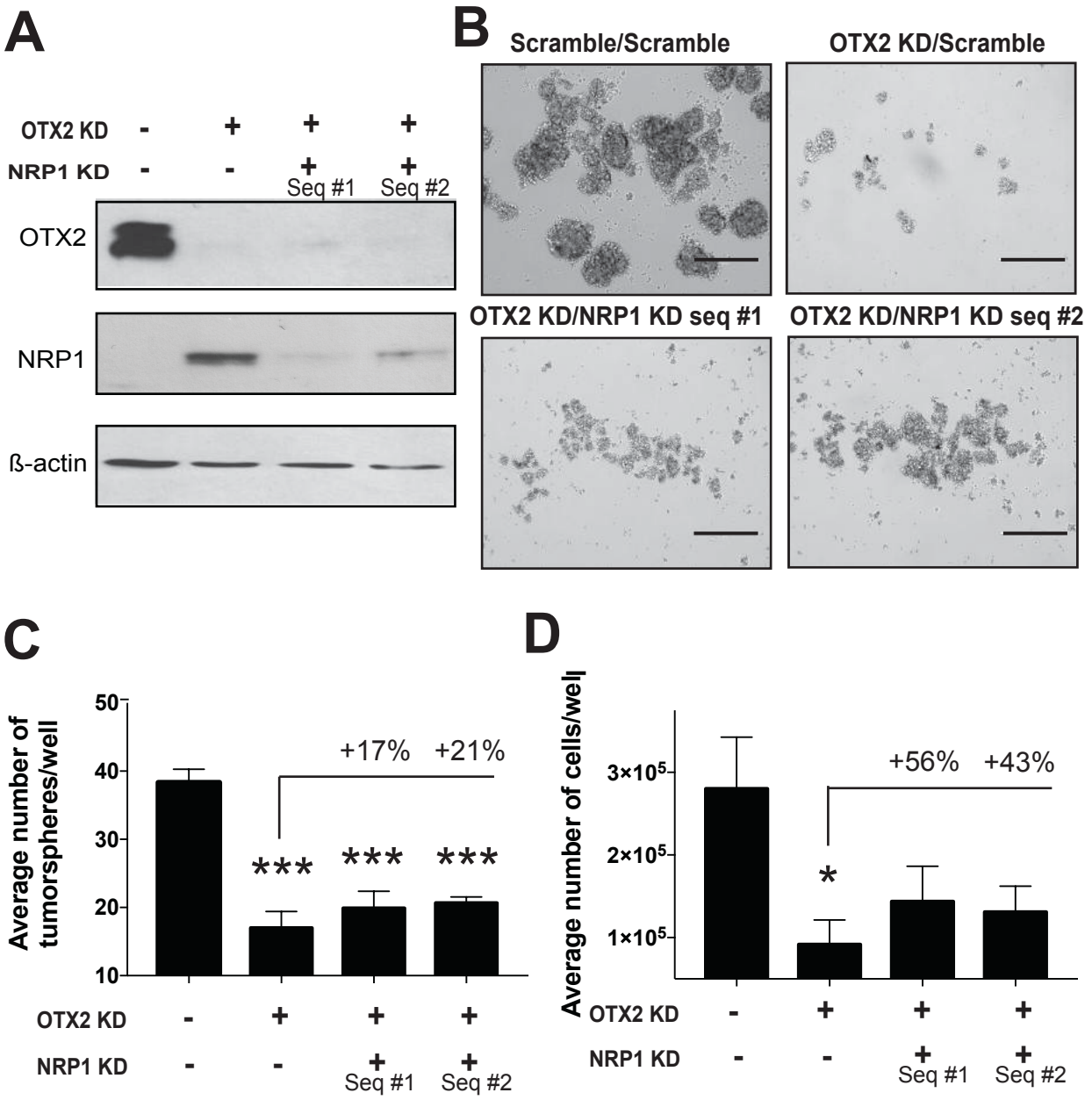

Figure 4.14: Decreased levels of NRP1 in OTX2 knockdown cells results in a partial rescue of tumorsphere formation and growth.

(**A**). Western blots depicting OTX2 and NRP1 protein levels following dual OTX2 and NRP1 knockdown in D283 tumorspheres over 5 days. β-actin serves as a loading control. (**B**). Representative images of D283 tumorspheres following dual OTX2 and NRP1 knockdown. Scale bar: 400 µm. (**C**). Quantification of tumorsphere number following dual OTX2 and NRP1 knockdown in D283 tumorspheres over 5 days. Error Bars: s.e.m., $p<0.001$***. N=4 biological replicates and n=12 technical replicates. (**D**). Quantification of total cell number following dual OTX2 and either L1CAM knockdown in D283 tumorspheres over 5 days. Error Bars: s.e.m. $p<0.05$*. N=7 biological replicates.

A

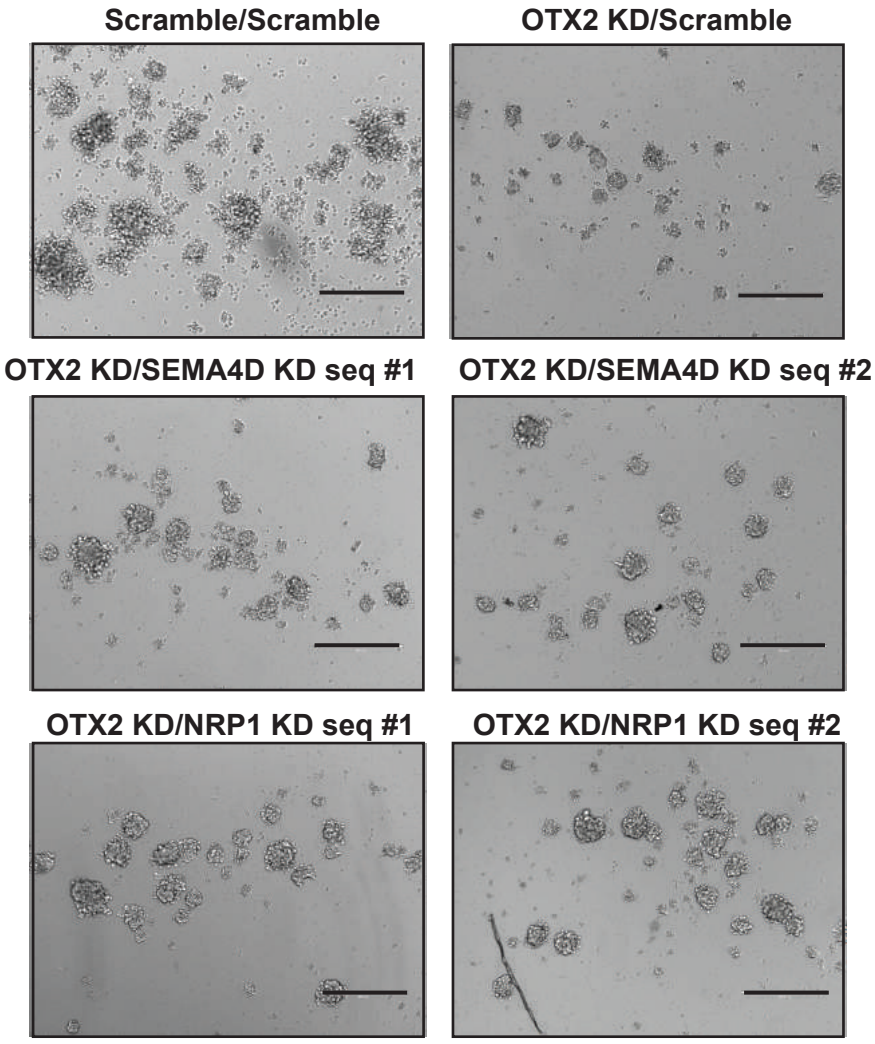
Scramble/Scramble
OTX2 KD/Scramble
OTX2 KD/SEMA4D KD seq #1
OTX2 KD/SEMA4D KD seq #2
OTX2 KD/NRP1 KD seq #1
OTX2 KD/NRP1 KD seq #2

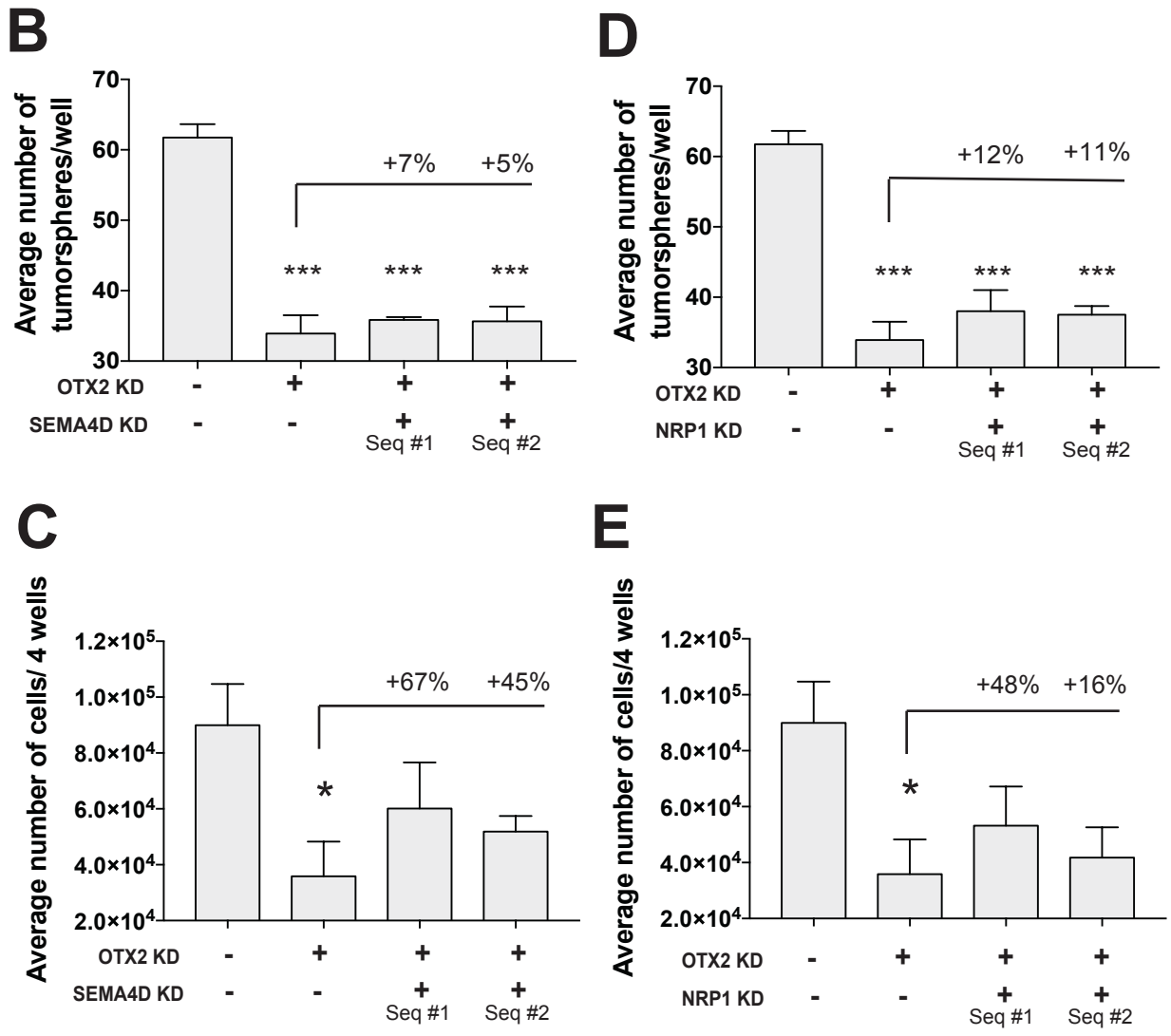

Figure 4.15: Decreased levels of semaphorin pathway genes in MB3W1 OTX2 knockdown tumorspheres results in a partial rescue of tumorsphere growth.
(A). Representative images of MB3W1 tumorspheres following dual OTX2 and either SEMA4D or NRP1 knockdown. Scale bar: 400 µm. (**B-C**). Quantification of tumorsphere number following dual OTX2 and either SEMA4D (**B**) or NRP1 (**B**) knockdown in MB3W1 tumorspheres over 5 days. Error Bars: s.e.m. $p<0.001$***. N=3 biological replicates and n=12 knockdown technical replicates. (**D-E**). Quantification of total cell number following dual OTX2 and either SEMA4D (**D**) or NRP1 (**E**) knockdown in MB3W1 tumorspheres over 5 days. Error Bars: s.e.m. $p<0.05$*. N=4 biological replicates and n=8 knockdown technical replicates were performed.

by Trypan Blue staining, despite an overall increase in cell number in both cell lines following dual KD (Figure 4.16). Collectively, these results provide further evidence that SEMA genes are associated with a tumor suppressive role and are negatively correlated with the OTX2-driven phenotype in OTX2 KD MB tumorspheres.

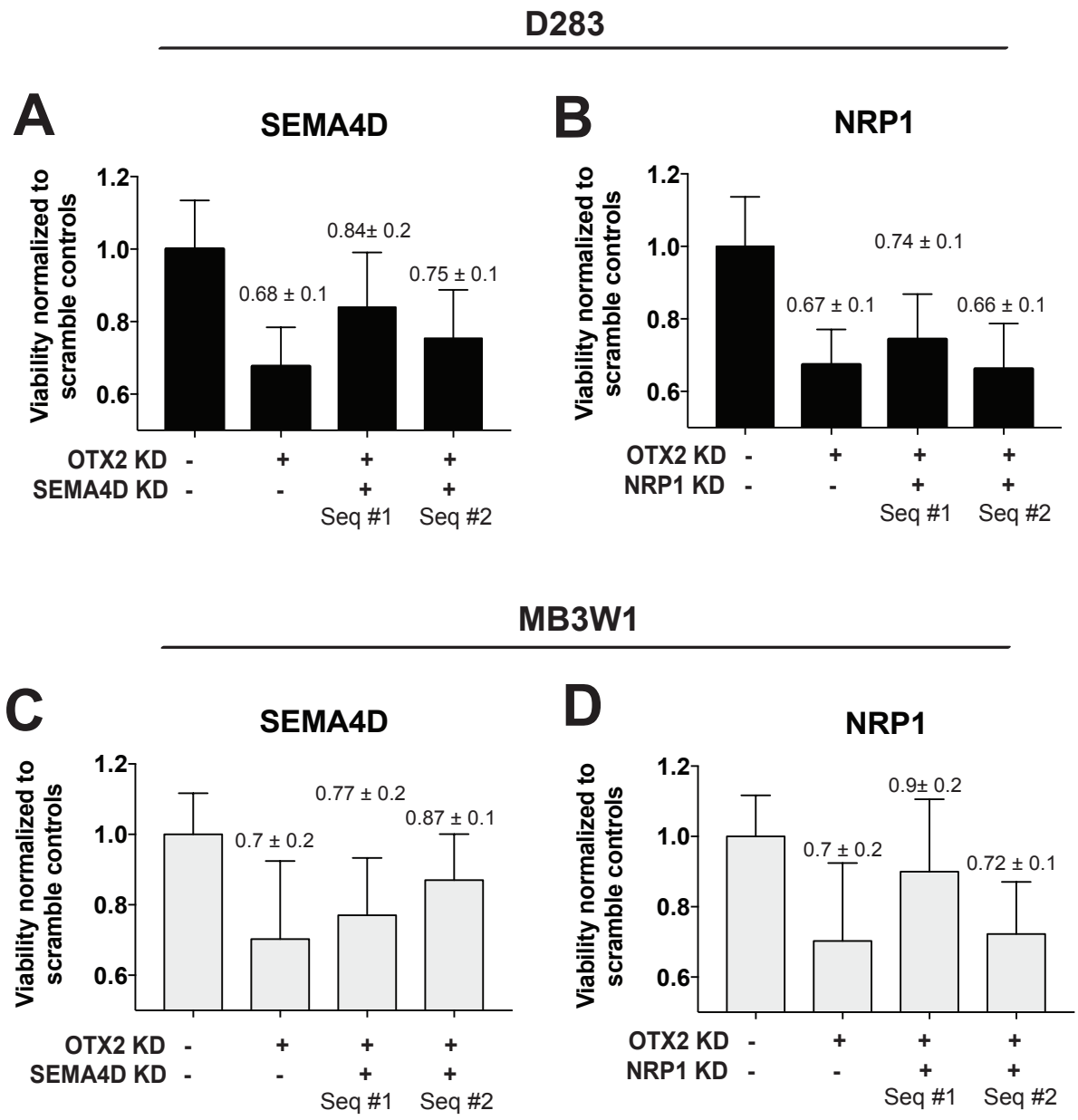

Figure 4.16: Decreased levels of semaphorin pathway genes in D283 and MB3W1 OTX2 knockdown tumorspheres does not significantly affect viability.
(**A-B**)**.** Viability in D283 tumorspheres following dual OTX2 and either SEMA4D (**A**) or NRP1 (**B**) knockdown over 5 days. Error Bars: s.e.m. N=7 and N=8 biological replicates for SEMA4D and NRP1 knockdown respectively. (**C-D**). Viability in MB3W1 tumorspheres following dual OTX2 and either SEMA4D (**C**) or NRP1 (**D**) knockdown over 5 days. Error Bars: s.e.m. N=4 biological replicates for SEMA4D and NRP1 knockdown.

4.3 AIM 3: To investigate the downstream pathways known to modulate the effects of select neural differentiation genes following OTX2 knockdown in Group 3 and Group 4 MB stem/progenitor cells.

4.3.1 OTX2 limits Rho pathway activation

As SEMA genes are contributing to the OTX2 KD phenotypes, we also wanted to investigate the downstream pathways known to mediate the effects of SEMA signaling such as Rho and MAPK (both ERK1/2 and p38) in OTX2 KD cells. Indeed, further interrogation of our gene expression profiling data revealed that Rho and MAPK signaling pathways were differentially expressed in OTX2 KD D283 relative to OTX2 scramble tumorspheres (Table 1.4). Genes associated with L1CAM interactions as well as SEMA Interactions/SEMA4D Signaling including the Rho pathway members *ROCK1*/*ROCK2* and several Rho guanine nucleotide exchange factors were significantly enriched in gene sets that were upregulated following OTX2 KD (Figure 4.17A-C, Table 1.4, Table S2, Table S3). Similarly, genes associated with MAPK signalling (both ERK1/2 and p38) were enriched in gene sets that were upregulated in the OTX2 KD cells; however, there was also enrichment in the scramble controls (Figure 4.17D). In support of these findings, we observed an increase in Rho activity in D283 tumorspheres as well as HD-MB03 tumorspheres following OTX2 KD (Figure 4.18A-B). However, MAPK pathway activation (both ERK1/2 and p38) was inconsistent following OTX2 KD (Figure 4.18 C-D). These results suggest an unexpected, yet novel role for Rho signaling in Group 3 and Group 4 MB stem/progenitor cell populations.

Table 1.4: Gene Set Enrichment Analysis revealed that genes associated with SEMA4D signaling were enriched in gene sets that were downregulated in D283 scramble relative to OTX2 knockdown tumorspheres.

Gene Symbol	Gene Title	Running Enrichment Score[A]
ARHGEF12	Rho guanine nucleotide exchange factor (GEF) 12	-0.5662338
ROCK2	Rho-associated, coiled-coil containing protein kinase 2	-0.54986334
ROCK1	Rho-associated, coiled-coil containing protein kinase 1	-0.55364746
MYL6	myosin, light chain 6, alkali, smooth muscle and non-muscle	-0.54413474
MYL12B	null	-0.5143689
MYH10	myosin, heavy chain 10, non-muscle	-0.48504782
PLXNB1	plexin B1	-0.4504612
MYH9	myosin, heavy chain 9, non-muscle	-0.40517303
MYL9	myosin, light chain 9, regulatory	-0.3621211
ARHGEF11	Rho guanine nucleotide exchange factor (GEF) 11	-0.29258606
SEMA4D	sema domain, immunoglobulin domain (Ig), transmembrane domain (TM) and short cytoplasmic domain, (semaphorin) 4D	-0.19715172
RHOB	ras homolog gene family, member B	-0.098245345
ARHGAP35	null	0.011831163

[A]Running Enrichment Score; calculated running-sum statistic looking at the correlation of a gene set with a phenotype [156].

Table 1.5: Gene Set Enrichment Analysis results for Reactome and KEGG databases identified pathways significantly enriched in gene sets that were downregulated in D283 scramble relative to OTX2 knockdown tumorspheres.

Name (Reactome Database)	Size[A]	ES	NES	NOM p-value	FDR q-value	FWER p-value
SEMAPHORIN INTERACTIONS	63	-0.65	-1.96	0	0.0411	0.047
AXON GUIDANCE	237	-0.52	-1.88	0	0.0640	0.139
DEVELOPMENTAL BIOLOGY	377	-0.49	-1.84	0	0.0780	0.237
INTERACTION BETWEEN L1 AND ANKYRINS	21	-0.74	-1.84	0.0026	0.0591	0.240
SIGNALING BY ROBO RECEPTOR	28	-0.71	-1.81	0	0.0661	0.315
L1CAM INTERACTIONS	82	-0.52	-1.65	0.0030	0.3009	0.894
NETRIN1 SIGNALING	37	-0.58	-1.63	0.0078	0.3097	0.926
BOTULINUM NEUROTOXICITY	17	-0.67	-1.57	0.0300	0.4194	0.982
INSULIN SYNTHESIS AND PROCESSING	19	-0.65	-1.54	0.0389	0.4923	0.995
SEMA4D IN SEMAPHORIN SIGNALING	29	-0.59	-1.53	0.0354	0.4746	0.995
Name (KEGG Database)	**Size**	**ES**	**NES**	**NOM p-val**	**FDR q-val**	**FWER p-val**
AXON GUIDANCE	126	-0.66	-2.21	0	0	0
ERBB SIGNALING PATHWAY	86	-0.51	-1.57	0.0185	0.5618	0.641
VASOPRESSIN REGULATED WATER REABSORPTION	43	-0.53	-1.48	0.0256	0.7283	0.873
CELL ADHESION MOLECULES CAMS	125	-0.43	-1.45	0.0101	0.6949	0.926
MAPK SIGNALING PATHWAY	260	-0.40	-1.43	0.0046	0.6085	0.938
TYPE I DIABETES MELLITUS	36	-0.52	-1.41	0.0635	0.5669	0.956
LONG TERM DEPRESSION	66	-0.46	-1.40	0.0483	0.5385	0.969
LONG TERM POTENTIATION	70	-0.46	-1.38	0.0718	0.5132	0.979
TYPE II DIABETES MELLITUS	46	-0.48	-1.37	0.0507	0.5142	0.987
T CELL RECEPTOR SIGNALING PATHWAY	105	-0.42	-1.36	0.0401	0.4860	0.988

[A]Size; number of genes.
Abbreviations: ES; enrichment score, NES; normalized enrichment score, NOM; nominal, FWER; family-wise error rate.

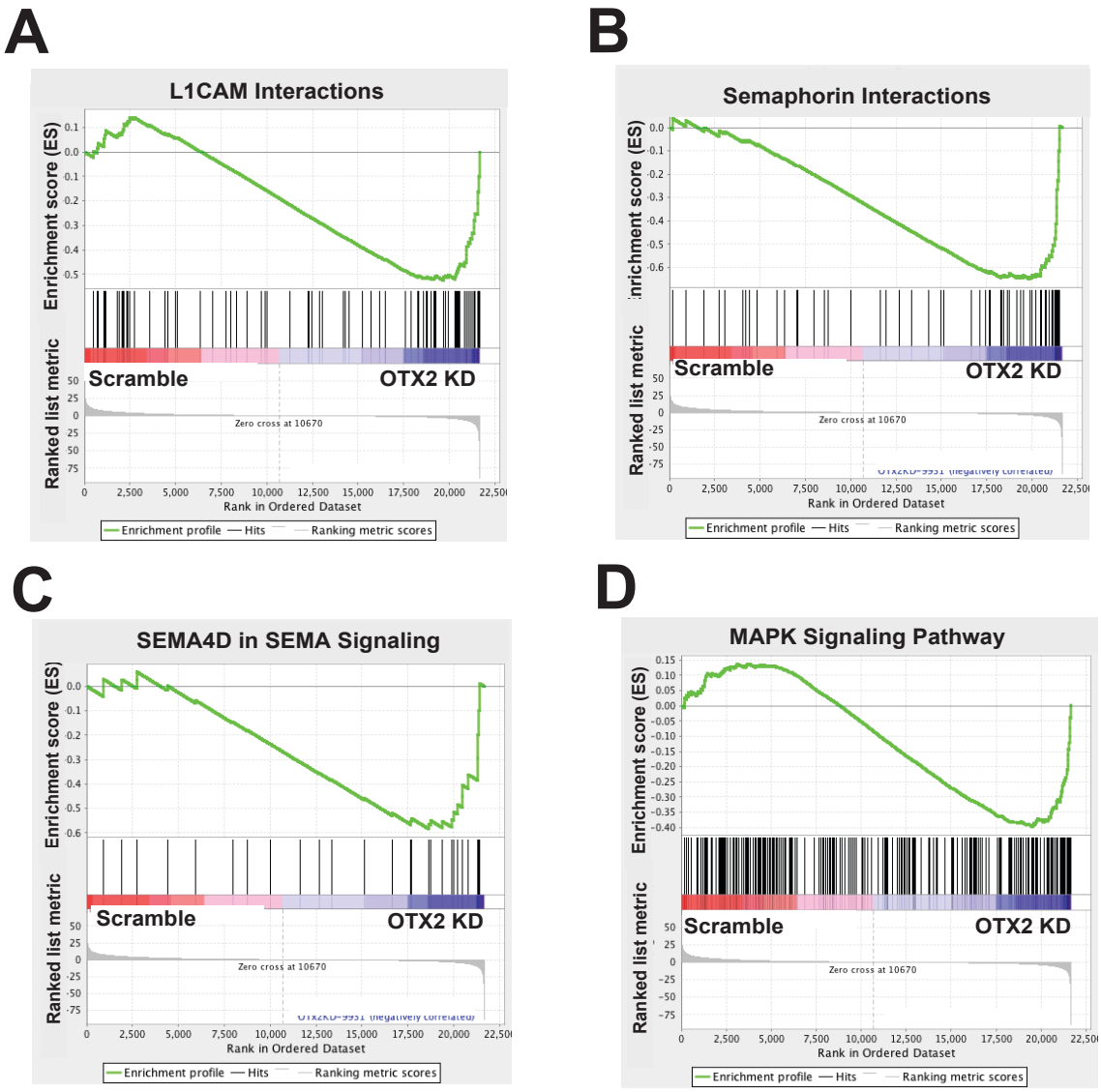

Figure 4.17: OTX2 levels are negatively correlated with activation of RHO signaling genes.

(**A-D**). Gene set enrichment analysis (GSEA) demonstrating that genes associated with L1CAM interactions (**A**), SEMA interactions (**B**), SEMA4D signaling (**C**), and MAPK signaling (**D**) were enriched in genes sets that are downregulated in the scramble and upregulated in the OTX2 knockdown D283 tumorspheres.

4.3.2 Decreased Rho activity partially rescues tumorsphere formation in OTX2 knockdown MB stem cells

To further interrogate the functional role of the Rho pathway in MB stem/progenitor cell populations, we treated scramble and OTX2 KD tumorspheres from D283, D341 and recently established MB3W1 cells with the Y-27632 ROCK inhibitor at concentrations ranging from 5-50 μM (Figure 4.18E, G, I). While ROCK inhibition had no significant effect on tumorsphere formation in scramble controls from the D283 and D341 cell lines, there was a statistically significant rescue in OTX2 KD tumorspheres using 20 and/or 50 μM (Figure 4.18E, G). For D341, in addition to the treatment effect, we also observed a strong statistically significant difference between the effects of ROCK on OTX2 KD relative to scramble tumorspheres ($p=0.005$). Importantly, there was also an increase in MB3W1 OTX2 KD tumorsphere number following ROCK treatment (Figure 4.18I). For this recently established cell line, higher concentrations were toxic; thus, the assays were performed at 5 and 10 μM. Moreover, there was an increase in cell number for D283, D341 and MB3W1 (Figure 4.18F, H, J). These results highlight a novel inhibitory role for the Rho pathway activation in MB stem/progenitor cell function. Thus, both SEMA genes and their downstream effectors are negatively correlated with the OTX2-driven phenotype in Group 3 and Group 4 MB tumorspheres. Collectively, our results reveal a novel role for an OTX2-SEMA-Rho pathway in Group 3 and Group 4 MB stem/progenitor cells.

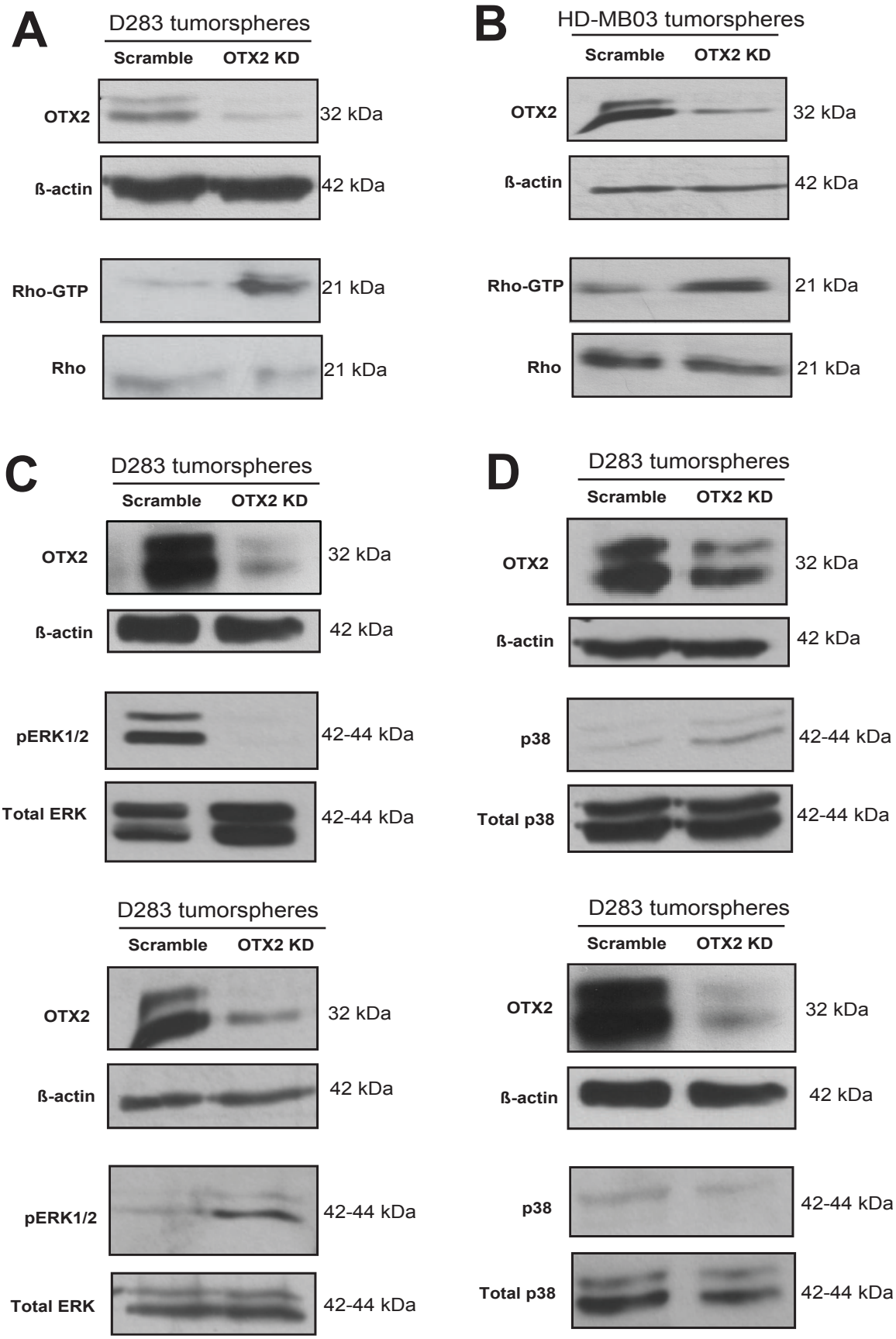
A
D283 tumorspheres
Scramble
OTX2 KD
OTX2
32 kDa
ß-actin
42 kDa
Rho-GTP
21 kDa
Rho
21 kDa
B
HD-MB03 tumorspheres
Scramble
OTX2 KD
OTX2
32 kDa
ß-actin
42 kDa
Rho-GTP
21 kDa
Rho
21 kDa
C
D283 tumorspheres
Scramble
OTX2 KD
OTX2
32 kDa
ß-actin
42 kDa
pERK1/2
42-44 kDa
Total ERK
42-44 kDa
D
D283 tumorspheres
Scramble
OTX2 KD
OTX2
32 kDa
ß-actin
42 kDa
p38
42-44 kDa
Total p38
42-44 kDa
D283 tumorspheres
Scramble
OTX2 KD
OTX2
32 kDa
ß-actin
42 kDa
pERK1/2
42-44 kDa
Total ERK
42-44 kDa
D283 tumorspheres
Scramble
OTX2 KD
OTX2
32 kDa
ß-actin
42 kDa
p38
42-44 kDa
Total p38
42-44 kDa

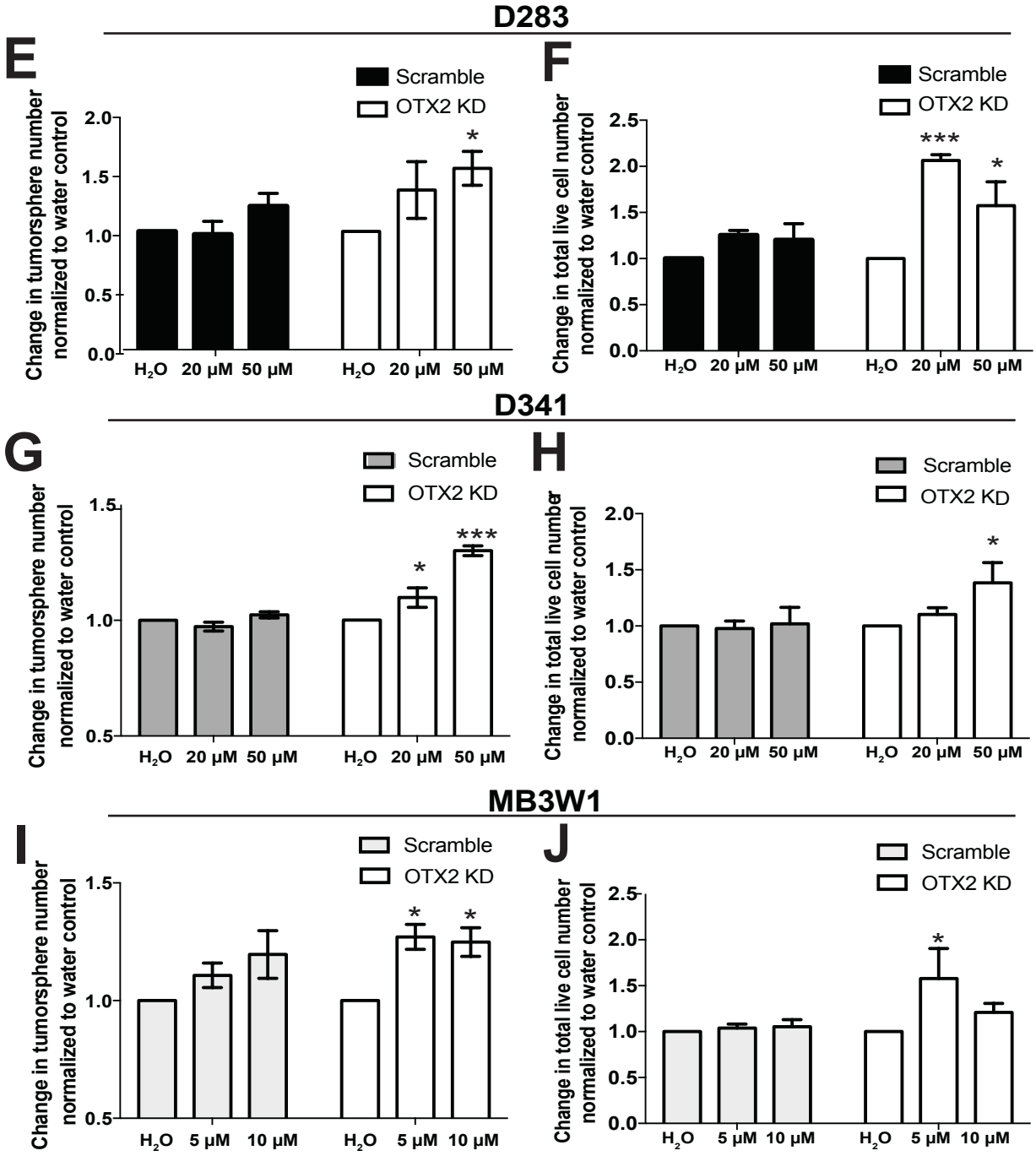

Figure 4.18: OTX2 levels are negatively correlated with activation of RHO signaling. (**A-B**) Western blots depicting increased Rho activity in D283 (**A**) and HD-MB03 (**B**) tumorspheres after OTX2 KD. (**C-D**) Western blots depicting increased and decreased pERK (**C**) activity and p38 (**D**) in D283 tumorspheres after OTX2 KD. (**E-J**) Treatment of D283 (**E, F**), D341 (**G, H**) and MB3W1 (**I, J**) scramble (SC) and OTX2 KD tumorspheres with the ROCK inhibitor Y-27632 results in a partial recovery of tumorsphere number and live cell number in OTX2 knockdown cells. N=3 biological replicates for tumorsphere numbers and n=12 D283, n=11 scramble D341, n=14 OTX2 knockdown D341, and n=12 MB3W1 technical replicates. N=3 biological replicates for D283 and MB3W1 live cell number and N=4 biological replicates for D341. Error bars: s.e.m. $p<0.05$ *, $p<0.001$***.

CHAPTER 5: DISCUSSION

5.1 *In vitro* MB studies in stem cell-enriched conditions are the most biologically relevant

These studies provide the first comprehensive list of OTX2 pathway genes in Group 3 and 4 MB stem/progenitor cell populations. As mentioned in section 1.3.6, studies to date have focused on OTX2-mediated control of cell cycle genes in MB cell lines grown in serum or as adherent cultures [132]. A more comprehensive understanding of OTX2-mediated regulation of MB stem cell populations is critical, as these cells are the major contributors to therapeutic resistance, tumor initiation, recurrence, and poor prognosis. Moreover, the genetic and phenotypic changes observed in human tumors are more accurately recapitulated in xenografts derived from brain tumor cells grown in stem cell-enriched conditions [169]. For instance, as previously mentioned, all *trans*-retinoic acid (ATRA) downregulated OTX2 expression while inhibiting growth of $OTX2^+$ MB cells *in vitro* [170]. However, subsequent testing of ATRA and other retinoic acids in stem cell-enriched tumorsphere conditions and in intracranial transplant models rendered the cells resistant to treatment [73]. Thus, tumorspheres are the most biologically relevant *in vitro* model system to use for characterizing the OTX2 regulatory network in MB. This is supported by changes in OTX2 levels during the later stages of human cerebellar development where OTX2 is expressed in the progenitor cells of the EGL but is not detected at the post-natal stage [112]. Moreover, OTX2 levels in the adult tissues are restricted to the choroid plexus, pineal gland, and retinal photoreceptor cells [110]. These data are consistent with the idea that OTX2 is associated with a more primitive cell population.

5.2 OTX2 inhibits neural differentiation and axon guidance gene expression in MB stem/progenitor cells

Using complementary bioinformatics approaches and functional validation studies, we have identified a novel role for OTX2 in regulating a cohort of axon guidance genes and their

downstream targets in Group 3 and Group 4 MB stem/progenitor cells. The majority of genes associated with neural differentiation and axon guidance pathways were negatively correlated with OTX2 expression and self-renewal suggesting a tumor suppressive role in Group 3 and Group 4 MB. Importantly, this negative correlation was demonstrated in both well established and recently derived cell lines [153, 154], as well as primary patient samples with *SEMA4D* serving as a novel prognostic indicator. Interestingly, low expression of another SEMA ligand, *SEMA6A*, has also been associated with shorter median survival in glioblastoma patients [171]. While the genes that regulate axon guidance are well known for their roles in neuronal migration and cell motility [164], our results reveal a novel connection between these neurodevelopmental cues and self-renewal in the most highly aggressive MB cells and extend current knowledge that axon guidance genes are differentially expressed between the MB subtypes [26] and can undergo alternative splicing in these tumors [172]. Indeed, a large number of genes from our neuronal differentiation list (Table S1) including, but not limited to, calcium/calmodulin dependent protein kinase IV (*CAMK4),* cerebellin-1 precursor *(CBLN1),* neuronal differentiation 1 *(NEUROD1),* nuclear receptor subfamily 2 group F member 1 *(NR2F1),* and neurexin (*NRXN1)* [173-175] have all been implicated in cerebellar morphology and/or granule cell development thus further validating the biological relevance of our tumorsphere model system to characterize the OTX2 network in Group 3 and Group 4 MB. Interestingly, several differentially expressed SEMA genes such SEMA6A [176, 177], PLXNA2 [16], NRP1 [178]and L1CAM [179] have also been shown to play a role in cerebellar development and granular precursor cell motility further underscoring the notion that an early cerebellar stem/progenitor is the cell of origin for Group 3 and Group 4 MB. To our knowledge, a negative correlation between OTX2 and axon guidance gene expression has not been functionally explored in Group 3 and 4 MB. We propose a working

model in which OTX2 promotes MB self-renewal/growth and suppresses differentiation by inhibiting the expression of axon guidance pathway genes and their downstream effectors (Figure 5.0).

5.3 Axon guidance cues can promote or inhibit tumor progression in a cell context dependent manner

Axon guidance cues within the SLIT, NETRIN, EPH/EPHRIN, and SEMA families are critical for nervous system development, functioning both as attractive and repulsive axon growth cone cues [180]. Interestingly, the mechanisms by which these neural connections unfold are highly conserved. Once multipotent neural progenitors proliferate and differentiate, axons guidance cues regulate axon branching, pruning and degeneration [181]. Accordingly, the neuronal axon growth cone tips fasciculate, turn and extend towards their targets to produce synaptic innervations between neurons in the nervous system [182]. Each of these steps is regulated by secreted and membrane bound axon guidance cues; which not only control cell motility, but also cell proliferation and cell survival during neural development and cancer progression [183]. For instance, aberrant expression of SLIT and/or its receptor ROBO has been shown to play a role in cancer progression and metastasis in melanoma, small cell lung cancer, and neuroblastoma [184, 185]. While in glioblastoma and MB tumors, SLIT2 is repressed and studies suggest that the SLIT/ROBO pathway plays a tumor suppressive role inhibiting cell invasion and motility both *in vitro* and *in vivo* [185, 186]. Moreover, SEMA6A suppressed proliferation, migration and invasion in glioblastoma cells *in vitro* [171], and PLXNC1 is a potential tumor suppressor in melanoma [187]. Following OTX2 KD in our tumorspheres, 90 axon guidance genes including those from the SLIT, NETRIN, EPH/EPHRIN, and SEMA families were differentially expressed. The presence of activated neural developmental signaling pathways and expression of neural lineage

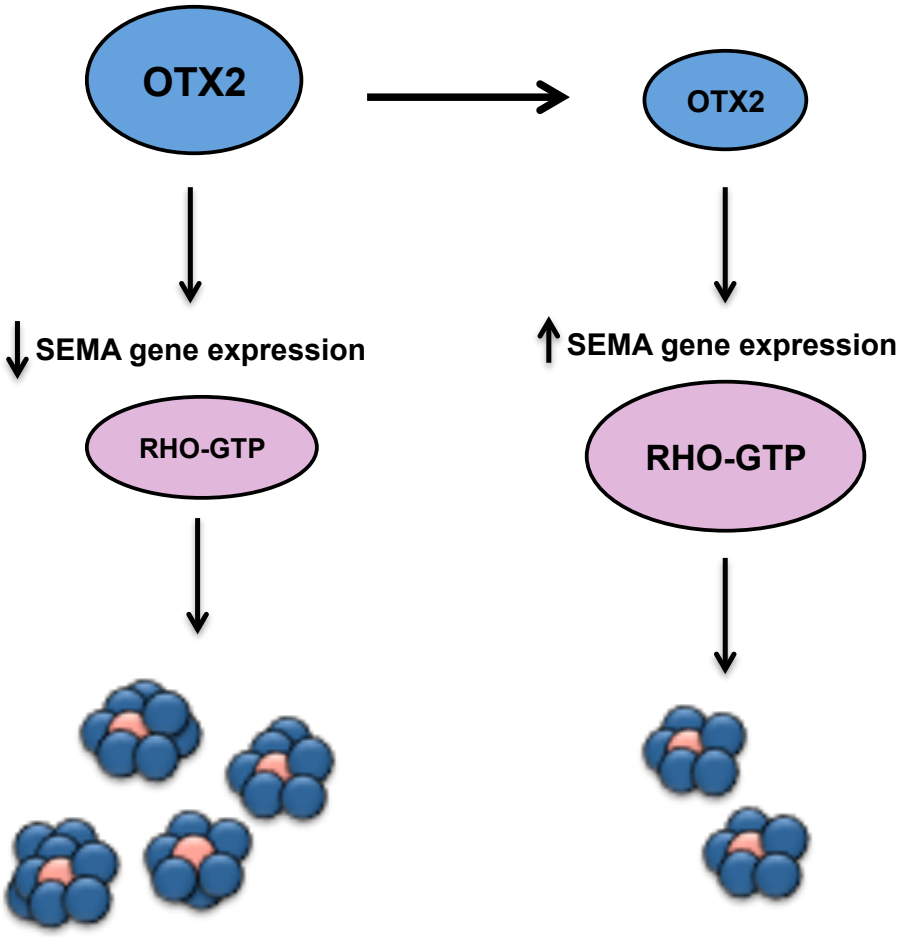

Figure 5.0: Working model depicting the oncogenic role OTX2 plays in high OTX2 expressing Group 3 and Group 4 MBs.
In high OTX2 expressing Group 3 and 4 MBs OTX2 decreases semaphorin gene expression, Rho activity and increases self-renewal capacity. When OTX2 is knocked down semaphorin gene expression increases, Rho activity increases, self-renewal decreases.

phenotypes in MBs provide support for the theory that these tumors have a stem/progenitor cell of origin.

5.4 Semaphorin signaling genes increases with OTX2 KD in Group 3 and 4 MB stem/progenitors cells demonstrating a potential tumor suppressive role

As the SEMA genes were the most significantly and differentially expressed across all of our data sets, we propose that the repression of SEMA gene expression by OTX2 contributes to inhibition of neural differentiation. SEMA molecules play important roles during development of the nervous system, namely as neuronal chemorepellent cues, and in the immune and vascular system [166]. There are eight main subclasses of 20 membrane bound or secreted SEMA proteins. Class I and II are found in invertebrates, while classes III-VII are found within vertebrates (Figure 5.1) [166, 188]. These SEMAs share a common, sema domain, consisting of a 500 amino acid beta-propeller fold structure [166, 188]. This structure is cysteine-rich and binds to a family of PLXN receptors that possess a similar sema domain (Figure 5.1) [166]. As briefly mentioned in section 4.2.1, some SEMAs also bind to NRP receptors alongside a PLXN and/or L1CAM receptors (Figure 5.1) [29]. While we have identified a role for *SEMA4D, NRP1,* and *L1CAM* genes in regulating tumorsphere formation and self-renewal capacity in MB, a recent study has also shown that SEMA genes regulate brain tumor stem cell survival [189]. Specifically, the SEMA ligand SEMA3C regulates and promotes glioblastoma stem cell survival through RAC1 activation, a small GTP-binding protein, without affecting expression of stem cell markers or differentiation [189] suggesting that the effect of SEMA genes on brain tumor stem cells is cell context specific. Furthermore, SEMA3C coimmunoprecipitated with PLXNA2, PLXND1 and NRP1 in glioblastoma stem cells enriched for the stem cell markers, CD133, Olig2, and Sox2 [189]. Conversely, SEMA3B is known to induce apoptosis and suppress tumorigenesis via NRP

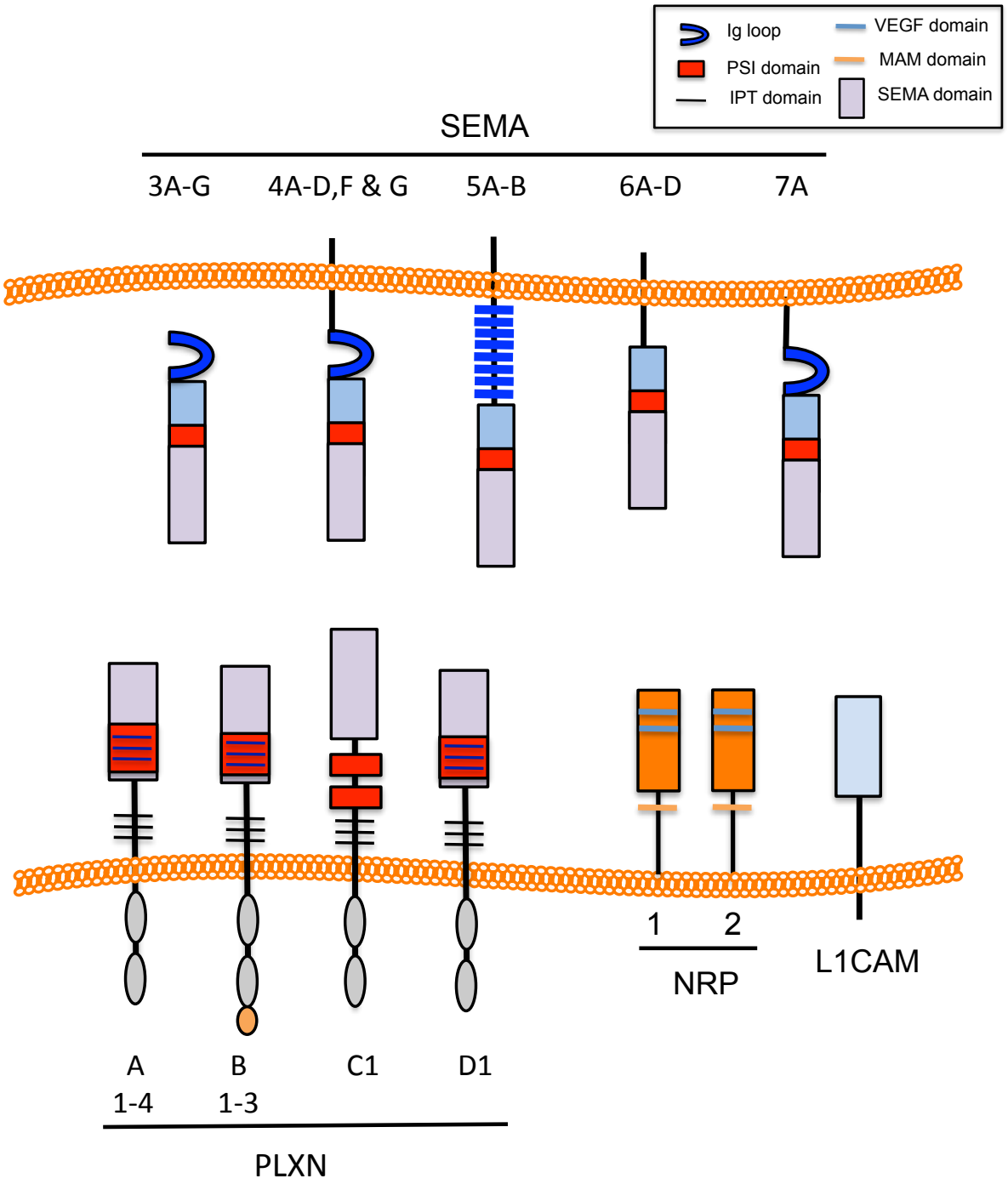

Figure 5.1: Vertebrate membrane bound and secreted semaphorin signaling molecules and receptors.

Schematic representation of vertebrate semaphorin (SEMA) ligands, the receptors, PLXN and NRP, and co-receptor L1CAM divided into subclasses based on sequence homology and structural similarities. Class 3 SEMAs are secreted, SEMAs of other subclasses are transmembrane (Class 4-6) or membrane-associated (Class 7). PLXN receptors are divided into 9 subclasses, all of which contain a GTPase-activating protein domain. Some SEMAs can only bind to PLXN receptors when NRP and/or L1CAM are associated. Adapted from Worzfeld and Offermanns, 2014.

binding and downregulation of PI3K signaling in lung cancer and glioblastoma cells [190]. While SEMA4D expression has been associated with increased tumor angiogenesis in a variety of cancers [191], overexpression of the SEMA4D receptor, PLXNB1, has also been linked with reduced tumor growth in melanoma xenografts [192]. Moreover, NRP1 and L1CAM, two of our target SEMA molecules, have been linked with many oncogenic functions. For instance, NRP1 has been associated with aggressive tumor growth and spread in both D283 and Daoy MB cells [193], while L1CAM have been implicated in CSC function in gliomas [194]. Overall these data again demonstrate how the effects of SEMA genes are likely cell-type and context specific; thus, further investigation into which ligand and receptor pairs cluster together in our stem cell conditions would provide some biological clarity.

As our dual OTX2/SEMA gene KD studies only resulted in a partial rescue of self-renewal and cell growth, additional OTX2-axon guidance signaling pathways are likely contributing to the Group 3 and Group 4 MB self-renewing phenotype and will need to be explored. For example, ephrin/EPH family genes were also negatively correlated with OTX2 expression in our global gene expression (Table S2) and patient sample datasets (Table 1.3). As EPH and SEMA signaling share many downstream targets including the Rho family of GTPases [195], the role of OTX2-EPH signaling in regulating MB self-renewal and differentiation will need to be examined, and will likely have overlapping roles with OTX2-SEMA pathways in Group 3 and 4 tumors. Interestingly, a recent study demonstrated that PLXNA1 serves as a receptor for SLIT C-terminal fragments further underscoring the complexity and cross talk between axon guidance signaling pathways [196].

As these pathways have been shown to be critical regulators of invasion/metastasis and angiogenesis in other cancers [166], it will also be imperative to evaluate the role of SEMA

pathway genes in regulating Group 3 and Group 4 MB motility and metastasis. For example, the SEMA3B ligand has been shown to inhibit tumor cell growth while increasing metastatic dissemination in melanoma and non-small cell lung carcinoma cells [197]. Other axon guidance cues have shown variable effects on MB cell motility with NETRIN-1 serving as a positive regulator of invasion [106] while SLIT2 inhibits MB invasion [186]. SLIT2 has also been shown to inhibit glioma motility and invasion by suppressing the activity of the small GTP-binding protein family member CDC42 [198, 186, 199]. While EPHB1 and EPHB2 have been shown to increase migration and cell adhesion in SHH MB cell lines, *EPHA3* and *EPHA5* were upregulated in our OTX2 KD MB tumorspheres [200, 201]. We have previously shown that higher self-renewing MB tumorspheres exhibit a downregulated motility transcription program [155]; thus, it is possible that the effects of axon guidance genes on Group 3 and Group 4 MB cells will be dependent on whether they are stem, progenitors or differentiated cells.

5.5 Transcriptional regulation of the semaphorin genes by OTX2

Our results demonstrate that OTX2 is either a direct or indirect repressor of SEMA gene expression. To date, the vast majority of studies have investigated the mechanisms by which OTX2 positively regulates expression of cell cycle genes [130, 202, 203]. The oncogenic role of OTX2 as a transcriptional repressor is underexplored. Interestingly, Bai *et al.* showed that OTX2 represses myogenic differentiation by binding to the 258 bp *MYOD1* core enhancer through its homeodomain in MB cells as compared to medullomyoblastomas [131]. In this study, the authors also suggested that OTX2 may recruit yet unidentified additional factors that will aid in suppressing multiple differentiation pathways, including those associated with the neuronal lineage [131]. Bunt and colleagues proposed that the transcription factors NEUROD1 and NR2F1, both direct targets of OTX2 as demonstrated by ChIP-on-ChIP experiments, may contribute to

OTX2-mediated regulation of neuronal differentiation [37], but the functional roles of these two proteins were not explored. Indeed, *NEUROD1* and *NR2F1* were both significantly upregulated following OTX2 KD in our MB tumorspheres (Table S1). In addition, OTX2 is associated with regulation of histone modifications [59] and has recently been found to cooperatively control the active enhancer landscape in Group 3 MB [203]. However, unlike the decreased *NEUROD1* expression we and Bunt *et al*. observed, Bouley *et al*. noted increased *NEUROD1* expression alongside OTX2 KD in their MB cell lines cultured in serum [202-204]. This discrepancy could be explained by the utilization of different cell lines or by differences in culture conditions (ie. serum vs. serum free defined media) between laboratories. Interestingly, SLIT2 promoter regions are epigenetically hypermethylated and inactivated in a variety of tumors [205, 206], while SLIT1 promoter methylation can be detected in glioma tumor cell lines as well [207]. Other studies also report TSS methylation of SEMA3B in lung cancer, glioma, and liver tumors [190, 208, 209]. In Group 3 and Group 4 MB, OTX2 may therefore co-localize with specific histone modifications (ie. H3K4me3 and H3K27m3) on select SEMA pathway genes in the context of a self-renewing and/or differentiating phenotype.

5.6 Downstream semaphorin pathway signaling is negatively correlated with OTX2

Our results reveal a novel role for Rho activity in regulating the balance between MB self-renewal and differentiation and open up new avenues for studying the effects of the Rho has been shown to either activate or inactivate Rho depending on the coupling of the PLXNB1 receptor with the ERBB2 or MET receptor tyrosine kinase [210]. For example, through the involvement of a PLXN-associated PDZ-Rho-guanine nucleotide exchange factor (GEF), RhoA activates cell migration via the PLXN-ERBB2 complex in normal neural stem like cells [210]. family of small GTP-binding proteins in MB stem cell function (Figure 5.2). SEMA4D signaling

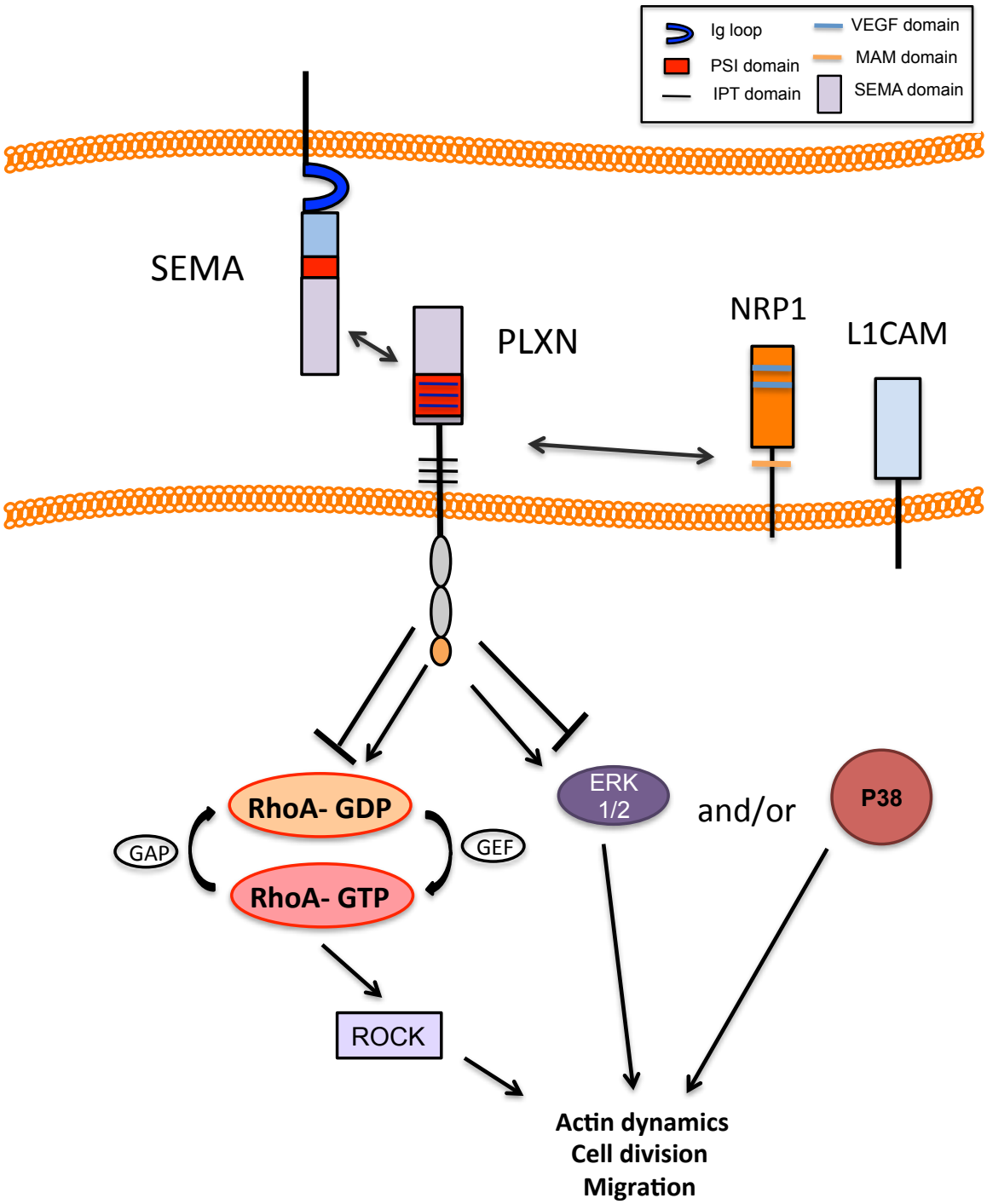

Figure 5.2: Downstream semaphorin pathway signaling.
SEMA receptors can elicit multiple intracellular signaling cascades, including RhoA and MAPK (ERK1/2, p38) activation. MAPK is activated by RAS and CDC42 molecules, in a variety of mechanisms, while RhoA is activated by guanine nucleotide exchange factors (GEFs) and inactivated by GTPase-activating proteins (GAP). Binding of active Rho-GTP to the Rho binding domain of ROCK disrupts the negative regulation, and activates its kinase.

These results suggest that our recombinant protein data could be due to interactions with a number of specific co-factors, and that additional biochemical ligand binding assays would be beneficial. However, in our MB models, increased Rho activity is associated with a more differentiated phenotype and treating OTX2 KD tumorspheres with the Y-27632 ROCK inhibitor resulted in a partial recovery of tumorsphere formation. These results are consistent with previous findings in glioblastoma stem cells in which treatment with the ROCK inhibitor enhanced tumorsphere formation [211]. Interestingly, RAC1 activity is positively correlated with survival and tumorsphere formation [189] in glioblastoma stem cell populations demonstrating that Rho/Rac play opposing roles in regulating stem cell function in this brain tumor cell population.

5.7 Future Directions

Our results highlight, for the first time, a connection between stem/progenitor cells and axon guidance signaling genes in MB and extend current knowledge that axon guidance genes are differentially expressed between the MB subtypes. Future studies include, stable gain/loss of function of select SEMA genes and subsequent transplantation into non-obese diabetic/severe combined immunodeficient (NOD-SCID) mice to evaluate the effects on tumor progression *in vivo*. Further, we will also evaluate the effects of constitutively active RhoA or RhoB on our Group 3 and Group 4 MB tumorspheres *in vitro*. This would complement our existing studies with the ROCK inhibitor, which increased the number of OTX2 KD tumorspheres. The antibody used for our Rho pulldown studies detects RhoA, RhoB, and RhoC activity; thus, we cannot be sure which Rho, or if all, are contributing to the OTX2 KD phenotype. While many studies focus on RhoA activity in cancer, there is evidence for RhoB acting as a tumor suppressor. For example, in clear cell renal cell carcinoma, RhoB is found at low levels in patient samples and when overexpressed, inhibits cell proliferation, colony formation, migration and promotes

apoptosis [212]. In fact, low expression of *RHOB* is commonly found in a variety of cancers [213, 214] but has never been explored in MB or in CSCs. Indeed, *RHOB* was significantly upregulated in our OTX2 KD tumorspheres relative to controls (Table 1.4). In contrast, RhoA exhibits both oncogenic and tumor suppressive roles depending on the cancer being studied [215]. If constitutive activation of RhoA and/or RhoB in cells results in tumor suppressive effects on our MB tumorspheres *in vitro*, transplantation into NOD-SCID mice to evaluate the effects on tumor progression *in vivo* will also be performed. In addition to the constitutive activation of RhoA and/or RhoB, we will also evaluate the effects of recombinant SEMA protein treatment on Rho activity. This would strengthen our finding that Rho activity is increased following OTX2 KD in our Group 3 and Group 4 tumorspheres.

Furthermore, as previously mentioned, it is possible that SEMA and RHO genes will impart different effects on MB motility and spread. Thus, we cannot be sure that SEMAs would not induce a more aggressive phenotype *in vivo* by increasing motility. Additional studies assessing MB cell motility are warranted using either a transwell or hanging drop aggregate migration assay, both of which are well established in our lab.

Lastly, while ChIP provides information on promoter occupancy, it does not distinguish between direct or indirect actions of OTX2 in regulating SEMA gene promoters. To test for direct interactions, specific OTX2-DNA complexes would need to be verified using electrophoretic mobility gel shift assays (EMSA) for *SEMA4D*, *NRP1* and *L1CAM*. Moreover, luciferase reporter gene assays assessing OTX2/SEMA promoter interactions could be performed to determine the exact molecular relationship between OTX2 and SEMA genes.

5.8 Summary

In summary, we have found that OTX2 is a critical regulator of Group 3 and Group 4

self-renewal and differentiation through modulation of a large cohort of axon guidance genes and downstream targets such as Rho activity. Published literature demonstrates the presence of activated developmental signaling pathways in MB and evidence for a cerebellar multipotent cell of origin. This study offers novel insights into the molecular drivers of the most aggressive MB tumors, provides further support for the notion that MB is a disease of dysregulated cerebellar development, and presents an informed framework to pursue novel targeted therapies aimed at targeting the axon guidance genes pathways that facilitate differentiation of MB tumors cells. Group 3 and 4 MB typically exhibit the worst prognosis with 33-50% of patients exhibiting metastasis at the time of diagnosis [1, 4]. Further defining the role of OTX2 and its associated targets, including the SEMA pathway genes, is thus imperative to reduce the aggressive nature of these tumors. Retrospective studies have also shown that patients whose MB show higher levels of neuronal differentiation experience greater overall survival [216, 217]. Thus, therapies aimed at differentiating Group 3 and Group 4 MB stem cells should be further developed.

CHAPTER 6: REFERENCES

1. Taylor, M.D. et al. Molecular subgroups of medulloblastoma: the current consensus. *Acta Neuropathol* **123**, 465-472 (2012).
2. Louis, D.N. et al. The 2007 WHO classification of tumours of the central nervous system. *Acta Neuropathol* **114**, 97-109 (2007).
3. Northcott, P.A., Dubuc, A.M., Pfister, S. & Taylor, M.D. Molecular subgroups of medulloblastoma. *Expert Rev Neurother* **12**, 871-884 (2012).
4. Ramaswamy, V. et al. Risk stratification of childhood medulloblastoma in the molecular era: the current consensus. *Acta Neuropathol* **131**, 821-831 (2016).
5. Gibson, P. et al. Subtypes of medulloblastoma have distinct developmental origins. *Nature* **468**, 1095-1099 (2010).
6. Wang, J. & Wechsler-Reya, R.J. The role of stem cells and progenitors in the genesis of medulloblastoma. *Exp Neurol* **260**, 69-73 (2014).
7. Wu, X. et al. Clonal selection drives genetic divergence of metastatic medulloblastoma. *Nature* **482**, 529-533 (2012).
8. Acampora, D. et al. Forebrain and midbrain regions are deleted in Otx2-/- mutants due to a defective anterior neuroectoderm specification during gastrulation. *Development* **121**, 3279-3290 (1995).
9. Simeone, A. Otx1 and Otx2 in the development and evolution of the mammalian brain. *EMBO J* **17**, 6790-6798 (1998).
10. Beby, F. & Lamonerie, T. The homeobox gene Otx2 in development and disease. *Exp Eye Res* **111**, 9-16 (2013).
11. Kaur, R. et al. OTX2 exhibits cell-context-dependent effects on cellular and molecular properties of human embryonic neural precursors and medulloblastoma cells. *Dis Model Mech* **8**, 1295-1309 (2015).
12. Louis, D.N. et al. The 2016 World Health Organization Classification of Tumors of the Central Nervous System: a summary. *Acta Neuropathol* **131**, 803-820 (2016).
13. Hatten, M.E. & Roussel, M.F. Development and cancer of the cerebellum. *Trends Neurosci* **34**, 134-142 (2011).
14. Albright, A.L. et al. Effects of medulloblastoma resections on outcome in children: a report from the Children's Cancer Group. *Neurosurgery* **38**, 265-271 (1996).
15. in PDQ Cancer Information Summaries (Bethesda (MD); 2002).
16. Srinivasan, V.M. et al. Modern management of medulloblastoma: Molecular classification, outcomes, and the role of surgery. *Surg Neurol Int* **7**, S1135-S1141 (2016).
17. Packer, R.J., Cogen, P., Vezina, G. & Rorke, L.B. Medulloblastoma: clinical and biologic aspects. *Neuro Oncol* **1**, 232-250 (1999).
18. Crawford, J.R., MacDonald, T.J. & Packer, R.J. Medulloblastoma in childhood: new biological advances. *Lancet Neurol* **6**, 1073-1085 (2007).
19. Brown, H.G. et al. "Large cell/anaplastic" medulloblastomas: a Pediatric Oncology Group Study. *J Neuropathol Exp Neurol* **59**, 857-865 (2000).
20. Ellison, D.W. et al. beta-Catenin status predicts a favorable outcome in childhood medulloblastoma: the United Kingdom Children's Cancer Study Group Brain Tumour Committee. *J Clin Oncol* **23**, 7951-7957 (2005).

21. Coluccia, D., Figuereido, C., Isik, S., Smith, C. & Rutka, J.T. Medulloblastoma: Tumor Biology and Relevance to Treatment and Prognosis Paradigm. *Curr Neurol Neurosci Rep* **16**, 43 (2016).
22. Packer, R.J. Craniospinal radiation therapy followed by adjuvant chemotherapy for newly diagnosed average-risk medulloblastoma. *Curr Neurol Neurosci Rep* **7**, 130-132 (2007).
23. Packer, R.J. Standard-risk medulloblastoma treated by adjuvant chemotherapy followed by reduced-dose craniospinal radiation therapy. *Curr Neurol Neurosci Rep* **7**, 129, 132 (2007).
24. Morfouace, M. et al. Pemetrexed and gemcitabine as combination therapy for the treatment of Group3 medulloblastoma. *Cancer Cell* **25**, 516-529 (2014).
25. Callu, D. et al. Remediation of learning difficulties in children after treatment for a cerebellar medulloblastoma: a single-case study. *Dev Neurorehabil* **11**, 16-24 (2008).
26. Northcott, P.A. et al. Medulloblastoma comprises four distinct molecular variants. *J Clin Oncol* **29**, 1408-1414 (2011).
27. Kool, M. et al. Molecular subgroups of medulloblastoma: an international meta-analysis of transcriptome, genetic aberrations, and clinical data of WNT, SHH, Group 3, and Group 4 medulloblastomas. *Acta Neuropathol* **123**, 473-484 (2012).
28. MacDonald, B.T., Tamai, K. & He, X. Wnt/beta-catenin signaling: components, mechanisms, and diseases. *Dev Cell* **17**, 9-26 (2009).
29. Parsons, D.W. et al. The genetic landscape of the childhood cancer medulloblastoma. *Science* **331**, 435-439 (2011).
30. Ramaswamy, V. et al. Recurrence patterns across medulloblastoma subgroups: an integrated clinical and molecular analysis. *Lancet Oncol* **14**, 1200-1207 (2013).
31. Koch, A. et al. Somatic mutations of WNT/wingless signaling pathway components in primitive neuroectodermal tumors. *Int J Cancer* **93**, 445-449 (2001).
32. Huang, H. et al. APC mutations in sporadic medulloblastomas. *Am J Pathol* **156**, 433-437 (2000).
33. Robinson, G. et al. Novel mutations target distinct subgroups of medulloblastoma. *Nature* **488**, 43-48 (2012).
34. Phoenix, T.N. et al. Medulloblastoma Genotype Dictates Blood Brain Barrier Phenotype. *Cancer Cell* **29**, 508-522 (2016).
35. Baryawno, N. et al. Small-molecule inhibitors of phosphatidylinositol 3-kinase/Akt signaling inhibit Wnt/beta-catenin pathway cross-talk and suppress medulloblastoma growth. *Cancer Res* **70**, 266-276 (2010).
36. Pietsch, T. & Haberler, C. Update on the integrated histopathological and genetic classification of medulloblastoma - a practical diagnostic guideline. *Clin Neuropathol* **35**, 344-352 (2016).
37. Smith, M.J. et al. Germline mutations in SUFU cause Gorlin syndrome-associated childhood medulloblastoma and redefine the risk associated with PTCH1 mutations. *J Clin Oncol* **32**, 4155-4161 (2014).
38. Choudhry, Z. et al. Sonic hedgehog signalling pathway: a complex network. *Ann Neurosci* **21**, 28-31 (2014).
39. Hui, C.C. & Angers, S. Gli proteins in development and disease. *Annu Rev Cell Dev Biol* **27**, 513-537 (2011).

40. Skowron, P., Ramaswamy, V. & Taylor, M.D. Genetic and molecular alterations across medulloblastoma subgroups. *J Mol Med (Berl)* **93**, 1075-1084 (2015).
41. Wang, X. et al. Sonic hedgehog regulates Bmi1 in human medulloblastoma brain tumor-initiating cells. *Oncogene* **31**, 187-199 (2012).
42. Wechsler-Reya, R.J. & Scott, M.P. Control of neuronal precursor proliferation in the cerebellum by Sonic Hedgehog. *Neuron* **22**, 103-114 (1999).
43. Martirosian, V., Chen, T.C., Lin, M. & Neman, J. Medulloblastoma initiation and spread: Where neurodevelopment, microenvironment and cancer cross pathways. *J Neurosci Res* **94**, 1511-1519 (2016).
44. Marzban, H. et al. Cellular commitment in the developing cerebellum. *Front Cell Neurosci* **8**, 450 (2014).
45. Salsano, E., Pollo, B., Eoli, M., Giordana, M.T. & Finocchiaro, G. Expression of MATH1, a marker of cerebellar granule cell progenitors, identifies different medulloblastoma sub-types. *Neurosci Lett* **370**, 180-185 (2004).
46. Goodrich, L.V., Milenkovic, L., Higgins, K.M. & Scott, M.P. Altered neural cell fates and medulloblastoma in mouse patched mutants. *Science* **277**, 1109-1113 (1997).
47. Yang, Z.J. et al. Medulloblastoma can be initiated by deletion of Patched in lineage-restricted progenitors or stem cells. *Cancer Cell* **14**, 135-145 (2008).
48. Thompson, E.M. et al. Prognostic value of medulloblastoma extent of resection after accounting for molecular subgroup: a retrospective integrated clinical and molecular analysis. *Lancet Oncol* **17**, 484-495 (2016).
49. Moxon-Emre, I. et al. Intellectual Outcome in Molecular Subgroups of Medulloblastoma. *J Clin Oncol* **34**, 4161-4170 (2016).
50. Gajjar, A. et al. Phase I study of vismodegib in children with recurrent or refractory medulloblastoma: a pediatric brain tumor consortium study. *Clin Cancer Res* **19**, 6305-6312 (2013).
51. Dijkgraaf, G.J. et al. Small molecule inhibition of GDC-0449 refractory smoothened mutants and downstream mechanisms of drug resistance. *Cancer Res* **71**, 435-444 (2011).
52. Rodon, J. et al. A phase I, multicenter, open-label, first-in-human, dose-escalation study of the oral smoothened inhibitor Sonidegib (LDE225) in patients with advanced solid tumors. *Clin Cancer Res* **20**, 1900-1909 (2014).
53. Hallahan, A.R. et al. The SmoA1 mouse model reveals that notch signaling is critical for the growth and survival of sonic hedgehog-induced medulloblastomas. *Cancer Res* **64**, 7794-7800 (2004).
54. Metcalfe, C. et al. PTEN loss mitigates the response of medulloblastoma to Hedgehog pathway inhibition. *Cancer Res* **73**, 7034-7042 (2013).
55. Gajjar, A.J. & Robinson, G.W. Medulloblastoma-translating discoveries from the bench to the bedside. *Nat Rev Clin Oncol* **11**, 714-722 (2014).
56. Adamson, D.C. et al. OTX2 is critical for the maintenance and progression of Shh-independent medulloblastomas. *Cancer Res* **70**, 181-191 (2010).
57. Kool, M. et al. Integrated genomics identifies five medulloblastoma subtypes with distinct genetic profiles, pathway signatures and clinicopathological features. *PLoS One* **3**, e3088 (2008).
58. Boon, K., Eberhart, C.G. & Riggins, G.J. Genomic amplification of orthodenticle homologue 2 in medulloblastomas. *Cancer Res* **65**, 703-707 (2005).

59. Bunt, J. et al. OTX2 sustains a bivalent-like state of OTX2-bound promoters in medulloblastoma by maintaining their H3K27me3 levels. *Acta Neuropathol* **125**, 385-394 (2013).
60. Northcott, P.A., Korshunov, A., Pfister, S.M. & Taylor, M.D. The clinical implications of medulloblastoma subgroups. *Nat Rev Neurol* **8**, 340-351 (2012).
61. Northcott, P.A. et al. Medulloblastomics: the end of the beginning. *Nat Rev Cancer* **12**, 818-834 (2012).
62. Northcott, P.A. et al. Enhancer hijacking activates GFI1 family oncogenes in medulloblastoma. *Nature* **511**, 428-434 (2014).
63. Schroeder, K. & Gururangan, S. Molecular variants and mutations in medulloblastoma. *Pharmgenomics Pers Med* **7**, 43-51 (2014).
64. Pei, Y. et al. An animal model of MYC-driven medulloblastoma. *Cancer Cell* **21**, 155-167 (2012).
65. Kawauchi, D. et al. A mouse model of the most aggressive subgroup of human medulloblastoma. *Cancer Cell* **21**, 168-180 (2012).
66. Kawauchi, D. et al. Novel MYC-driven medulloblastoma models from multiple embryonic cerebellar cells. *Oncogene* (2017).
67. Wortham, M. et al. Aberrant Otx2 expression enhances migration and induces ectopic proliferation of hindbrain neuronal progenitor cells. *PLoS One* **7**, e36211 (2012).
68. Adesina, A.M. et al. FOXG1 dysregulation is a frequent event in medulloblastoma. *J Neurooncol* **85**, 111-122 (2007).
69. Lin, C.Y. et al. Active medulloblastoma enhancers reveal subgroup-specific cellular origins. *Nature* **530**, 57-62 (2016).
70. Swartling, F.J. et al. Pleiotropic role for MYCN in medulloblastoma. *Genes Dev* **24**, 1059-1072 (2010).
71. Swartling, F.J. et al. Distinct neural stem cell populations give rise to disparate brain tumors in response to N-MYC. *Cancer Cell* **21**, 601-613 (2012).
72. Mubarak, N. et al. A randomized, phase 2 study comparing pemetrexed plus best supportive care versus best supportive care as maintenance therapy after first-line treatment with pemetrexed and cisplatin for advanced, non-squamous, non-small cell lung cancer. *BMC Cancer* **12**, 423 (2012).
73. Bai, R. et al. Evaluation of retinoic acid therapy for OTX2-positive medulloblastomas. *Neuro Oncol* **12**, 655-663 (2010).
74. Azevedo, F.A. et al. Equal numbers of neuronal and nonneuronal cells make the human brain an isometrically scaled-up primate brain. *J Comp Neurol* **513**, 532-541 (2009).
75. Roussel, M.F. & Hatten, M.E. Cerebellum development and medulloblastoma. *Curr Top Dev Biol* **94**, 235-282 (2011).
76. Schmahmann, J.D. & Caplan, D. Cognition, emotion and the cerebellum. *Brain* **129**, 290-292 (2006).
77. Wiser, A.K. et al. Dysfunctional cortico-cerebellar circuits cause 'cognitive dysmetria' in schizophrenia. *Neuroreport* **9**, 1895-1899 (1998).
78. Butts, T., Green, M.J. & Wingate, R.J. Development of the cerebellum: simple steps to make a 'little brain'. *Development* **141**, 4031-4041 (2014).

79. Limperopoulos, C. et al. Does cerebellar injury in premature infants contribute to the high prevalence of long-term cognitive, learning, and behavioral disability in survivors? *Pediatrics* **120**, 584-593 (2007).
80. Altman, J. & Bayer, S.A. Embryonic development of the rat cerebellum. I. Delineation of the cerebellar primordium and early cell movements. *J Comp Neurol* **231**, 1-26 (1985).
81. Martinez, S., Andreu, A., Mecklenburg, N. & Echevarria, D. Cellular and molecular basis of cerebellar development. *Front Neuroanat* **7**, 18 (2013).
82. Araujo, A.P. et al. Effects of Transforming Growth Factor Beta 1 in Cerebellar Development: Role in Synapse Formation. *Front Cell Neurosci* **10**, 104 (2016).
83. Leto, K. & Rossi, F. Specification and differentiation of cerebellar GABAergic neurons. *Cerebellum* **11**, 434-435 (2012).
84. Dusart, I. & Flamant, F. Profound morphological and functional changes of rodent Purkinje cells between the first and the second postnatal weeks: a metamorphosis? *Front Neuroanat* **6**, 11 (2012).
85. Daz, C. & Puelles, L. Plurisegmental vestibulocerebellar projections and other hindbrain cerebellar afferents in midterm chick embryos: biotinylated dextranamine experiments in vitro. *Neuroscience* **117**, 71-82 (2003).
86. Gray's Anatomy. *Bookseller*, 32-32 (2011).
87. Muller, F. & O'Rahilly, R. The human brain at stages 21-23, with particular reference to the cerebral cortical plate and to the development of the cerebellum. *Anat Embryol (Berl)* **182**, 375-400 (1990).
88. Martinez, S. The cerebellum: from development to structural complexity and motor learning. *Front Neuroanat* **8**, 118 (2014).
89. Broccoli, V., Boncinelli, E. & Wurst, W. The caudal limit of Otx2 expression positions the isthmic organizer. *Nature* **401**, 164-168 (1999).
90. Danielian, P.S. & McMahon, A.P. Engrailed-1 as a target of the Wnt-1 signalling pathway in vertebrate midbrain development. *Nature* **383**, 332-334 (1996).
91. Hidalgo-Sanchez, M., Martinez-de-la-Torre, M., Alvarado-Mallart, R.M. & Puelles, L. A distinct preisthmic histogenetic domain is defined by overlap of Otx2 and Pax2 gene expression in the avian caudal midbrain. *J Comp Neurol* **483**, 17-29 (2005).
92. Blaess, S., Corrales, J.D. & Joyner, A.L. Sonic hedgehog regulates Gli activator and repressor functions with spatial and temporal precision in the mid/hindbrain region. *Development* **133**, 1799-1809 (2006).
93. Vieira, C. et al. Molecular mechanisms controlling brain development: an overview of neuroepithelial secondary organizers. *Int J Dev Biol* **54**, 7-20 (2010).
94. Wingate, R.J. & Hatten, M.E. The role of the rhombic lip in avian cerebellum development. *Development* **126**, 4395-4404 (1999).
95. Bally-Cuif, L. & Wassef, M. Determination events in the nervous system of the vertebrate embryo. *Curr Opin Genet Dev* **5**, 450-458 (1995).
96. Wingate, R.J. The rhombic lip and early cerebellar development. *Curr Opin Neurobiol* **11**, 82-88 (2001).
97. Lavezzi, A.M., Ottaviani, G., Terni, L. & Matturri, L. Histological and biological developmental characterization of the human cerebellar cortex. *Int J Dev Neurosci* **24**, 365-371 (2006).

98. Zecevic, N. & Rakic, P. Differentiation of Purkinje cells and their relationship to other components of developing cerebellar cortex in man. *J Comp Neurol* **167**, 27-47 (1976).
99. Tsekhmistrenko, T.A. Quantitative changes in human cerebellar pyriform neurons from birth to the age of 20 years. *Neurosci Behav Physiol* **29**, 405-409 (1999).
100. Schuller, U. et al. Acquisition of granule neuron precursor identity is a critical determinant of progenitor cell competence to form Shh-induced medulloblastoma. *Cancer Cell* **14**, 123-134 (2008).
101. Hagan, N. & Zervas, M. Wnt1 expression temporally allocates upper rhombic lip progenitors and defines their terminal cell fate in the cerebellum. *Mol Cell Neurosci* **49**, 217-229 (2012).
102. Pei, Y. et al. WNT signaling increases proliferation and impairs differentiation of stem cells in the developing cerebellum. *Development* **139**, 1724-1733 (2012).
103. Wortham, M. et al. Chromatin accessibility mapping identifies mediators of basal transcription and retinoid-induced repression of OTX2 in medulloblastoma. *PLoS One* **9**, e107156 (2014).
104. Larsen, K.B., Lutterodt, M.C., Mollgard, K. & Moller, M. Expression of the homeobox genes OTX2 and OTX1 in the early developing human brain. *J Histochem Cytochem* **58**, 669-678 (2010).
105. Acampora, D. et al. Visceral endoderm-restricted translation of Otx1 mediates recovery of Otx2 requirements for specification of anterior neural plate and normal gastrulation. *Development* **125**, 5091-5104 (1998).
106. Chatelain, G., Fossat, N., Brun, G. & Lamonerie, T. Molecular dissection reveals decreased activity and not dominant negative effect in human OTX2 mutants. *J Mol Med (Berl)* **84**, 604-615 (2006).
107. Puelles, E. et al. Otx2 regulates the extent, identity and fate of neuronal progenitor domains in the ventral midbrain. *Development* **131**, 2037-2048 (2004).
108. Hoch, R.V., Lindtner, S., Price, J.D. & Rubenstein, J.L. OTX2 Transcription Factor Controls Regional Patterning within the Medial Ganglionic Eminence and Regional Identity of the Septum. *Cell Rep* **12**, 482-494 (2015).
109. Boncinelli, E. & Morgan, R. Downstream of Otx2, or how to get a head. *Trends Genet* **17**, 633-636 (2001).
110. Fossat, N., Chatelain, G., Brun, G. & Lamonerie, T. Temporal and spatial delineation of mouse Otx2 functions by conditional self-knockout. *EMBO Rep* **7**, 824-830 (2006).
111. Matsuo, I., Kuratani, S., Kimura, C., Takeda, N. & Aizawa, S. Mouse Otx2 functions in the formation and patterning of rostral head. *Genes Dev* **9**, 2646-2658 (1995).
112. de Haas, T. et al. OTX1 and OTX2 expression correlates with the clinicopathologic classification of medulloblastomas. *J Neuropathol Exp Neurol* **65**, 176-186 (2006).
113. Frantz, G.D., Weimann, J.M., Levin, M.E. & McConnell, S.K. Otx1 and Otx2 define layers and regions in developing cerebral cortex and cerebellum. *J Neurosci* **14**, 5725-5740 (1994).
114. Chung, C.Y. et al. The transcription factor orthodenticle homeobox 2 influences axonal projections and vulnerability of midbrain dopaminergic neurons. *Brain* **133**, 2022-2031 (2010).

115. Omodei, D. et al. Anterior-posterior graded response to Otx2 controls proliferation and differentiation of dopaminergic progenitors in the ventral mesencephalon. *Development* **135**, 3459-3470 (2008).
116. Nguyen Ba-Charvet, K.T., von Boxberg, Y., Guazzi, S., Boncinelli, E. & Godement, P. A potential role for the OTX2 homeoprotein in creating early 'highways' for axon extension in the rostral brain. *Development* **125**, 4273-4282 (1998).
117. Wieschaus, E., Perrimon, N. & Finkelstein, R. orthodenticle activity is required for the development of medial structures in the larval and adult epidermis of Drosophila. *Development* **115**, 801-811 (1992).
118. Puelles, L. & Rubenstein, J.L. Forebrain gene expression domains and the evolving prosomeric model. *Trends Neurosci* **26**, 469-476 (2003).
119. Puelles, E. et al. Otx2 controls identity and fate of glutamatergic progenitors of the thalamus by repressing GABAergic differentiation. *J Neurosci* **26**, 5955-5964 (2006).
120. Johansson, P.A. et al. The transcription factor Otx2 regulates choroid plexus development and function. *Development* **140**, 1055-1066 (2013).
121. Nishida, A. et al. Otx2 homeobox gene controls retinal photoreceptor cell fate and pineal gland development. *Nat Neurosci* **6**, 1255-1263 (2003).
122. Nishihara, D. et al. Otx2 is involved in the regional specification of the developing retinal pigment epithelium by preventing the expression of sox2 and fgf8, factors that induce neural retina differentiation. *PLoS One* **7**, e48879 (2012).
123. Nishida, S. et al. Immunization with ACE (Angiotensin Converting Enzyme) develops diabetic changes in the kidney and retina in diabetogenic rats. *Endocr J* **50**, 801-807 (2003).
124. Furukawa, T., Morrow, E.M. & Cepko, C.L. Crx, a novel otx-like homeobox gene, shows photoreceptor-specific expression and regulates photoreceptor differentiation. *Cell* **91**, 531-541 (1997).
125. Furukawa, E. & Omura, Y. Scanning and transmission electron microscopic study on a multilayered basement membrane in the pineal organ of the ayu Plecoglossus altivelis. *Arch Histol Cytol* **60**, 511-517 (1997).
126. Koike, C. et al. Functional roles of Otx2 transcription factor in postnatal mouse retinal development. *Mol Cell Biol* **27**, 8318-8329 (2007).
127. Baas, D. et al. The subcellular localization of Otx2 is cell-type specific and developmentally regulated in the mouse retina. *Brain Res Mol Brain Res* **78**, 26-37 (2000).
128. Fossat, N. et al. A new GFP-tagged line reveals unexpected Otx2 protein localization in retinal photoreceptors. *BMC Dev Biol* **7**, 122 (2007).
129. Beby, F. et al. Otx2 gene deletion in adult mouse retina induces rapid RPE dystrophy and slow photoreceptor degeneration. *PLoS One* **5**, e11673 (2010).
130. Bunt, J. et al. Regulation of cell cycle genes and induction of senescence by overexpression of OTX2 in medulloblastoma cell lines. *Mol Cancer Res* **8**, 1344-1357 (2010).
131. Bai, R.Y., Staedtke, V., Lidov, H.G., Eberhart, C.G. & Riggins, G.J. OTX2 represses myogenic and neuronal differentiation in medulloblastoma cells. *Cancer Res* **72**, 5988-6001 (2012).
132. Bunt, J. et al. Joint binding of OTX2 and MYC in promotor regions is associated with high gene expression in medulloblastoma. *PLoS One* **6**, e26058 (2011).

133. Bernstein, B.E. et al. A bivalent chromatin structure marks key developmental genes in embryonic stem cells. *Cell* **125**, 315-326 (2006).
134. Al-Hajj, M. Cancer stem cells and oncology therapeutics. *Curr Opin Oncol* **19**, 61-64 (2007).
135. Dick, J.E. Stem cell concepts renew cancer research. *Blood* **112**, 4793-4807 (2008).
136. Potten, C.S., Al-Barwari, S.E., Hume, W.J. & Searle, J. Circadian rhythms of presumptive stem cells in three different epithelia of the mouse. *Cell Tissue Kinet* **10**, 557-568 (1977).
137. Lapidot, T. et al. A cell initiating human acute myeloid leukaemia after transplantation into SCID mice. *Nature* **367**, 645-648 (1994).
138. Pastrana, E., Silva-Vargas, V. & Doetsch, F. Eyes wide open: a critical review of sphere-formation as an assay for stem cells. *Cell Stem Cell* **8**, 486-498 (2011).
139. Dontu, G., Al-Hajj, M., Abdallah, W.M., Clarke, M.F. & Wicha, M.S. Stem cells in normal breast development and breast cancer. *Cell Prolif* **36 Suppl 1**, 59-72 (2003).
140. Al-Hajj, M., Wicha, M.S., Benito-Hernandez, A., Morrison, S.J. & Clarke, M.F. Prospective identification of tumorigenic breast cancer cells. *Proc Natl Acad Sci U S A* **100**, 3983-3988 (2003).
141. Singh, S.K. et al. Identification of a cancer stem cell in human brain tumors. *Cancer Res* **63**, 5821-5828 (2003).
142. Liang, L. et al. Characterization of novel biomarkers in selecting for subtype specific medulloblastoma phenotypes. *Oncotarget* **6**, 38881-38900 (2015).
143. Read, T.A. et al. Identification of CD15 as a marker for tumor-propagating cells in a mouse model of medulloblastoma. *Cancer Cell* **15**, 135-147 (2009).
144. Ward, R.J. et al. Multipotent CD15+ cancer stem cells in patched-1-deficient mouse medulloblastoma. *Cancer Res* **69**, 4682-4690 (2009).
145. Capela, A. & Temple, S. LeX/ssea-1 is expressed by adult mouse CNS stem cells, identifying them as nonependymal. *Neuron* **35**, 865-875 (2002).
146. Kreso, A. & Dick, J.E. Evolution of the cancer stem cell model. *Cell Stem Cell* **14**, 275-291 (2014).
147. Friedman, H.S. et al. Establishment and characterization of the human medulloblastoma cell line and transplantable xenograft D283 Med. *J Neuropathol Exp Neurol* **44**, 592-605 (1985).
148. Snuderl, M. et al. Targeting placental growth factor/neuropilin 1 pathway inhibits growth and spread of medulloblastoma. *Cell* **152**, 1065-1076.
149. Siu, I.M., Lal, A., Blankenship, J.R., Aldosari, N. & Riggins, G.J. c-Myc promoter activation in medulloblastoma. *Cancer Res* **63**, 4773-4776 (2003).
150. Thompson, E.M. et al. The role of angiogenesis in Group 3 medulloblastoma pathogenesis and survival. *Neuro Oncol* (2017).
151. Friedman, H.S. et al. Phenotypic and genotypic analysis of a human medulloblastoma cell line and transplantable xenograft (D341 Med) demonstrating amplification of c-myc. *Am J Pathol* **130**, 472-484 (1988).
152. He, X.M. et al. Differentiation characteristics of newly established medulloblastoma cell lines (D384 Med, D425 Med, and D458 Med) and their transplantable xenografts. *Lab Invest* **64**, 833-843 (1991).

153. Dietl, S. et al. MB3W1 is an orthotopic xenograft model for anaplastic medulloblastoma displaying cancer stem cell- and Group 3-properties. *BMC Cancer* **16**, 115 (2016).
154. Milde, T. et al. HD-MB03 is a novel Group 3 medulloblastoma model demonstrating sensitivity to histone deacetylase inhibitor treatment. *J Neurooncol* **110**, 335-348 (2012).
155. Morrison, L.C. et al. Deconstruction of medulloblastoma cellular heterogeneity reveals differences between the most highly invasive and self-renewing phenotypes. *Neoplasia* **15**, 384-398 (2013).
156. Subramanian, A. et al. Gene set enrichment analysis: a knowledge-based approach for interpreting genome-wide expression profiles. *Proc Natl Acad Sci U S A* **102**, 15545-15550 (2005).
157. Milacic, M. et al. Annotating cancer variants and anti-cancer therapeutics in reactome. *Cancers* **4**, 1180-1211 (2012).
158. Croft, D. et al. The Reactome pathway knowledgebase. *Nucleic Acids Res* **42**, D472-477 (2014).
159. Kanehisa, M., Sato, Y., Kawashima, M., Furumichi, M. & Tanabe, M. KEGG as a reference resource for gene and protein annotation. *Nucleic Acids Res* **44**, D457-462 (2016).
160. Kanehisa, M. & Goto, S. KEGG: kyoto encyclopedia of genes and genomes. *Nucleic Acids Res* **28**, 27-30 (2000).
161. Kanehisa, M., Furumichi, M., Tanabe, M., Sato, Y. & Morishima, K. KEGG: new perspectives on genomes, pathways, diseases and drugs. *Nucleic Acids Res* **45**, D353-D361 (2017).
162. Northcott, P.A. et al. Subgroup-specific structural variation across 1,000 medulloblastoma genomes. *Nature* **488**, 49-56.
163. Remke, M. et al. FSTL5 is a marker of poor prognosis in non-WNT/non-SHH medulloblastoma. *J Clin Oncol* **29**, 3852-3861.
164. Mehlen, P., Delloye-Bourgeois, C. & Chedotal, A. Novel roles for Slits and netrins: axon guidance cues as anticancer targets? *Nat Rev Cancer* **11**, 188-197 (2011).
165. Neufeld, G. et al. The role of the semaphorins in cancer. *Cell Adh Migr*, 1-23 (2016).
166. Worzfeld, T. & Offermanns, S. Semaphorins and plexins as therapeutic targets. *Nat Rev Drug Discov* **13**, 603-621 (2014).
167. Castellani, V., De Angelis, E., Kenwrick, S. & Rougon, G. Cis and trans interactions of L1 with neuropilin-1 control axonal responses to semaphorin 3A. *EMBO J* **21**, 6348-6357 (2002).
168. Northcott, P.A. et al. Subgroup-specific structural variation across 1,000 medulloblastoma genomes. *Nature* **488**, 49-56 (2012).
169. Huszthy, P.C. et al. Remission of invasive, cancer stem-like glioblastoma xenografts using lentiviral vector-mediated suicide gene therapy. *PLoS One* **4**, e6314 (2009).
170. Di, C. et al. Identification of OTX2 as a medulloblastoma oncogene whose product can be targeted by all-trans retinoic acid. *Cancer Res* **65**, 919-924 (2005).
171. Zhao, J. et al. SEMA6A is a prognostic biomarker in glioblastoma. *Tumour Biol* **36**, 8333-8340 (2015).
172. Dubuc, A.M. et al. Subgroup-specific alternative splicing in medulloblastoma. *Acta Neuropathol* **123**, 485-499 (2012).

173. Kokubo, M. et al. BDNF-mediated cerebellar granule cell development is impaired in mice null for CaMKK2 or CaMKIV. *J Neurosci* **29**, 8901-8913 (2009).
174. Schuller, U., Kho, A.T., Zhao, Q., Ma, Q. & Rowitch, D.H. Cerebellar 'transcriptome' reveals cell-type and stage-specific expression during postnatal development and tumorigenesis. *Mol Cell Neurosci* **33**, 247-259 (2006).
175. Uemura, T. et al. Trans-synaptic interaction of GluRdelta2 and Neurexin through Cbln1 mediates synapse formation in the cerebellum. *Cell* **141**, 1068-1079 (2010).
176. Kerjan, G. et al. The transmembrane semaphorin Sema6A controls cerebellar granule cell migration. *Nat Neurosci* **8**, 1516-1524 (2005).
177. Renaud, J. et al. Plexin-A2 and its ligand, Sema6A, control nucleus-centrosome coupling in migrating granule cells. *Nat Neurosci* **11**, 440-449 (2008).
178. Telley, L. et al. Dual Function of NRP1 in Axon Guidance and Subcellular Target Recognition in Cerebellum. *Neuron* **91**, 1276-1291 (2016).
179. Huang, X. et al. The cell adhesion molecule L1 regulates the expression of FGF21 and enhances neurite outgrowth. *Brain Res* **1530**, 13-21 (2013).
180. Bloch-Gallego, E., Causeret, F., Ezan, F., Backer, S. & Hidalgo-Sanchez, M. Development of precerebellar nuclei: instructive factors and intracellular mediators in neuronal migration, survival and axon pathfinding. *Brain Res Brain Res Rev* **49**, 253-266 (2005).
181. Rehman, M. & Tamagnone, L. Semaphorins in cancer: biological mechanisms and therapeutic approaches. *Semin Cell Dev Biol* **24**, 179-189 (2013).
182. Hollis, E.R., 2nd & Zou, Y. Expression of the Wnt signaling system in central nervous system axon guidance and regeneration. *Front Mol Neurosci* **5**, 5 (2012).
183. Chedotal, A., Kerjan, G. & Moreau-Fauvarque, C. The brain within the tumor: new roles for axon guidance molecules in cancers. *Cell Death Differ* **12**, 1044-1056 (2005).
184. Wang, B. et al. Induction of tumor angiogenesis by Slit-Robo signaling and inhibition of cancer growth by blocking Robo activity. *Cancer Cell* **4**, 19-29 (2003).
185. Mertsch, S. et al. Slit2 involvement in glioma cell migration is mediated by Robo1 receptor. *J Neurooncol* **87**, 1-7 (2008).
186. Werbowetski-Ogilvie, T.E. et al. Inhibition of medulloblastoma cell invasion by Slit. *Oncogene* **25**, 5103-5112 (2006).
187. Scott, G.A., McClelland, L.A., Fricke, A.F. & Fender, A. Plexin C1, a receptor for semaphorin 7a, inactivates cofilin and is a potential tumor suppressor for melanoma progression. *J Invest Dermatol* **129**, 954-963 (2009).
188. Yazdani, U. & Terman, J.R. The semaphorins. *Genome Biol* **7**, 211 (2006).
189. Man, J. et al. Sema3C promotes the survival and tumorigenicity of glioma stem cells through Rac1 activation. *Cell Rep* **9**, 1812-1826 (2014).
190. Tomizawa, Y. et al. Inhibition of lung cancer cell growth and induction of apoptosis after reexpression of 3p21.3 candidate tumor suppressor gene SEMA3B. *Proc Natl Acad Sci U S A* **98**, 13954-13959 (2001).
191. Sierra, J.R. et al. Tumor angiogenesis and progression are enhanced by Sema4D produced by tumor-associated macrophages. *J Exp Med* **205**, 1673-1685 (2008).
192. Argast, G.M. et al. Plexin B1 is repressed by oncogenic B-Raf signaling and functions as a tumor suppressor in melanoma cells. *Oncogene* **28**, 2697-2709 (2009).

193. Snuderl, M. et al. Targeting placental growth factor/neuropilin 1 pathway inhibits growth and spread of medulloblastoma. *Cell* **152**, 1065-1076 (2013).
194. Bao, S. et al. Targeting cancer stem cells through L1CAM suppresses glioma growth. *Cancer Res* **68**, 6043-6048 (2008).
195. Lisabeth, E.M., Falivelli, G. & Pasquale, E.B. Eph receptor signaling and ephrins. *Cold Spring Harb Perspect Biol* **5** (2013).
196. Delloye-Bourgeois, C. et al. PlexinA1 is a new Slit receptor and mediates axon guidance function of Slit C-terminal fragments. *Nat Neurosci* **18**, 36-45 (2015).
197. Rolny, C. et al. The tumor suppressor semaphorin 3B triggers a prometastatic program mediated by interleukin 8 and the tumor microenvironment. *J Exp Med* **205**, 1155-1171 (2008).
198. Xu, Y., Li, W.L., Fu, L., Gu, F. & Ma, Y.J. Slit2/Robo1 signaling in glioma migration and invasion. *Neurosci Bull* **26**, 474-478 (2010).
199. Wong, K. et al. Signal transduction in neuronal migration: roles of GTPase activating proteins and the small GTPase Cdc42 in the Slit-Robo pathway. *Cell* **107**, 209-221 (2001).
200. Sikkema, A.H. et al. EphB2 activity plays a pivotal role in pediatric medulloblastoma cell adhesion and invasion. *Neuro Oncol* **14**, 1125-1135 (2012).
201. Bhatia, S. et al. Knockdown of EphB1 receptor decreases medulloblastoma cell growth and migration and increases cellular radiosensitization. *Oncotarget* **6**, 8929-8946 (2015).
202. Bunt, J. et al. OTX2 directly activates cell cycle genes and inhibits differentiation in medulloblastoma cells. *Int J Cancer* **131**, E21-32 (2012).
203. Boulay, G. et al. OTX2 Activity at Distal Regulatory Elements Shapes the Chromatin Landscape of Group 3 Medulloblastoma. *Cancer Discov* **7**, 288-301 (2017).
204. Viskov, C. et al. Isolation and characterization of contaminants in recalled unfractionated heparin and low-molecular-weight heparin. *Clin Appl Thromb Hemost* **15**, 395-401 (2009).
205. Dallol, A. et al. Frequent epigenetic inactivation of the SLIT2 gene in gliomas. *Oncogene* **22**, 4611-4616 (2003).
206. Dallol, A. et al. SLIT2, a human homologue of the Drosophila Slit2 gene, has tumor suppressor activity and is frequently inactivated in lung and breast cancers. *Cancer Res* **62**, 5874-5880 (2002).
207. Dickinson, R.E. et al. Epigenetic inactivation of SLIT3 and SLIT1 genes in human cancers. *Br J Cancer* **91**, 2071-2078 (2004).
208. Kuroki, T. et al. Allelic loss on chromosome 3p21.3 and promoter hypermethylation of semaphorin 3B in non-small cell lung cancer. *Cancer Res* **63**, 3352-3355 (2003).
209. Braga, E.A. et al. [New tumor suppressor genes in hot spots of human chromosome 3: new methods of identification]. *Mol Biol (Mosk)* **37**, 194-211 (2003).
210. Swiercz, J.M., Worzfeld, T. & Offermanns, S. ErbB-2 and met reciprocally regulate cellular signaling via plexin-B1. *J Biol Chem* **283**, 1893-1901 (2008).
211. Tilson, S.G. et al. ROCK Inhibition Facilitates In Vitro Expansion of Glioblastoma Stem-Like Cells. *PLoS One* **10**, e0132823 (2015).
212. Chen, W. et al. RhoB Acts as a Tumor Suppressor That Inhibits Malignancy of Clear Cell Renal Cell Carcinoma. *PLoS One* **11**, e0157599 (2016).

213. Liu, M. et al. miR-21 targets the tumor suppressor RhoB and regulates proliferation, invasion and apoptosis in colorectal cancer cells. *FEBS Lett* **585**, 2998-3005 (2011).
214. Xu, J. et al. The neddylation-cullin 2-RBX1 E3 ligase axis targets tumor suppressor RhoB for degradation in liver cancer. *Mol Cell Proteomics* **14**, 499-509 (2015).
215. Battistini, C. & Tamagnone, L. Transmembrane semaphorins, forward and reverse signaling: have a look both ways. *Cell Mol Life Sci* **73**, 1609-1622 (2016).
216. Grotzer, M.A., Janss, A.J., Phillips, P.C. & Trojanowski, J.Q. Neurotrophin receptor TrkC predicts good clinical outcome in medulloblastoma and other primitive neuroectodermal brain tumors. *Klin Padiatr* **212**, 196-199 (2000).
217. Miyahara, H. et al. Neuronal differentiation associated with Gli3 expression predicts favorable outcome for patients with medulloblastoma. *Neuropathology* **34**, 1-10 (2014).

APPENDIX A: SUPPLEMENARY TABLES

Table S1: Neuronal differentiation genes that are significantly and differentially expressed following OTX2 knockdown in D283 tumorspheres.

Gene Assignment	Predictive effect on neuronal differentiation (based on measurement direction and literature compiled in Ingenuity® Knowledge Base)	Fold change
DPYSL2	Increased	2.284692494
NEUROD2	Increased	2.470837274
NTRK3	Increased	3.721798631
HMGB2	Increased	0.334250124
EFNA3	Increased	3.294364069
GAP43	Increased	10.4468783
MID1	Increased	0.398320048
NRXN1	Increased	7.459091891
NSG1	Increased	2.187070915
CNR1	Increased	9.787904329
EPHA4	Increased	2.713208655
LRP1	Increased	2.435132037
NR2F1	Increased	3.140512475
KLF7	Increased	2.797232165
DLG5	Increased	2.100889088
ACTL6B	Increased	2.239225777
CNTNAP2	Increased	9.493894381
NCAM2	Increased	13.78473856
TSC1	Increased	2.037782393
PAX6	Increased	3.031433133
RELN	Increased	4.00277355
SEMA6A	Increased	5.544279543
NUMBL	Increased	2.0265138
SDK1	Increased	2.396618043
CRMP1	Increased	8.190775203
DPYSL3	Increased	2.261061134
SNCA	Increased	5.95045505
DPYSL5	Increased	2.223758315
CIT	Increased	0.377356492
KIDINS220	Increased	2.979354926
SLIT2	Increased	3.365917929
KIF3A	Increased	2.844154821
GRIA1	Increased	6.520578659
BCL2	Increased	2.63170905
FNBP1	Increased	2.488023307
KIF1A	Increased	3.38932974

PDGFRA	Increased	4.982949662
RIMS1	Increased	4.161201066
APP	Increased	2.360348687
KALRN	Increased	4.806544198
ELAVL4	Increased	26.6857934
FYN	Increased	3.280691645
mir-181	Increased	2.987626914
CAMK4	Increased	3.431882122
TRIP10	Increased	0.219912269
CAMK1G	Increased	3.020945171
NEUROD1	Increased	2.193143177
CDK5R1	Increased	2.756810306
ADGRB2	Increased	2.494931144
MAPT	Increased	4.17564771
NEUROG2	Increased	2.797232165
SEMA4D	Increased	3.45575275
HES1	Increased	0.400257405
ID1	Increased	0.4181232
NEFH	Increased	0.291587342
RYR2	Increased	11.03488737
TNFRSF21	Increased	0.494142826
PRKCE	Increased	3.396384986
TBR1	Increased	2.698205069
CHRNA1	Increased	0.410940094
NEUROD6	Increased	2.946495372
SV2A	Increased	2.352182501
MAP6	Increased	12.92417244
ADGRL3	Increased	10.70342044
PCYT1B	Increased	2.200757219
LRRTM2	Increased	3.415270858
ASCL1	Increased	3.640155296
ADGRB3	Increased	2.040609318
CLSTN2	Increased	6.315951094
SOX11	Increased	2.380063393
NLGN3	Increased	2.136130816
DAGLA	Increased	2.319799309
SLITRK5	Increased	2.265767771
CAPRIN2	Increased	2.926142441
TENM4	Increased	8.24774655
LRRN3	Increased	6.050271989
FLRT1	Increased	4.23393758
CLSTN3	Increased	2.233025924
LRRTM1	Increased	4.334903867
CBLN2	Increased	2.11696879

NEUROD4	Increased	4.401514437
RIMS3	Increased	2.713208655
EPHB2	Increased	2.72829567
SEPT4	Decreased	0.276241121
ERBB2	Decreased	0.438910899
SULF1	Decreased	0.458819941
MUSK	Decreased	0.368311921
BMP7	Decreased	0.414659773
EEF2K	Decreased	0.281654807
PPP3CA	Decreased	2.488023307
RIT1	Decreased	2.051956291
DOCK10	Decreased	0.403880389
SMAD3	Decreased	0.44844408
TGFB1	Decreased	0.279709275
FGF2	Decreased	0.281069731
FGFR2	Decreased	0.248445273
SDC2	Decreased	0.492433221
COL25A1	Decreased	0.5
GDI1	Decreased	2.09216988
KIF23	Decreased	0.146807746
DCX	Decreased	5.241573615
SLC12A2	Decreased	0.334713814
SERPINF1	Decreased	0.195467411
SYNGAP1	Decreased	2.522754818
RTN4	Decreased	2.057653416
CBLN1	Decreased	0.342695701
GAS7	Decreased	0.185436867
RAPGEF2	Decreased	3.655325801
NTF3	Decreased	0.321078952
DCLK1	Decreased	4
RYR1	Decreased	0.483973513
CHRNA7	Decreased	0.295452887
GLI3	Decreased	0.243163737
KLF9	Decreased	0.219912269
NGF	Decreased	0.220064753
GEM	Decreased	0.268501118
L1CAM	Decreased	5.105315075
MYO5A	Decreased	2.324628215
IGF1	Decreased	0.467163673
DOCK1	Decreased	0.464902471
MAPK8IP1	Decreased	2.67585511
PARD3	Decreased	0.431071773
PLPPR5	Decreased	0.336108749
RAB17	Decreased	0.16747295

REM2	Decreased	2.270484204
ROBO2	Decreased	2.406606052
MDGA1	Decreased	2.236123702
BARHL2	Affected	2.202283196
LRP4	Affected	0.400812665
NYAP2	Affected	9.553305497
CELSR2	Affected	4.597979392
CPT1C	Affected	2.236123702
PCDHB9	Affected	2.020902893
RNF165	Affected	3.073750363
PRICKLE2	Affected	0.267757706
BRSK1	Affected	2.043440165
PCDHB14	Affected	3.673104649
ATL1	Affected	2.37676621
PDZRN3	Affected	0.321747312
GPM6A	Affected	2.430073584
LRRC7	Affected	22.7059737
RUFY3	Affected	2.496661098
SHTN1	Affected	4.717426369
NSMF	Affected	4.319906239
CCDC88A	Affected	2.069095163
BBS4	Affected	0.395842933
CLMN	Affected	0.221288441
FEZF2	Affected	2.687006851
SEZ6	Affected	2.944453724
TULP1	Affected	0.385552706
PCDH8	Affected	2.360348687
CACNA1F	Affected	0.406126198
CNTN4	Affected	5.158673003
CPEB4	Affected	2.150988781
ATCAY	Affected	11.08855909
PREX2	Affected	0.441351498
PLXND1	Affected	2.284692494
LRRC4C	Affected	3.69609029
CASP6	Affected	0.480630464
GABRA5	Affected	0.252437824
GFRA1	Affected	2.615342697
SPR	Affected	0.272815969
CACNA2D2	Affected	8.299359493
HSPB1	Affected	0.407253782
SYN1	Affected	2.599078125
LZTS1	Affected	2.350552657
MAP1B	Affected	2.711328654
NPTXR	Affected	22.54913208

SLC1A3	Affected	0.257563488
NCAN	Affected	4.422922613
SHC1	Affected	0.486327474
NOTCH1	Affected	0.384751805
PARD6B	Affected	0.283417353
ETV4	Affected	0.483973513
SYP	Affected	2.125791349
DMD	Affected	0.498615626
LAMA1	Affected	0.242322454
SNAP91	Affected	4.948529915
CACNB4	Affected	0.489370825
SNCB	Affected	4.319906239
MPP5	Affected	0.340328529
CD44	Affected	2.615342697
GJA1	Affected	0.095127086
BTG3	Affected	0.334250124
HCN1	Affected	3.048289661
NRG1	Affected	3.60500185
PCDHB13	Affected	4.456774603
CXCR4	Affected	0.35013908
EPB41L3	Affected	3.977880675
DNER	Affected	4.707626949
NR4A2	Affected	3.906834116
CTNNA2	Affected	2.327853069
CAST	Affected	0.41065535
TP73	Affected	5.045509635
SPTBN4	Affected	2.507066041
NRP2	Affected	5.392670927
PLXNA3	Affected	3.431882122
ONECUT1	Affected	4.352969767
THRA	Affected	3.928558381
RAB3A	Affected	2.353813474
ERBB3	Affected	0.416099367
ARHGEF28	Affected	2.170458744
MYOD1	Affected	0.172898829
LOX	Affected	0.35404386
RDX	Affected	0.498615626
CADM1	Affected	2.096524951
C3	Affected	0.190650207
UNC5A	Affected	3.647732662
UGT8	Affected	0.335875856
FZD5	Affected	0.456599125
VIM	Affected	0.355765865
OPTN	Affected	3.518596304

WNT7B	Affected	3.035638506
VLDLR	Affected	0.280097304
DISC1	Affected	0.278548413
COL4A1	Affected	0.240148716
PLPPR4	Affected	0.409802304
DCC	Affected	19.91798777
NRP1	Affected	4.525257851
GABRG2	Affected	5.172995728
ARHGAP33	Affected	3.786854525
CLU	Affected	0.393926943
CACNA1S	Affected	0.47204621
RAB29	Affected	0.206183387
MAP2	Affected	17.31559431
TOP2B	Affected	2.046274939
PRDM1	Affected	0.285982743
CDC20	Affected	0.178376813
LIF	Affected	0.414659773
SRCIN1	Affected	2.633533844
SRGAP2	Affected	2.106722072
SIPA1L1	Affected	2.049113646
HERC1	Affected	2.724516069
PDLIM5	Affected	0.454074209
EFNB2	Affected	8.456144324
WEE1	Affected	0.340800652
SIX4	Affected	0.346517471
BMP2	Affected	0.166200889
CACNA1A	Affected	14.89751712
LYN	Affected	0.185436867
PITPNA	Affected	0.47237352
NR2F6	Affected	0.469435874
NR1D1	Affected	2.30697121
KIF20B	Affected	0.33985706
PAK3	Affected	5.540437872
FNBP1L	Affected	2.648177821
PCDHB8	Affected	2.049113646
PCDHB10	Affected	4.23393758
PCDHB11	Affected	2.873880353
EPHA3	Affected	35.97692556
LAMB2	Affected	0.404160434
LINGO1	Affected	2.153972752

Transcripts differentially expressed at least 2.0-fold (up- or downregulated) and with a value of $P<0.05$ were considered significant.

Table S2: Axon guidance genes that are significantly and differentially expressed following OTX2 knockdown in D283 tumorspheres.

Gene Assignment	Entrez Gene Name	Fold change
ABLIM3	actin binding LIM protein family, member 3	0.358488812
ADAM11	ADAM metallopeptidase domain 11	4.629960868
ADAM23	ADAM metallopeptidase domain 23	2.298989696
ADAMTS7	ADAM metallopeptidase with thrombospondin type 1 motif, 7	2.484576564
ARPC1B	actin related protein 2/3 complex, subunit 1B, 41kDa	0.467163673
BMP1	bone morphogenetic protein 1	2.38998241
BMP2	bone morphogenetic protein 2	0.166200889
BMP7	bone morphogenetic protein 7	0.414659773
C9orf3	chromosome 9 open reading frame 3	0.428390977
CXCR4	chemokine (C-X-C motif) receptor 4	0.35013908
DCC	DCC netrin 1 receptor	19.91798777
DOCK1	dedicator of cytokinesis 1	0.464902471
DPYSL2	dihydropyrimidinase-like 2	2.284692494
DPYSL5	dihydropyrimidinase-like 5	2.223758315
EFNA3	ephrin-A3	3.294364069
EFNA4	ephrin-A4	0.178624267
EFNB2	ephrin-B2	8.456144324
EPHA2	EPH receptor A2	0.18595172
EPHA3	EPH receptor A3	35.97692556
EPHA4	EPH receptor A4	2.713208655
EPHA5	EPH receptor A5	29.79503423
EPHB2	EPH receptor B2	2.72829567
EPHB4	EPH receptor B4	0.273763118
ERBB2	erb-b2 receptor tyrosine kinase 2	0.438910899
FYN	FYN proto-oncogene, Src family tyrosine kinase	3.280691645
FZD1	frizzled class receptor 1	0.411510173
FZD5	frizzled class receptor 5	0.456599125
FZD7	frizzled class receptor 7	0.08207007
GLI3	GLI family zinc finger 3	0.243163737
GNAO1	guanine nucleotide binding protein (G protein), alpha activating activity polypeptide O	5.747760706
GNB3	guanine nucleotide binding protein (G protein), beta polypeptide 3	0.257206677
GNB4	guanine nucleotide binding protein (G protein), beta polypeptide 4	0.294226684
GNB5	guanine nucleotide binding protein (G protein), beta 5	2.131693472
GNG2	guanine nucleotide binding protein (G protein), gamma 2	3.020945171
GNG3	guanine nucleotide binding protein (G protein), gamma 3	6.143241079
GNG5	guanine nucleotide binding protein (G protein), gamma 5	0.40584479
GNG11	guanine nucleotide binding protein (G protein), gamma 11	0.367801686

GNG12	guanine nucleotide binding protein (G protein), gamma 12	0.300200857
IGF1	insulin-like growth factor 1 (somatomedin C)	0.467163673
ITGA4	integrin, alpha 4 (antigen CD49D, alpha 4 subunit of VLA-4 receptor)	2.25792881
KALRN	kalirin, RhoGEF kinase	4.806544198
KLC1	kinesin light chain 1	2.164449289
L1CAM	L1 cell adhesion molecule	5.105315075
LINGO1	leucine rich repeat and Ig domain containing 1	2.153972752
LRRC4C	leucine rich repeat containing 4C	3.69609029
MICAL1	microtubule associated monooxygenase, calponin and LIM domain containing 1	2.425025638
MYL4	myosin, light chain 4, alkali; atrial, embryonic	0.357000995
NGF	nerve growth factor (beta polypeptide)	0.220064753
NRP1	neuropilin 1	4.525257851
NRP2	neuropilin 2	5.392670927
NTF3	neurotrophin 3	0.321078952
NTRK3	neurotrophic tyrosine kinase, receptor, type 3	3.721798631
PAK3	p21 protein (Cdc42/Rac)-activated kinase 3	5.540437872
PAK7	p21 protein (Cdc42/Rac)-activated kinase 7	4.688089135
PAPPA2	pappalysin 2	0.147624083
PLCB4	phospholipase C, beta 4	9.428315262
PLCD3	phospholipase C, delta 3	0.392292049
PLCD4	phospholipase C, delta 4	3.267075964
PLCE1	phospholipase C, epsilon 1	0.341036959
PLCG1	phospholipase C, gamma 1	2.403272099
PLCL1	phospholipase C-like 1	4.500233939
PLXNA2	plexin A2	3.43664302
PLXNA3	plexin A3	3.431882122
PLXND1	plexin D1	2.284692494
PPP3CA	protein phosphatase 3, catalytic subunit, alpha isozyme	2.488023307
PRKAR2B	protein kinase, cAMP-dependent, regulatory, type II, beta	2.486299338
PRKCE	protein kinase C, epsilon	3.396384986
PRKD3	protein kinase D3	0.459456442
PTCH2	patched 2	3.164549205
ROBO2	roundabout guidance receptor 2	2.406606052
RRAS	related RAS viral (r-ras) oncogene homolog	0.323985241
RTN4	reticulon 4	2.057653416
SDC2	syndecan 2	0.492433221
SEMA4D	sema domain, immunoglobulin domain (Ig), transmembrane domain (TM) and short cytoplasmic domain, (semaphorin) 4D	3.45575275
SEMA6A	sema domain, transmembrane domain (TM), and cytoplasmic domain, (semaphorin) 6A	5.544279543
SEMA6C	sema domain, transmembrane domain (TM), and cytoplasmic domain, (semaphorin) 6C	2.8108374
SHC1	SHC (Src homology 2 domain containing) transforming protein	0.486327474

	1	
SLIT1	slit guidance ligand 1	13.04115732
SLIT2	slit guidance ligand 2	3.365917929
SMO	smoothened, frizzled class receptor	0.422786144
SOS2	son of sevenless homolog 2 (Drosophila)	2.033549347
SRGAP2	SLIT-ROBO Rho GTPase activating protein 2	2.106722072
TUBB6	tubulin, beta 6 class V	0.284204243
TUBB2A	tubulin, beta 2A class IIa	2.358713185
TUBB2B	tubulin, beta 2B class IIb	2.00416321
TUBB4A	tubulin, beta 4A class IVa	2.124318373
UNC5A	unc-5 netrin receptor A	3.647732662
UNC5B	unc-5 netrin receptor B	2.599078125
UNC5D	unc-5 netrin receptor D	8.094825608
WNT7B	wingless-type MMTV integration site family, member 7B	3.035638506

Transcripts differentially expressed at least 2.0-fold (up- or downregulated) and with a value of $P<0.05$ were considered significant.

Table S3: Gene Set Enrichment Analysis revealed that genes associated with semaphorin interactions were enriched in gene sets that were downregulated in D283 scramble relative to OTX2 knockdown tumorspheres.

Gene Symbol	Gene Title
MYL6	myosin, light chain 6, alkali, smooth muscle and non-muscle
MYL12B	null
MYH10	myosin, heavy chain 10, non-muscle
PLXNB1	plexin B1
MYH9	myosin, heavy chain 9, non-muscle
PAK1	p21/Cdc42/Rac1-activated kinase 1 (STE20 homolog, yeast)
PLXNA1	plexin A1
MYL9	myosin, light chain 9, regulatory
PLXND1	plexin D1
FYN	FYN oncogene related to SRC, FGR, YES
NRP1	neuropilin 1
PIP5K1C	phosphatidylinositol-4-phosphate 5-kinase, type I, gamma
ARHGEF11	Rho guanine nucleotide exchange factor (GEF) 11
SEMA4D	sema domain, immunoglobulin domain (Ig), transmembrane domain (TM) and short cytoplasmic domain, (semaphorin) 4D
DPYSL2	dihydropyrimidinase-like 2
RHOB	ras homolog gene family, member B
DPYSL3	dihydropyrimidinase-like 3
CDK5R1	cyclin-dependent kinase 5, regulatory subunit 1 (p35)
PLXNA3	plexin A3
PLXNA2	plexin A2
SEMA6A	sema domain, transmembrane domain (TM), and cytoplasmic domain, (semaphorin) 6A
DPYSL5	dihydropyrimidinase-like 5

All transcripts in the core enrichment were significantly different with a $P<0.05$.